

4-2018

Power Series Solutions of Nonlinear Partial Differential Equations: Applications in Nonlinear Physics

Laila Yahya Mohammed Al Sakkaf

Follow this and additional works at: https://scholarworks.uaeu.ac.ae/phys_theses

Part of the [Physics Commons](#)

Recommended Citation

Al Sakkaf, Laila Yahya Mohammed, "Power Series Solutions of Nonlinear Partial Differential Equations: Applications in Nonlinear Physics" (2018). *Physics Theses*. 1.
https://scholarworks.uaeu.ac.ae/phys_theses/1

This Thesis is brought to you for free and open access by the Physics at Scholarworks@UAEU. It has been accepted for inclusion in Physics Theses by an authorized administrator of Scholarworks@UAEU. For more information, please contact fadl.musa@uaeu.ac.ae.

United Arab Emirates University

College of Science

Department of Physics

POWER SERIES SOLUTIONS OF NONLINEAR PARTIAL
DIFFERENTIAL EQUATIONS: APPLICATIONS IN NONLINEAR
PHYSICS

Laila Yahya Mohammed Al Sakkaf

This thesis is submitted in partial fulfillment of the requirements for the degree of
Master of Science in Physics

Under the Supervision of Professor Usama Al Khawaja

April 2018

Declaration of Original Work

I, Laila Yahya Mohammed Al Sakkaf, the undersigned, a graduate student at the United Arab Emirates University (UAEU), and the author of this thesis entitled "*Power Series Solutions of Nonlinear Partial Differential Equations: Applications in Nonlinear Physics*", hereby, solemnly declare that this thesis is my own original research work that has been done and prepared by me under the supervision of Professor Usama Al Khawaja, in the College of Science at UAEU. This work has not previously been presented or published, or formed the basis for the award of any academic degree, diploma or a similar title at this or any other university. Any materials borrowed from other sources (whether published or unpublished) and relied upon or included in my thesis have been properly cited and acknowledged in accordance with appropriate academic conventions. I further declare that there is no potential conflict of interest with respect to the research, data collection, authorship, presentation and/or publication of this thesis.

Student's Signature



Date

9/05/2018

2018 Copyright © 2018 Laila Yahya Mohammed Al Sakkaf

This is a book Copyright © 2018 Laila Yahya Mohammed Al Sakkaf
All Rights Reserved

Printed in Saudi Arabia

Advisory Committee

1) Advisor: Usama Al Khawaja

Title: Professor

Department of Physics

College of Science

2) Co-advisor: Qasem Al-Mdallal

Title: Professor

Department of Mathematical Science

College of Science

Approval of the Master Thesis

This Master Thesis is approved by the following Examining Committee Members:

1) Advisor (Committee Chair): Usama Al Khawaja

Title: Professor

Department of Physics

College of Science

Signature  _____

Date 23/4/2018

2) Member: Abdessamad Abada

Title: Professor

Department of Physics

College of Science

Signature  _____

Date 24/04/2018

3) Member (External Examiner): Basem Saleem Attali

Title: Professor

College of Graduate Studies and Research

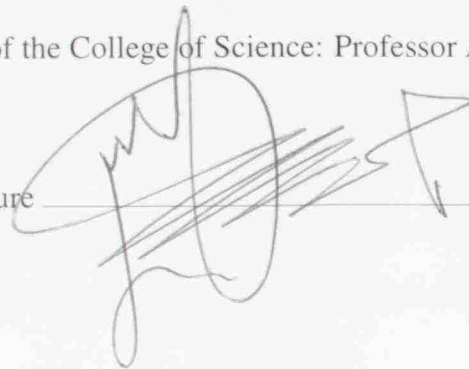
Institution: Sharjah University, UAE

Signature  _____

Date 15/4/2018

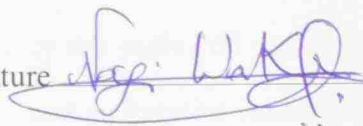
This Master Thesis is accepted by:

Dean of the College of Science: Professor Ahmed Murad

Signature 

Date 13/5/2018

Dean of the College of Graduate Studies: Professor Nagi T. Wakim

Signature 

Date 13/5/2018

Copy 8 of 9

Abstract

Obtaining analytical solutions for nonlinear partial differential equations (PDEs) is becoming a crucial role for many scientific researchers due to their importance in various physical systems. Many analytical and numerical techniques have been developed to solve PDEs, yet, there is no general applicable method for such equations.

In this study, we present an efficient iterative power series method for nonlinear boundary value problems that treats the typical divergence problem and increases arbitrarily the radius of convergence. This method is based on expanding the solution around an iterative initial point. Three nonlinear systems are considered here, the nonlinear Schrödinger equation (NLSE) with three interesting versions in which we include the nonintegrable higher order NLSE, the ordinary form of the unsteady nonlinear Navier-Stokes equations, and the chaotic Lorenz system.

The present method successfully captures the exact solitonic solutions for the fundamental NLSE and its higher-order versions including the localized and oscillating solutions for the nonintegrable higher order NLSE. The method reproduces also dual solutions for both the flow and heat transfer fields. Furthermore, the method solves accurately the Lorenz system. Some comparisons with previous works emphasized the validity, accuracy, and efficiency of the present method.

Keywords: Iterative power series solution; NLSE; Unsteady flow; Heat transfer; Contracting cylinder; Chaotic behaviour; Lorenz system.

Title and Abstract (in Arabic)

استخدام متسلسلات القوى في حل المعادلات التفاضلية الجزئية غير الخطية: تطبيقاتها في الفيزياء غير الخطية

الملخص

يعد الحصول على حلول تحليلية للمعادلات التفاضلية الجزئية غير الخطية مطلباً ملحاً للعديد من الباحثين في مختلف المجالات العلمية، وذلك لأهميتها في العديد من النظم الفيزيائية. و على الرغم من وجود الكثير من الطرق التحليلية و الرقمية التي طورت لحل المعادلات التفاضلية الجزئية غير الخطية، إلا أنه لم يتم التوصل إلى طريقة تطبيقية شاملة.

في هذه الدراسة قمنا بطرح آلية فاعلة من متسلسلات القوى، أطلقنا عليها متسلسلات القوى التتابعية، بحيث تعالج خلل التباعد في متسلسلات القوى فتزيد من قطر التقارب إلى المالا نهية. تعتمد هذه الطريقة على تمديد الحل حول نقطة بدء تتابعية.

قمنا بتطبيق هذه الآلية على ثلاث أنظمة فيزيائية غير خطية وهي كالتالي؛ معادلة شرودنجر غير الخطية مثل ذات الرتبة العليا غير التفاضلية و معادلات نافير ستوك غير الخطية غير الثابتة و نظام لورينز الفوضوي.

حققت هذه الآلية المطروحة نجاحاً في الحصول على حل سوليتوني صحيح لمعادلتى شرودنجر غير الخطية الأساسية و ذات القوى غير الخطية و حل موضعي و آخر تذبذبي لمعادلة شرودنجر غير الخطية ذات الرتبة العليا غير التفاضلية و حل ازدواجي لحقلَي التدفق و الانتقال الحراري و إيجاد جاذبات لورينز.

وتم التحقق من صحة و دقة و فاعلية هذه الآلية من خلال القيام بعدة مقارنات مع ما تم التوصل إليه سابقاً.

مفاهيم البحث الرئيسية: متسلسلات القوى التتابعية؛ معادلة شرودنجر غير الخطية؛ التدفق غير الثابت؛ نقل الحرارة؛ اسطوانة قابلة للتقلص؛ السلوك الفوضوي؛ نظام لورينز.

Acknowledgements

My first and deepest gratitude goes to my supervisor, Prof. Usama Al Khawaja, for supporting and encouraging me during the past three years, for his efforts, motivation, endless patience and for devoting a large part of his time to teach me the basics of Mathematica software.

I am extremely grateful to my co-advisor, Prof. Qasem Al-Modallal, department of Mathematical Science, for his continuous encouragement and openness.

I will forever be thankful to Prof. Abdessamad Abada, the Master program coordinator, department of Physics, for his enlightening suggestions, useful discussions and warm advising.

I thank and appreciate Dr. Sakthivinayagam Pattu, department of Physics, for his kind technical assistance in using the LaTeX program and his continuous help.

I would like also to express my acknowledgements to the members of Physics and Mathematical Science departments for their support and guidance through my graduate studies and to all of my lovely friends and colleagues for their encouragement and support.

Finally, special thanks go to my family, specially, my mother and sister Maryam for her everlasting hope, care, and concern to relieve my worries and stress.

Dedication

To my mother, for her advice, endless support and patience.

To the memory of my father, who inspired scientific thinking in our lives.

To my beloved sisters and brothers.

Table of Contents

Title	i
Declaration of Original Work	ii
Copyright	iii
Advisory Committee	iv
Approval of the Master Thesis	v
Abstract	vii
Title and Abstract (in Arabic)	viii
Acknowledgments	x
Dedication	xi
Table of Contents	xii
List of Tables	xiv
List of Figures	xv
List of Abbreviations	xviii
Chapter 1: Introduction	1
Chapter 2: Nonlinear Schrödinger Equation (NLSE)	5
2.1 Fundamental NLSE	5
2.1.1 Some Physical Solutions of the NLSE	6
2.1.2 Some Applications of the NLSE	7
2.2 Survey of Some Known Solutions of the NLSE	9

Chapter 3: Analytical Methods for Solving the NLSE	15
3.1 Separation of Variables (SoV) Method	15
3.1.1 SoV Method to NLSE with Power Law Nonlinearity	16
3.2 Similarity Transformation Method	18
3.2.1 Integrability Conditions	18
3.2.2 Generating Exact Solutions of the Nonautonomous NLSE from the Autonomous NLSE	19
3.3 Lax Pair (LP) and Darboux Transformation (DT) Method	23
3.3.1 LP and DT Method to the Fundamental NLSE	23
3.3.2 LP and DT Method to NLSE with Linear Potential	35
Chapter 4: Iterative Power Series (IPS) Method	41
4.1 Mathematical Formalism of the IPS Method	42
4.2 Application of IPS Method to NLSEs	46
4.2.1 IPS Method to the Fundamental NLSE	47
4.2.2 Mathematica Code	49
4.2.3 IPS Method to NLSE with Power Law Nonlinearity	52
4.2.4 IPS Method to Higher Order NLSE	52
Chapter 5: Application of IPS Method to Fluid Flow Dynamics	57
5.1 Heat and Mass Transfer Model	58
5.2 IPS Method to Heat and Mass Transfer Model	60
Chapter 6: Application of IPS Method to Chaotic Systems	72
6.1 Lorenz System	72
6.2 IPS Method to Lorenz System	75
Chapter 7: Conclusions and Future Remarks	82
References	84
Appendix	95

List of Tables

5.1	Stabilization of λ values with η_∞ at $\gamma = 1$ and $S = -1$	63
5.2	The upper bound of the error for the first solution at $\gamma = 2$ and $S = -1$ versus the CPU time at different values of n_{max}	64

List of Figures

2.1	Continuous wave solution given by Eq. (2.2) with $\sigma_1 = \sigma_2 = 1$	9
2.2	Bright soliton solution given by Eq.(2.3) with $\sigma_1 = \sigma_2 = 1$	10
2.3	Movable bright soliton solution given by Eq. (2.4) with $A = \sigma_1 = \sigma_2 = 1$, $v = 0.5$, and $x_0 = \phi_0 = 0$	10
2.4	Two-soliton solution given by Eq. (2.5) with $\sigma_1 = \sigma_2 = 0.5$, $v_1 = v_2 = 0$, $n_1 = 1$, $n_2 = 1.5$, and $\phi_{01} = \phi_{02} = 0$	12
2.5	Peregrine soliton solution given by Eq. (2.6) with $\sigma_1 = \sigma_2 = 1$ and $x_0 = \phi_0 = 0$	12
2.6	Kuznetsov-Ma breather solution given by Eq. (2.7) with $a = 0.2$	13
2.7	Akhmediev breather solution given by Eq. (2.7) with $a = 0.65$	13
2.8	Dark soliton solution given by Eq. (2.8) with $A = \sigma_1 = 1$ and $\sigma_2 = -1$	14
2.9	Movable dark soliton solution given by Eq. (2.9) with $A = \sigma_1 = \sigma_2 = 1$, $v = 0.5$, and $x_0 = \phi_0 = 0$	14
3.1	Movable solitonic solution of the fundamental NLSE, $A = 2$, $x_0 = 0$, and $v = 0.6$. Evolution of the movable soliton (left). Contour plot of the solution (right).	30
3.2	Non-movable solitonic solution of the fundamental NLSE, $A = 2$, $x_0 = 0$, and $v = 0$. Evolution of the non-movable soliton (left). Contour plot of the solution (right).	31
3.3	First order Rogue wave solution of the fundamental NLSE, $C_3 = C_4 = 1$. Evolution of the Peregrine soliton (left). Contour plot of the solution (right).	35
3.4	First order Rogue wave solution of the fundamental NLSE, $C_3 = C_4 = 1$. Spatial (left) and temporal (right) profiles of the Peregrine soliton.	36
3.5	Solitonic solution of the fundamental NLSE with linear potential, $x_0 = 1$, $A = 1$, and $\alpha = 1$. Evolution of the soliton (left). Contour plot of the solution (right).	40
4.1	<i>I</i> segments of the IPS method. The blue curve corresponds to the solitonic solution of the fundamental NLSE.	43
4.2	Schematic loop of the IPS method.	46
4.3	Solitonic solution of Eq. (4.14). The blue curve corresponds to the exact solution given by Eq. (4.15) and the diverging orange curves correspond to the IPS method at different iterations, with $\Delta = 0.02$, and $n_{max} = 8$	49
4.4	Solitonic solution of Eq. (4.14). Left: The IPS solution, with $a_0^0 = 1$, $a_1^0 = 0$, $n_{max} = 8$, $I = 1000$, and $\Delta = 0.005$. Right: The difference between the IPS solution and the exact solution given by (4.15).	49

4.5	Solitonic solution of Eq. (4.21). Left: The IPS solution, with initial values $a_0^0 = \left(\frac{3}{2}\right)^{\frac{1}{4}}$ and $a_1^0 = 0$. The power series is expanded up to $n_{max} = 8$, with the iteration number $I = 1000$ and $\Delta = 0.005$. Right: The difference between the IPS solution and the exact solution given by Eq. (3.12).	53
4.6	Oscillating solutions of Eq. (4.28) using IPS method with initial values $a_0^0 = 0.1$ and $a_1^0 = 0$. The power series is expanded up to $n_{max} = 8$, with the iteration number $I = 10000$ and $\Delta = 0.0085$. Left: The SRS factor is $\sigma_5 = +0.02$. Right: The SRS factor is $\sigma_5 = -0.02$	55
4.7	The IPS Localized solution of Eq. (4.28) with initial values $a_0^0 = 1.429660329$ and $a_1^0 = 0$, and the SRS factor is $\sigma_5 = -0.02$. The power series is expanded up to $n_{max} = 8$, with the iteration number $I = 10000$ and $\Delta = 0.002$	55
4.8	Left: Localized solutions of Eqs. (4.28) and (4.14), dotted curve corresponds to the normalized representation of Figure 4.7 and the blue curve corresponds to the solution in Figure 4.4. Right: The difference between the two solutions.	56
5.1	Velocity profiles, $f'(\eta)$, for the first solution; exact (blue) and approximate (dashed) solutions at different I with $S = -1$ and $\gamma = 1$. The power series is expanded up to $n_{max} = 8$, $\Delta = 0.014$	63
5.2	Error of the IPS method (left) and the ERK4 (right) for the case of $\gamma = 1$ and $S = -1$. The error is defined as the difference between the numerical solution and the exact solution (5.23). The power series is expanded up to $n_{max} = 8$, $I = 1000$ and $\Delta = 0.014$	64
5.3	Normalized skin friction coefficient, $f''(1)$, as a function of S for $\gamma = 0$. The IPS (solid blue), the Zaimi <i>et al.</i> [79] (\bullet), and the Elnajjar <i>et al.</i> [81] (\star) solutions.	65
5.4	Velocity profiles, $f'(\eta)$, for different values of γ at $S = 2$: First solution (left) and second solution (right). The power series is expanded up to $n_{max} = 8$, $I = 1000$ and $\Delta = 0.014$	66
5.5	Velocity profiles, $f'(\eta)$, for different values of S at $\gamma = 1$: First solution (left) and second solution (right). The power series is expanded up to $n_{max} = 8$, $I = 1000$ and $\Delta = 0.014$	66
5.6	Normalized skin friction coefficient, $f''(1)$, as a function of S for different values of γ : The first solution (solid) and second solution (dotted). The power series is expanded up to $n_{max} = 8$, $I = 1000$ and $\Delta = 0.014$	67
5.7	Temperature profiles, $\theta(\eta)$, for different values of γ at $S = 2$: First solution (left) and second solution (right). The power series is expanded up to $n_{max} = 8$, $I = 1000$ and $\Delta = 0.014$	69
5.8	Temperature profiles, $\theta(\eta)$, for different values of S at $\gamma = 1$: First solution (left) and second solution (right). The power series is expanded up to $n_{max} = 8$, $I = 1000$ and $\Delta = 0.014$	69
5.9	Heat transfer rate, $-\theta'(1)$, as a function of S for different values of γ : The first solution (solid) and second solution (dotted). The power series is expanded up to $n_{max} = 8$, $I = 1000$ and $\Delta = 0.014$	70

5.10	An overview of the solution for problems (5.10) and (5.11) subject to the boundary conditions (5.12) in the $\gamma-S$ domain.	71
6.1	Trajectory, $y(t)$ (blue), of the chaotic Lorenz model with $Pr = 10$, $Ra = 28$, and $\gamma = 8/3$ and initial condition $(a_0^0, b_0^0, c_0^0) = (0, 1, 0)$. The power series is expanded up to $n_{max} = 8$, with $I = 10000$ and $\Delta = 0.002$. The dashed curve represents the zeroth order series solution with $n_{max} = 20$	77
6.2	Trajectories, $x(t)$ (red), $y(t)$ (blue), and $z(t)$ (green) of the chaotic Lorenz model with $Pr = 10$, $Ra = 28$, and $\gamma = 8/3$ and initial condition $(a_0^0, b_0^0, c_0^0) = (0, 1, 0)$. The power series is expanded up to $n_{max} = 8$, with $I = 10000$ and $\Delta = 0.002$	77
6.3	Two $y(t)$ solutions of the Lorenz system with $Pr = 10$, $Ra = 28$, $\gamma = 8/3$ and the initial conditions $(a_0^0, b_0^0, c_0^0) = (0, 1, 0)$. The IPS solutions are expanded up to $n_{max} = 8$, with $I = 7500$ (green curve) and with $I = 8000$ (red curve).	78
6.4	Two $y(t)$ solutions of the Lorenz system with $Pr = 10$, $Ra = 28$, $\gamma = 8/3$ and the initial conditions $(a_0^0, b_0^0, c_0^0) = (0, 1, 0)$. The IPS solutions are expanded up to $n_{max} = 8$, with $I = 8000$ (red curve) and with $I = 8500$ (blue curve).	79
6.5	Two $y(t)$ solutions of the Lorenz system with $Pr = 10$, $Ra = 28$, $\gamma = 8/3$ and the initial conditions $(a_0^0, b_0^0, c_0^0) = (0, 1, 0)$. The IPS solution is expanded up to $n_{max} = 8$, with $I = 8000$ (red curve) and The ERK4 solution (black curve).	79
6.6	Two $y(t)$ solutions of the Lorenz system with $Pr = 10$, $Ra = 28$, and $\gamma = 8/3$ and the initial conditions $(a_0^0, b_0^0, c_0^0) = (0, 1, 0)$ (blue), and $(0, 1.0001, 0)$ (red). The power series is expanded up to $n_{max} = 8$, with $I = 10000$ and $\Delta = 0.005$	80
6.7	Three chaotic projections of the phase space of the Lorenz system with $Pr = 10$, $Ra = 28$, and $\gamma = 8/3$ and initial condition $(a_0^0, b_0^0, c_0^0) = (0, 1, 0)$. The power series is expanded up to $n_{max} = 8$, $I = 10000$ and $\Delta = 0.003$ for $t \in (0, 30]$	81

List of Abbreviations

BEC	Bose-Einstein condensate
BVPs	Boundary value problems
CPU	Central Processing Unit
DT	Darboux Transformation
ERK4	Explicit Runge-Kutta method of order four
HONLSE	Higher order Nonlinear Schrödinger equation
IPS	Iterative Power Series
LP	Lax Pair
NLSE	Nonlinear Schrödinger equation
ODEs	Ordinary differential equations
PDEs	Partial differential equations
PS	Power Series
SoV	Separation of Variables
SPM	Self-phase modulation
SRS	Stimulated Raman scattering
SS	Self steepening
TOD	Third-order dispersion
GVD	Group velocity dispersion
GPE	Gross-Pitaevskii equation

Chapter 1: Introduction

Many systems in physics represent nonlinear behaviour and thus are modeled by nonlinear equations. In fact, the majority of natural phenomena in the world are nonlinear systems, and hence, nonlinearity is the norm rather than the exception. The nonlinearity becomes significant when the input part of the system is large enough to make the nonlinearity noteworthy. Many nonlinear systems are approximately linear for small perturbations. An example of linear behaviour is an oscillating spring. The validity of Hook's law breaks down when the displacement of the spring (input part of the system) becomes large, therefore, it oscillates nonlinearly. Another well known example is a simple pendulum. The pendulum acts linearly only when the displacement angle (input part of the system) is small enough. Nonlinear optical interaction can be served as a profound example as well. The nonlinearity of a nonlinear material is non-notable unless with high enough optical intensity.

In the mathematical sense, breaking down the linearity is associated with breaking down the superposition principle, and hence states that the sum of two solutions of the equation is not a solution of the system any more. Nonlinear equations admit infinitely many independent solutions. This leads to difficulty in predicting the possible behaviours of the nonlinear systems, and thus, finding out some interesting physical solutions out of those infinite solutions became a considerable task for many researchers.

Nonlinear partial differential equations (PDEs) arise in diverse physical systems such as quantum mechanics, propagation of light pulses in nonlinear optical waveguides, Bose-Einstein condensates (BEC), plasma physics, Biological systems, ocean waves, chemical reactions, and others. In the frame of real physical system,

the term "Nonlinear boundary value problems (BVPs)" is used instead of nonlinear PDEs, where the boundary information of the interesting system is known. Numerous phenomena in engineering and applied science fields are governed by nonlinear BVPs. Therefore, the nonlinear BVPs have received a huge attention by mathematicians, physicists and engineers for the sake of finding and analyzing their solutions. Achieving solutions of such systems is very helpful in studying the nonlinear phenomena arising in these systems.

Generally speaking, finding analytical solutions in terms of well-known functions for nonlinear BVPs is often impossible. Many successful techniques have been developed to solve nonlinear PDEs, and recently, great interest was devoted to develop analytical and numerical techniques, such as Adomian Decomposition [1], Lax pair and Darboux Transformation [2], Inverse Scattering method [3], and Homotopy Analysis method [5, 6]. However, there is no general applicable method to solve such nonlinear equations.

Among these valuable techniques, Power Series (PS) method is one of the most traditional methods of solving linear equations. Its application extends to nonlinear PDEs as well. However, it suffers in many cases from a serious problem of divergence after a certain value of the independent variable. The divergence is intrinsic to the nature of the solution since it persists to exist even with an infinite power series expansion.

The PS method was used for solving different classes of differential equations. However, this method is not commonly used in nonlinear physical systems because of its accommodated typical problem of finite radius of convergence. As a result, the work done by the PS method is so limited in this area.

Some nonlinear systems whether nonlinear ordinary differential equations (ODEs)

or nonlinear PDEs were studied by the PS method. The power series expansion is constructed for some examples of nonlinear ODEs after they are converted into polynomial format [7]. Three versions of nonlinear time-dependent Burgers equation are solved by the PS method in [8]. Sandoval and Mello reported in [9] how it is easy to get out the recursion relations of different examples of nonlinear PDEs. They showed how this technique works in both the stationary (time-independent) and non-stationary (time-dependent) states of Burger equation. The authors also represented the recursion relations of the equations of a steady state laminar boundary on a flat plate; the Korteweg-de Vries equation, and the coupled Korteweg-de Vries equation. The researchers in [10] made a comparison between the obtained series solution and the well-known exact solution of number of nonlinear PDEs. Moreover, other efforts were devoted for building symbolic power series code for solving such equations [11].

Although the above examples of solving nonlinear PDEs by the PS technique gave a good approximated solution, further publications represented attempts to solve the divergence problem of this method. Scraton in [12] reported some successful functional transformations that enhance the radius of convergence, however, this enhancement results only in a slight increase in the radius of convergence.

In this work, we present a modified version of the power series method that delays the convergence point, and therefore extending the radius of convergence to an arbitrary value. This value could, in principle, approach infinity achieving exact solutions, see a materialized work relegated to Appendix. Along this manuscript, the method will be called Iterative Power Series (IPS) method.

Recognizing that a powerful numerical scheme based on this method is already established [13–19], we nonetheless present a thorough investigation of the error associated with this method with the aim of showing how we can systemically reduce errors to infinitesimal values. We will show robustness and efficiency of the method

via a number of highly-demanding boundary-value problems. Therefore, solving the problem of finite radius of convergence will open the door wide for applying the power series method to much larger class of differential equations, particularly the nonlinear ones.

The outline of this thesis is organized as follows. In chapter 2, we investigate the nonlinear Schrödinger equation (NLSE), one of the most universal nonlinear models. Specifically, we present some interesting solutions of the fundamental NLSE such as *Solitons*, *Peregrine soliton*, and *Breather solutions*. We present several real physical implementations of such solutions in nonlinear optics, ocean dynamics, quantum physics, and biological science. We close the discussion with a survey of some investigated exact solutions of the NLSE. In chapter 3, we present some analytical methods for solving the NLSE. We employ the *Separation of Variables* method to solve the NLSE with power law nonlinearity, the *Similarity Transformation* method to obtain exact solutions of the nonautonomous NLSE from the standard autonomous NLSE, and the *Lax Pair and Darboux Transformation* method to solve the same equation and the NLSE with linear potential. Chapter 4 illustrates the new *IPS* method. We begin by applying this technique on three versions of the NLSE, the fundamental NLSE, the NLSE with power law nonlinearity, and the nonintegrable higher order NLSE. Note that all the presented equations in this chapter are homogeneous nonlinear equations. The bulk of chapter 5 is devoted to apply the IPS method on the *Heat and Mass Transform Model*. This model is described by two inhomogeneous nonlinear equations. The governing equations for this system are the continuity, momentum, and energy equations. In chapter 6, we apply the IPS method on the *Lorenz Model*, one of the most important nonlinear systems that admits chaotic behaviour. We end with a summary of our main conclusions and future remarks in chapter 7.

Chapter 2: Nonlinear Schrödinger Equation (NLSE)

Among all nonlinear equations, the NLSE is one of the most universal integrable differential equations. It describes multiple physical phenomena, discrete and continuous systems. It is considered as a key of describing the BEC, the collapse of plasma waves, pulses in nonlinear optical fibers, the propagation of waves in nonlinear waveguides, and the interaction between solitons in nonlinear waveguides [20–25].

2.1 Fundamental NLSE

Here we present some physical applications of the fundamental version of the NLSE which is also called in some applications the homogeneous Gross-Pitaevskii equation (GPE)

$$i u_t + \sigma_1 u_{xx} + \sigma_2 |u|^2 u = 0, \quad (2.1)$$

where $u = u(x, t)$ stands for the amplitude of the envelope wave and respectively, x and t correspond to the position and time. Here $u_t = \partial u / \partial t$ and $u_{xx} = \partial^2 u / \partial x^2$. The constant coefficients, $\sigma_1 = \pm 1$, corresponds to the normal (+1) group velocity dispersion (GVD), which has responsibility to compress the pulse and anomalous (-1) GVD, which has responsibility to spread out the pulse, and $\sigma_2 = \pm 1$, corresponds to the type of the cubic nonlinearity, self-focusing (+1) or self-defocussing (-1), respectively. As a result of the source of nonlinearity of the later coefficient, the equation is named also NLSE with cubic nonlinearity, or commonly known as NLSE with Kerr law. In nonlinear optics, nonlinear Kerr effect is the variation of the refractive index of an optical medium with the intensity of optical beam as, $n(|u|^2) = n_0 + n_2 |u|^2$, where n_2 is the material nonlinearity coefficient and n_0 is the refractive index of the material in the

absence of optical field. This effect becomes significant only with very intense beams such as those from lasers. As a consequence of the Kerr effect, the phase is exposed to what is called a self-phase modulation (SPM), $\Delta\phi = \omega t - kL(n_0 + n_2|u|^2)$, where L is the propagation distance, ω is the wave frequency, and k is the wavenumber given by $2\pi/\lambda$, here λ is the wavelength.

2.1.1 Some Physical Solutions of the NLSE

Below, we list some of the most interesting exact solutions of the fundamental NLSE with a brief description of their appearance in some applications. In addition, mathematical representations of these solutions and other exact solutions will be shown in the next section.

Solitons

One of the admitted exact solutions of the fundamental NLSE is *Soliton* given by the solution in (2.3) and the corresponding figure in Figure 2.2. Such solution is considered as the most essential phenomenon of the equation. Solitons are localized nonlinear waves that remain stable and constant during the propagation. This is due to a dynamic balance between the group velocity dispersion, σ_1 , and the nonlinear Kerr effect, σ_2 . The first observation of soliton behaviour was in a narrow water channel in 1834 by J. S. Russell [26]. Such waves can interact between themselves elastically as if they are real particles, and return to their initial properties after the collision. They arise in diverse physical systems including propagation of light pulses in nonlinear optical waveguides and ocean waves [27, 28].

Peregrine Soliton

Another interesting solution of this nonlinear equation is the *Peregrine* soliton which models *Rogue* waves, see Figure 2.5. This type of solution is localized in both

space and time given by Eq. (2.6). It appears from nowhere, causes danger, and disappears without a trace. Rogue wave plays an important role in several physical nonlinear systems. It occurs in oceans, cold matter systems, and optics [29–34]. Peregrine soliton is one prototype of Rogue waves [35]. It is the lowest order rational solution of the NLSE. This solution takes the form of one dominant peak accompanied with two side holes that exist as a result of energy conservation. The highest amplitude of the Peregrine soliton equals three times the amplitude of the surrounding background. In 1983, the British mathematician H. Peregrine was the first one who proposed the Peregrine soliton of the NLSE [36].

Breather Solutions

Two interesting breather types of the soliton are localized in one dimension and periodic in the other dimension with constant amplitude. These two solutions are given by Eq. (2.7). *Ma breather*, Figure 2.6, was investigated in 1979 by Y. C. Ma [37]. It is localized in space but periodic in the time dimension. Thus, it appears several times in the same location. *Akhmediev breather*, Figure 2.7, is another soliton which was found by N. N. Akhmediev in 1985 [38–40]. Such solution is localized in time but periodic in the space. This means that, it appears at the same time in several places.

2.1.2 Some Applications of the NLSE

Some interesting applications of solitons and rogue wave solutions of the fundamental NLSE are listed below.

Nonlinear Optics

The fundamental NLSE describes the behaviour of optical waves and pulses passing through fiber optics and optical waveguides. Due to the merits of NLSE soliton, this solution provided an obvious shift in the optical communication. One of the

main characteristics of optical soliton communication is the ability of such kind of pulses to propagate for long distances without any distortion, and hence more accurate information transfer. The application of optical soliton was invented theoretically in 1973 and supported experimentally in 1980 [24, 25].

Ocean Dynamics

The fundamental NLSE is more studied in deep and shallow water. Both solitons and Rogue waves are highly applicable in water dynamics and oceanography. The first observation of soliton was water wave soliton as we already mentioned. Tsunami is an example of two dimensional soliton as a result of minor earthquakes and landslides. Tsunami occurred in many regions such as the Pacific Ocean, the Mediterranean Sea, the Atlantic Ocean, and the Indian Ocean. Oceanic Rogue waves have been seen in various seas and oceans of the world. The highest recorded observation of the Rogue wave, with 34 m in height, was in 1933 in the Pacific Northwest. Another miserable case happened in the Indian Ocean in 1968 which broke the tanker World Glory and caused the death of more than 20 crews. More recorded cases can be found in [33, 41].

Cold Quantum Gases

Atomic waves of the fundamental NLSE arise due to the atomic interactions in dilute gases. During the cooling of gas, the atoms start to transfer from fermions to bosons condense in the same quantum state and induce the fifth state of matter, the BEC. These condense bosons could take the form of three dimensional solitons or rogue waves [42, 43].

Biomembranes and Nerves

In 2005 the two scientists, T. Heimburg and A. D. Jackson declared the classical theory of nerve signals which states that the voltage differences in and out neurons create electrical signals. Under several circumstances, they proved that such signals are not electrical signals but sound signals. The researchers reported that these signals

move along long distances through nerve cells which could in length be from a few milliliters to a few meters, these sound waves should not expand in all directions, and hence supported their idea and constructed their new model of the nerves communication that states that nerves communicate via sound waves, but not any sounds, the nerve signals are acoustic solitons [44].

2.2 Survey of Some Known Solutions of the NLSE

Below we demonstrate some of the known exact solutions of Eq. (2.1).

Continuous Wave

$$u(x, t) = \sqrt{\frac{\sigma_1}{\sigma_2}} e^{i \sigma_1 t}. \quad (2.2)$$

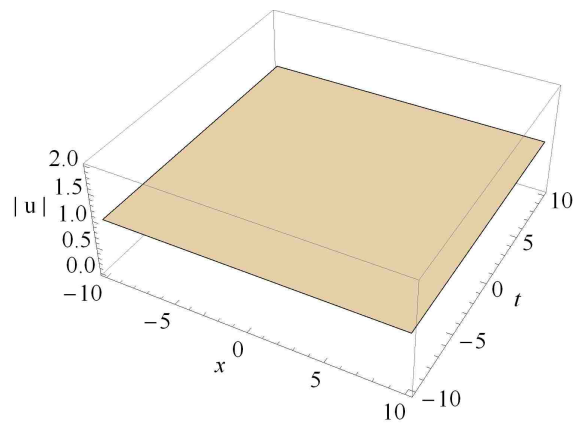


Figure 2.1: Continuous wave solution given by Eq. (2.2) with $\sigma_1 = \sigma_2 = 1$.

Bright Soliton

$$u(x,t) = \sqrt{\frac{2\sigma_1}{\sigma_2}} \operatorname{sech}(x) e^{i\sigma_1 t}. \quad (2.3)$$

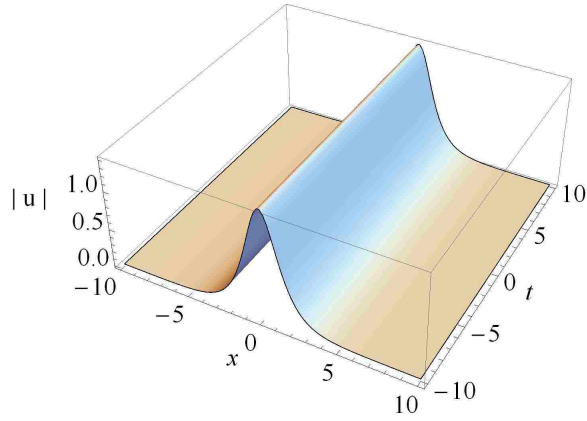


Figure 2.2: Bright soliton solution given by Eq.(2.3) with $\sigma_1 = \sigma_2 = 1$.

Movable Bright Soliton

$$u(x,t) = A \operatorname{sech}[A(c x - \sigma_2 v t - x_0)] e^{i[v(c x - x_0) + \frac{1}{2} \sigma_2 (A^2 - v^2) t + \phi_0]}, \quad (2.4)$$

where $c = \sqrt{\frac{\sigma_2}{2\sigma_1}}$.

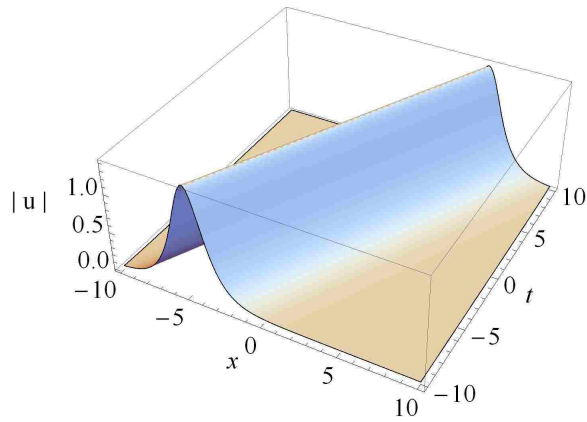


Figure 2.3: Movable bright soliton solution given by Eq. (2.4) with $A = \sigma_1 = \sigma_2 = 1$, $v = 0.5$, and $x_0 = \phi_0 = 0$.

Two-soliton

$$\begin{aligned}
u(x,t) &= \sqrt{\frac{n_1}{8}} e^{i(\phi_{01} + \phi_1(x,t))} \operatorname{sech} \left[\frac{n_1}{4} (x - (x_1 + t v_1)) \right] \\
&+ \sqrt{\frac{n_2}{8}} e^{i(\phi_{01} + \phi_{02} + \phi_2(x,t) + \tan^{-1} [\frac{\alpha_2}{\alpha_1}] + \tan^{-1} [\frac{\alpha_4}{\alpha_3}])} \\
&\times \operatorname{sech} \left[\frac{n_1}{4} (x - (x_2 + t v_2)) + \frac{1}{2} \log \left[\frac{\alpha_1^2 + \alpha_2^2}{\alpha_3^2 + \alpha_4^2} \right] \right], \tag{2.5}
\end{aligned}$$

where

$$\begin{aligned}
\phi_j(x,t) &= v_j (x - (x_j + t v_j)) + \frac{t}{8} (4 v_j^2 + \frac{1}{4} n_j^2), \\
\alpha_1 &= f_1 + e^{y_m} \cos z, & \alpha_2 &= f_2 + e^{y_m} \sin z, \\
\alpha_3 &= \frac{f_3}{n_1} - n_1 e^{y_p} \cos z, & \alpha_4 &= \frac{f_2}{n_1} - n_1 e^{y_p} \sin z, \\
f_1 &= \frac{(n_2 + n_1)}{2} + \frac{(n_2 - n_1)}{2} e^y, & f_2 &= 2 (v_2 - v_1) (1 + e^y), \\
f_3 &= -\frac{1}{2} ((n_2 - n_1) + (n_2 + n_1) e^y), \\
y_m &= \frac{1}{4} ((n_1 - n_2) x + (n_1 (x_1 + t v_1) - n_2 (x_2 + t v_2))), \\
y_p &= \frac{1}{4} ((n_1 + n_2) x - (n_1 (x_1 + t v_1) + n_2 (x_2 + t v_2))), \\
y &= \frac{1}{2} n_1 (x - (x_1 + t v_1)), & z_{jj} &= -x_j v_j + x v_j - \frac{t}{8} (4 v_j^2 - \frac{1}{4} n_j^2), \\
z &= -\phi_{02} + z_{11} - z_{22}, \text{ and } j = 1, 2.
\end{aligned}$$

It should be mentioned here that, the first sech term corresponds to the first soliton ($j = 1$), while the second sech term corresponds to the second soliton ($j = 2$) with a shift in both, the position and the phase. Here x_j , v_j , n_j , and $\phi_{0j} + \phi_j(x,t)$ correspond to the center-of-mass position, the speed, the normalization, and the phase of the two solitons, respectively [46].

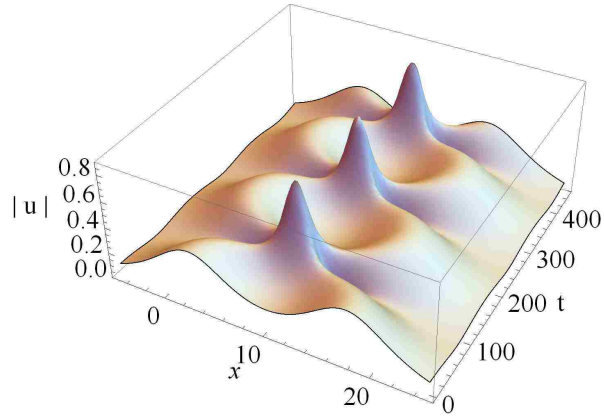


Figure 2.4: Two-soliton solution given by Eq. (2.5) with $\sigma_1 = \sigma_2 = 0.5$, $\nu_1 = \nu_2 = 0$, $n_1 = 1$, $n_2 = 1.5$, and $\phi_{01} = \phi_{02} = 0$.

Peregrine Soliton

$$u(x,t) = \left[1 - \frac{4(1 + 2i\sigma_2 t)}{1 + 4(cx - x_0)^2 + 4\sigma_2^2 t^2} \right] e^{i\sigma_2 t + i\phi_0}. \quad (2.6)$$

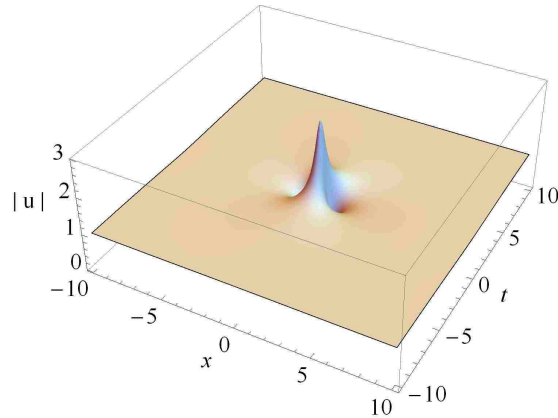


Figure 2.5: Peregrine soliton solution given by Eq. (2.6) with $\sigma_1 = \sigma_2 = 1$ and $x_0 = \phi_0 = 0$.

Kuznetsov-Ma Breather and Akhmediev Breather

$$u(x,t) = \left[1 + \frac{2(1 - 2a) \cosh(bt) + ib \sinh(bt)}{\sqrt{2a} \cos(wx) - \cosh(bt)} \right] e^{it}, \quad (2.7)$$

where a is the single governing parameter determines the physical behaviour of the solution. Here, $w = 2\sqrt{(1-2a)}$ and $b = \sqrt{8a(1-2a)}$. The Kuznetsov-Ma breather is obtained when $0 < a < 1/2$, Figure 2.6, while the Akhmediev breather is obtained when $1/2 < a < \infty$, Figure 2.7. However, when $a \rightarrow 1/2$, a Peregrine soliton is achieved [47].

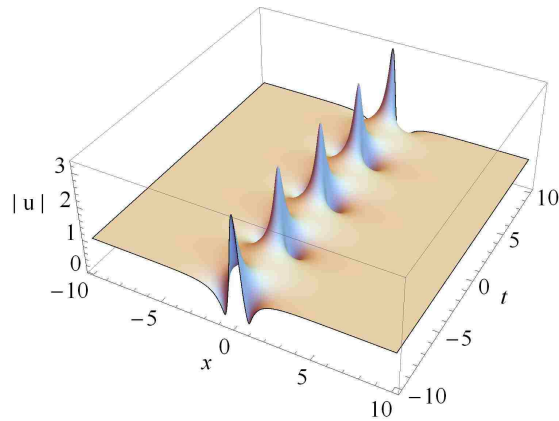


Figure 2.6: Kuznetsov-Ma breather solution given by Eq. (2.7) with $a = 0.2$.

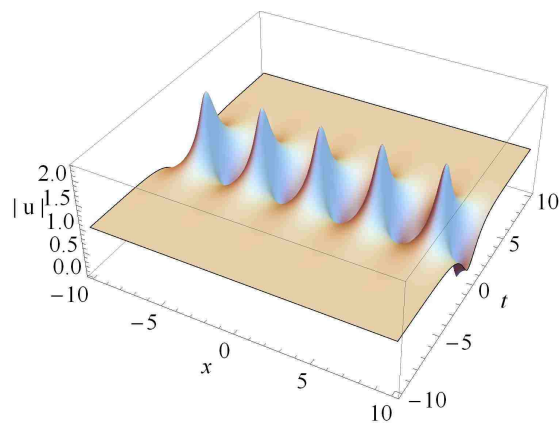


Figure 2.7: Akhmediev breather solution given by Eq. (2.7) with $a = 0.65$.

Dark Soliton

$$u(x, t) = A \tanh \left[A \sqrt{-\frac{\sigma_2}{2\sigma_1}} x \right] e^{i A^2 \sigma_2 t} \quad (2.8)$$

[48].

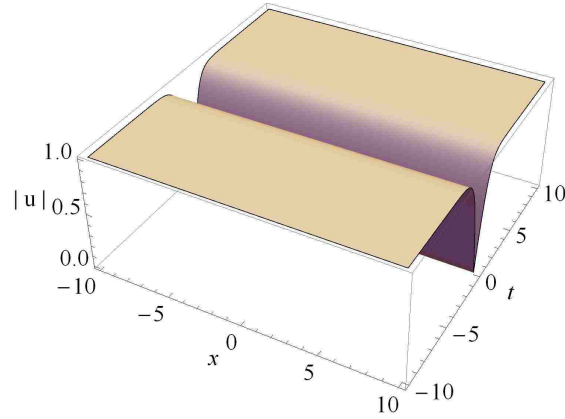


Figure 2.8: Dark soliton solution given by Eq. (2.8) with $A = \sigma_1 = 1$ and $\sigma_2 = -1$.

Movable Dark Soliton

$$u(x, t) = A \tanh[A(c x + \sigma_2 v t - x_0)] e^{i[v(c x - x_0) + \frac{1}{2} \sigma_2 (2A^2 + v^2) t + \phi_0]}. \quad (2.9)$$

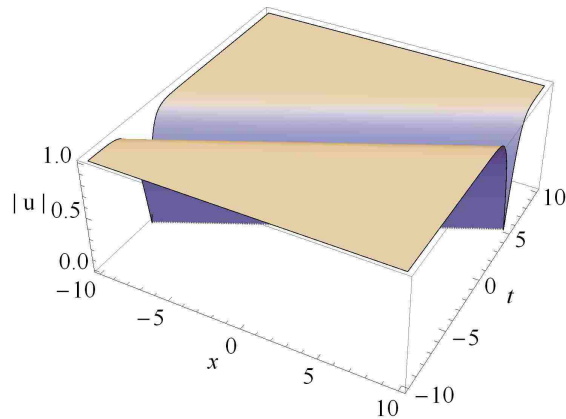


Figure 2.9: Movable dark soliton solution given by Eq. (2.9) with $A = \sigma_1 = \sigma_2 = 1$, $v = 0.5$, and $x_0 = \phi_0 = 0$.

Chapter 3: Analytical Methods for Solving the NLSE

Various analytical methods are used to handle nonlinear equations such as the Inverse Scattering Transform [3, 4], the Adomian Decomposition method [1], and the Homotopy Analysis method [5, 6]. This chapter presents three useful techniques that are used frequently for solving nonlinear PDEs. Separation of Variables method is our first technique that is used in solving the NLSE with power law nonlinearity. The second presented technique is the Similarity Transformation method which will be employed to find exact solution of the NLSE with linear potential from the fundamental version. Last but not least is the Lax pair and Darboux Transformation method which will be used to solve two versions of the NLSE, the fundamental NLSE and the NLSE with linear potential. These techniques are explained with the help of these illustrative examples.

3.1 Separation of Variables (SoV) Method

In this section we deal with an elementary and powerful technique for solving PDEs known as Separation of Variables (SoV) method which is also known as Fourier method. This method is based on seeking a solution of the PDE in the form of a product of functions of one variable, $u(x, t) = X(x) T(t)$, where $u(x, t)$ is the desired solution. Substituting the product of functions of one variable in the original PDE will separate it into a set of ODEs, each involving only one independent variable. Although, this technique is quite simple, it requires a previous knowledge about the solutions of the equation that appear. Add to that, the ability of solving the ODEs that are obtained.

3.1.1 SoV Method to NLSE with Power Law Nonlinearity

Let us employ the SoV method to the NLSE with power law nonlinearity written as

$$\frac{i}{2} u_t + \frac{1}{2} u_{xx} + |u|^{2s} u = 0, \quad (3.1)$$

where we set $\sigma_1 = +1$, $\sigma_2 = +2$ and $s > 0$ is an integer. This equation was studied in several works [49–51] due to its importance in plasma physics and nonlinear fiber optics. The well-known general stationary solution of Eq. (3.1) is written in the form of

$$u(x, t) = Z(x) \exp(i\omega t). \quad (3.2)$$

Substituting this solution in Eq. (3.1) yields to the ODE given by

$$\frac{1}{2} Z - \frac{1}{2} Z'' - Z^{2s+1} = 0. \quad (3.3)$$

Using $Z'' = Z' (dZ'/dZ)$ in Eq. (3.3)

$$\frac{1}{2} Z - Z^{2s+1} = \frac{1}{2} Z' \frac{d}{dZ} Z'. \quad (3.4)$$

Multiplying by 2 and rearranging

$$(Z - 2 Z^{2s+1}) dZ = Z' dZ'. \quad (3.5)$$

Integrating both sides

$$\frac{1}{2} Z^2 - \frac{1}{s+1} Z^{2s+2} = \frac{1}{2} Z'^2 + C_0, \quad (3.6)$$

where C_0 is the integration constant. Multiplying by 2 and rearranging, we achieve

$$Z'^2 = Z^2 - \frac{2}{s+1} Z^{2s+2} - C_1, \quad (3.7)$$

where $C_1 = 2 C_0$. Now $Z' = dZ/dx$ will be

$$\frac{d}{dx} Z = \sqrt{Z^2 - \frac{2}{s+1} Z^{2s+2} - C_1}, \quad (3.8)$$

then, separating variables, we get

$$\frac{d}{\sqrt{Z^2 - \frac{2}{s+1} Z^{2s+2} - C_1}} Z = dx, \quad (3.9)$$

and integrating both sides to find the form of the independent variable, x ,

$$x = \frac{Z \sqrt{-1-s+2Z^{2s}} \tanh\left(\frac{\sqrt{-1-s+2Z^{2s}}}{\sqrt{1+s}}\right)}{s \sqrt{1+s} \sqrt{Z^2 - \frac{2Z^{2s+2}}{1+s}}} + C_2, \quad (3.10)$$

where we put $C_1 = 0$, and C_2 is the integration constant. Solving Eq. (3.10) for Z with $C_2 = 0$, the general solution reads

$$Z(x) = 2^{\frac{-1}{2s}} \left(\sqrt{1+s} \operatorname{sech}(s x) \right)^{\frac{1}{s}}. \quad (3.11)$$

At $s = 2$, exact solitonic solution is obtained

$$Z(x) = \left(\sqrt{\frac{3}{2}} \operatorname{sech}(2x) \right)^{\frac{1}{2}}. \quad (3.12)$$

3.2 Similarity Transformation Method

We present here another useful technique that is used to handle nonlinear PDEs, namely, the Similarity Transformation method. This method is employed frequently to generate new solutions of a nonautonomous NLSE from those of the fundamental homogeneous NLSE [52–57], via transforming the coordinates and the solution function. The two equations are similar if a similarity transformation will carry the first equation to the second equation, and then one can obtain solutions of the second equation from the solutions of the first equation and vice versa.

3.2.1 Integrability Conditions

Considering the most general NLSE written as

$$\begin{aligned} f(x,t) \Psi_{xx}(x,t) + g(x,t) |\Psi(x,t)|^2 \Psi(x,t) + v(x,t) \Psi(x,t) + \\ i \gamma(x,t) \Psi(x,t) + i \Psi(x,t) = 0. \end{aligned} \quad (3.13)$$

This equation was considered in [58] where the following Painlevé integrability conditions were obtained

$$f(x,t) = f(t), \quad g(x,t) = g(t), \quad \gamma(x,t) = \gamma(t), \quad (3.14)$$

$$v(x,t) = v_0(t) + v_1(t) x + v_2(t) x^2. \quad (3.15)$$

Here the function coefficients, $f(x,t)$, $g(x,t)$, and $\gamma(x,t)$ denote the dispersion, nonlinearity, and gain/loss, respectively, and $v(x,t)$ indicates the external potential applied. The functions, $v_0(t)$ and $v_1(t)$ are arbitrary, while $v_2(t)$ is given by

$$4 f(x,t)^3 g(x,t)^2 v_2(t) + f(x,t) g(x,t) (f_t(x,t) g_t(x,t) + f(x,t) g_{tt}(x,t) +$$

$$g(x,t)^2(f_t(x,t)^2 - f(x,t) f_{tt}(x,t)) - 2 f_{tt}(x,t) g_t(x,t)^2 = 0, \quad (3.16)$$

where the subscripts indicate differentiation with respect to t and x .

While our aim is not to study or derive the integrability conditions, it is worth mentioning that deciding whether an equation is integrable depends on the method used. Another definition defines the integrable system as system that provides an infinite set of conserved quantities.

3.2.2 Generating Exact Solutions of the Nonautonomous NLSE from the Autonomous NLSE

We write the fundamental or autonomous NLSE as

$$\Psi_T = \frac{i}{2} \Psi_{XX} + i \gamma |\Psi|^2 \Psi, \quad (3.17)$$

where $X = X(x,t)$ and γ is used here to represent the Kerr effect. The nonautonomous NLSE with a linear external potential is

$$i \Phi_t + \frac{1}{2} \Phi_{xx} - c x \Phi + \gamma |\Phi|^2 \Phi = 0, \quad (3.18)$$

where c is the strength of the potential. The integrability condition (3.16) can be obtained by performing the following transformation

$$\Phi(x,t) = A(x,t) \Psi(X(x,t), T(x,t)), \quad (3.19)$$

where $A(x,t)$ is a general complex function and $X(x,t)$ and $T(x,t)$ are the transformed coordinates to be found. Due to their conformity in involving the independent variable

t , one can simply represent this transformation as the following

$$\Phi(x, t) = A(x, t) \Psi(X(x, t), t). \quad (3.20)$$

From Eq. (3.20) we obtain

$$\Phi_t = A_t \Psi + A \Psi_t + A \Psi_X X_t, \quad (3.21)$$

$$\Phi_x = A_x \Psi + A \Psi_X X_x, \quad (3.22)$$

$$\Phi_{xx} = A_{xx} \Psi + 2 A_x \Psi_X X_x + A \Psi_{XX} X_x^2 + A \Psi_X X_{xx}, \quad (3.23)$$

and

$$|\Phi|^2 \Phi = |A|^2 |\Psi|^2 A \Psi. \quad (3.24)$$

Substituting Eqs. (3.21)-(3.24) in Eq. (3.18), we get

$$\begin{aligned} & i (A_t \Psi + A \Psi_t + A \Psi_X X_t) + \frac{1}{2} (A_{xx} \Psi + 2 A_x \Psi_X X_x + A \Psi_{XX} X_x^2 + A \Psi_X X_{xx}) - \\ & c x A \Psi + \gamma |A|^2 |\Psi|^2 A \Psi = 0. \end{aligned} \quad (3.25)$$

Using Eq. (3.17) to simplify Eq. (3.25), we find

$$\begin{aligned} & i (A_t \Psi + \frac{iA}{2} \Psi_{XX} + i A \gamma |\Psi|^2 \Psi + A \Psi_X X_t) + \frac{1}{2} (A_{xx} \Psi + 2 A_x \Psi_X X_x + \\ & A \Psi_{XX} X_x^2 + A \Psi_X X_{xx}) - c x A \Psi + \gamma |A|^2 |\Psi|^2 A \Psi = 0. \end{aligned} \quad (3.26)$$

Collecting coefficients of Ψ , Ψ_X , Ψ_{XX} , and $|\Psi|^2 \Psi$, separately, and equating to zero, the following equations are obtained

$$\Psi: \quad i A_t + \frac{1}{2} A_{xx} - c x A = 0, \quad (3.27)$$

$$\Psi_X: \quad i A X_t + A_x X_x + \frac{1}{2} A X_{xx} = 0, \quad (3.28)$$

$$\Psi_{XX}: \quad \frac{A}{2} (X_x^2 - 1) = 0, \quad (3.29)$$

$$|\Psi|^2 \Psi: \quad \gamma A (|A|^2 - 1) = 0. \quad (3.30)$$

Solving Eq. (3.29) for $X(x, t)$, we get

$$X(x, t) = x + C(t), \quad (3.31)$$

where $C(t)$ is the integration constant.

From Eq. (3.30), one can observe that $A(x, t)$ should take the form of $e^{iG(x, t)}$. Solving Eq. (3.28) for $A(x, t)$, we get

$$A(x, t) = e^{-i \int X_t dx + S(t)}, \quad (3.32)$$

which reads

$$A(x, t) = e^{-i C'(t) x + H(t)}, \quad (3.33)$$

where $S(t)$ and $H(t)$ are the integration constants and the prime denotes differentiation with respect to t . Employing this result in Eq. (3.27), we find

$$x C''(t) + i H'(t) - c x - \frac{1}{2} C'(t)^2 = 0, \quad (3.34)$$

which implies the following two relations

$$x C''(t) = c x, \quad (3.35)$$

and

$$i H'(t) = \frac{1}{2} C'(t)^2. \quad (3.36)$$

These relations, (3.35) and (3.36), deduce

$$C(t) = \frac{c t^2}{2} + \lambda_1, \quad (3.37)$$

and

$$H(t) = \frac{-i c^2 t^3}{6} + \lambda_2, \quad (3.38)$$

where λ_1 and λ_2 are the integration constants. Once these results are achieved, one can construct the wave function, $A(x, t)$, and the transformed coordinate, $X(x, t)$, as the following

$$A(x, t) = e^{-i c t - \frac{i c^2 t^3}{6} + \lambda_3}, \quad (3.39)$$

and

$$X(x, t) = x + \frac{c t^2}{2} + \lambda_1, \quad (3.40)$$

where λ_3 is the combined integration constant. Finally, forming $\Phi(x, t)$ reads

$$\Phi(x, t) = e^{-i c t - \frac{i c^2 t^3}{6} + \lambda_3} \Psi\left(x + \frac{c t^2}{2} + \lambda_1, t\right). \quad (3.41)$$

3.3 Lax Pair (LP) and Darboux Transformation (DT) Method

In this section we analyze the NLSEs using the Lax Pair (LP) and Darboux Transformation (DT) technique. In principle, Darboux Transformation method is only useful for linear systems and can not be directly applied for nonlinear systems. A crucial additional step to Darboux Transformation method is required to make it applicable for nonlinear systems as well. It is to search for an appropriate pair that associates the nonlinear equation to a linear system. This pair was introduced firstly in 1968 by P. D. Lax [59], and accordingly named Lax Pair. The Lax Pair should be associated with the nonlinear model through what is called a compatibility condition. The next step is to solve the obtained linear system using a seed solution, which is a known exact solution of the nonlinear system. This technique gives the applicability to perform new exact solutions which is a remarkable merit. Each seed solution performs another exact solution that belongs to the family of the seed solution. The latter obtained solution could be used as a new seed solution for the next performance round. Notice that all achieved solutions will be under the same family of the initial seed solution. This technique was first employed in 1972 on the NLSE by V. E. Zakharov and A. B. Shabat [2] and then rolled up through many works, some are listed in [60–64].

Here, we present this technique through two equations, the fundamental NLSE and the NLSE with linear potential.

3.3.1 LP and DT Method to the Fundamental NLSE

To illustrate the LP and DT technique, we start with the fundamental NLSE written as

$$i u_t + \frac{1}{2} u_{xx} + |u|^2 u = 0, \quad (3.42)$$

Using the search method proposed in [65], the Lax Pair of Eq. (3.42) is defined as

$$\Phi_x = U_0 \Phi + U_1 \Phi \Lambda, \quad (3.43)$$

$$\Phi_t = V_0 \Phi + V_1 \Phi \Lambda + V_2 \Phi \Lambda^2, \quad (3.44)$$

where U and V , the two objects forming the Lax Pair, are defined as

$$U_0 = \begin{bmatrix} 0 & u \\ -u^* & 0 \end{bmatrix}, \quad V_0 = \frac{i}{2} \begin{bmatrix} |u|^2 & u_x \\ u_x^* & -|u|^2 \end{bmatrix}, \quad (3.45)$$

$$U_1 = \begin{bmatrix} 1 & 0 \\ 0 & -1 \end{bmatrix}, \quad V_1 = i U_0, \quad V_2 = i U_1, \quad (3.46)$$

$$\Lambda = \begin{bmatrix} \lambda_{1r} + i \lambda_{1i} & 0 \\ 0 & \lambda_{2r} + i \lambda_{2i} \end{bmatrix}, \quad (3.47)$$

where u^* is the complex conjugate of $u(x, t)$, U_1 and V_2 are constant matrices, and λ_{1r} , λ_{1i} , λ_{2r} , and λ_{2i} are real constants. The auxiliary field Φ is given by

$$\Phi = \begin{bmatrix} \psi_1(x, t) & \psi_2(x, t) \\ \phi_1(x, t) & \phi_2(x, t) \end{bmatrix}, \quad (3.48)$$

where the symmetry reduction requires

$$\phi_1^* = \psi_2, \quad \phi_2^* = -\psi_1, \quad (3.49)$$

and Φ_x and Φ_t are the derivatives of Φ with respect to x and t . The compatibility condition reads

$$\Phi_{xt} = \Phi_{tx}. \quad (3.50)$$

Substituting Eqs. (3.43) and (3.44) in (3.50), another representation of the compatibility condition can be given as a set of the following equations

$$U_{0t} - V_{0x} + [U_0, V_0] = 0, \quad (3.51)$$

$$U_{1t} - V_{1x} + [U_0, V_1] + [U_1, V_0] = 0, \quad (3.52)$$

$$V_{2x} + [V_1, U_1] + [V_2, U_0] = 0, \quad (3.53)$$

$$[U_1, V_2] = 0, \quad (3.54)$$

where U_{nt} is the derivative of U_n with respect to t , V_{mx} is the derivative of V_m with respect to x , and $[U_n, V_m]$ is the commutator between U_n and V_m , where $n = 0, 1$ and $m = 0, 1, 2$.

Soliton Solution of the Fundamental NLSE

For the sake of illustration, we solve the linear system given by Eqs. (3.43) and (3.44) with zero seed solution

$$u_0(x, t) = 0. \quad (3.55)$$

The corresponding Lax Pair terms of this seed solution will read

$$U_0 = V_0 = V_1 = \begin{bmatrix} 0 & 0 \\ 0 & 0 \end{bmatrix}, \quad (3.56)$$

while U_1 , V_2 , and Λ are independent of the seed solution. From Eqs. (3.43) and (3.44) we have

$$\Phi_x = \begin{bmatrix} (i \lambda_{1i} + \lambda_{1r}) \psi_1 & (i \lambda_{2i} + \lambda_{2r}) \psi_2 \\ -(i \lambda_{1i} + \lambda_{1r}) \phi_1 & -(i \lambda_{2i} + \lambda_{2r}) \phi_2 \end{bmatrix}, \quad (3.57)$$

and

$$\Phi_t = \begin{bmatrix} i (i \lambda_{1i} + \lambda_{1r})^2 \psi_1 & i (i \lambda_{2i} + \lambda_{2r})^2 \psi_2 \\ -i (i \lambda_{1i} + \lambda_{1r})^2 \phi_1 & -i (i \lambda_{2i} + \lambda_{2r})^2 \phi_2 \end{bmatrix}. \quad (3.58)$$

Matching these two matrices with the derivatives of (3.48), we get the following eight linear equations

$$\psi_{1x} = (i \lambda_{1i} + \lambda_{1r}) \psi_1, \quad (3.59)$$

$$\psi_{2x} = (i \lambda_{2i} + \lambda_{2r}) \psi_2, \quad (3.60)$$

$$\phi_{1x} = -(i \lambda_{1i} + \lambda_{1r}) \phi_1, \quad (3.61)$$

$$\phi_{2x} = -(i \lambda_{2i} + \lambda_{2r}) \phi_2, \quad (3.62)$$

$$\psi_{1t} = i (i \lambda_{1i} + \lambda_{1r})^2 \psi_1, \quad (3.63)$$

$$\psi_{2t} = i (i \lambda_{2i} + \lambda_{2r})^2 \psi_2, \quad (3.64)$$

$$\phi_{1t} = -i (i \lambda_{1i} + \lambda_{1r})^2 \phi_1, \quad (3.65)$$

$$\phi_{2t} = -i (i \lambda_{2i} + \lambda_{2r})^2 \phi_2. \quad (3.66)$$

Solving the above eight equations leads to

$$\psi_1(x, t) = C_1 e^{i(\lambda_{1i} - i \lambda_{1r})x} e^{-i(\lambda_{1i}^2 - 2i \lambda_{1i} \lambda_{1r} - \lambda_{1r}^2)t}, \quad (3.67)$$

$$\psi_2(x,t) = C_2 e^{i(\lambda_{2i}-i\lambda_{2r})x} e^{-i(\lambda_{2i}^2-2i\lambda_{2i}\lambda_{2r}-\lambda_{2r}^2)t}, \quad (3.68)$$

$$\phi_1(x,t) = C_3 e^{-i(\lambda_{1i}-i\lambda_{1r})x} e^{(i\lambda_{1i}^2+2i\lambda_{1i}\lambda_{1r}-i\lambda_{1r}^2)t}, \quad (3.69)$$

$$\phi_2(x,t) = C_4 e^{-i(\lambda_{2i}-i\lambda_{2r})x} e^{(i\lambda_{2i}^2+2i\lambda_{2i}\lambda_{2r}-i\lambda_{2r}^2)t}, \quad (3.70)$$

where $C_1, C_2, C_3,$ and C_4 are real constants. From Eqs. (3.67)-(3.70), one can construct the seed of the auxiliary field, Φ_0 .

Considering the definition of Darboux Transformation in [66]

$$\Phi[1] = \Phi \Lambda - \sigma \Phi, \quad (3.71)$$

$$U_0[1] = U_0 + [U_1, \sigma], \quad (3.72)$$

where $\Phi[1]$ is the transformed field and $[U_1, \sigma]$ is the commutator between U_1 and σ , with σ is given by

$$\sigma = \Phi_0 \Lambda \Phi_0^{-1}. \quad (3.73)$$

Constructing the four elements of $U_0[1]$ matrix

$$U_0[1] = \begin{bmatrix} U_0[1]_{(11)} & U_0[1]_{(12)} \\ U_0[1]_{(21)} & U_0[1]_{(22)} \end{bmatrix}, \quad (3.74)$$

as follows

$$U_0[1]_{(11)} = 0, \quad (3.75)$$

$$U_0[1]_{(12)} = \frac{2C_1C_2(-i\lambda_{1i} - \lambda_{1r} + i\lambda_{2i} + \lambda_{2r})e^{2(i\lambda_{1i}+\lambda_{1r}+i\lambda_{2i}+\lambda_{2r})x}}{C_1C_4e^{2(i\lambda_{1i}+\lambda_{1r})x+2i(\lambda_{2i}-i\lambda_{2r})^2t} - C_2C_3e^{2(i\lambda_{2i}+\lambda_{2r})x+2i(\lambda_{1i}-i\lambda_{1r})^2t}}, \quad (3.76)$$

$$U_0[1]_{(21)} = \frac{2C_3C_4(i\lambda_{1i} + \lambda_{1r} - i\lambda_{2i} - \lambda_{2r})e^{2i(\lambda_{1i}^2-2i\lambda_{1i}\lambda_{1r}-\lambda_{1r}^2+(\lambda_{2i}-i\lambda_{2r})^2)t}}{-C_1C_4e^{2(i\lambda_{1i}+\lambda_{1r})x+2i(\lambda_{2i}-i\lambda_{2r})^2t} + C_2C_3e^{2(i\lambda_{2i}+\lambda_{2r})x+2i(\lambda_{1i}-i\lambda_{1r})^2t}}, \quad (3.77)$$

$$U_0[1]_{(22)} = 0. \quad (3.78)$$

Based on the expression of U_0 matrix in Eq. (3.45), $U_0[1]_{(12)}$ represents u_1 , while $U_0[1]_{(21)}$ represents $-u_1^*$, where u_1 is the achieved new exact solution of Eq. (3.42). Although they do not seem to be the complex conjugate of each other at first sight, yet we found them as complex conjugate of each other after some simplification. From Eqs. (3.76) and (3.77), we can write the relation between the four parameters C_1 , C_2 , C_3 , and C_4 as

$$C_1 = \frac{-C_3 C_4}{C_2}. \quad (3.79)$$

Next, let us reform the solution in Eq. (3.76) to the more applicable form of the soliton solution. We set an assumption that describes the relation between λ_{1r} and λ_{2r} as

$$\lambda_{1r} = -\lambda_{2r}. \quad (3.80)$$

Applying Eqs. (3.79) and (3.80) in Eq. (3.76), the solution reads

$$u_1(x, t) = \frac{2(-i\lambda_{1i} + i\lambda_{2i} + 2\lambda_{2r})}{\frac{C_2}{C_4} e^{E_1} + \frac{C_4}{C_2} e^{E_2}}, \quad (3.81)$$

where

$$E_1 = -2i\lambda_{1i}x + 2i\lambda_{1i}^2t + 2\lambda_{2r}x - 4\lambda_{1i}\lambda_{2r}t - 2i\lambda_{2r}^2t, \quad (3.82)$$

and

$$E_2 = -2i\lambda_{2i}x + 2i\lambda_{2i}^2t - 2\lambda_{2r}x + 4\lambda_{2i}\lambda_{2r}t - 2i\lambda_{2r}^2t. \quad (3.83)$$

Renaming $C_4/C_2 \rightarrow \gamma$

$$u_1(x, t) = \frac{2(-i\lambda_{1i} + i\lambda_{2i} + 2\lambda_{2r})}{e^{E_3} + e^{E_4}}, \quad (3.84)$$

where

$$E_3 = E_1 - \ln\gamma, \quad (3.85)$$

and

$$E_4 = E_2 + \ln\gamma. \quad (3.86)$$

The solitonic solution is achieved when the following condition is satisfied

$$\lambda_{1i} = \lambda_{2i}, \quad (3.87)$$

and thus, the solution in Eq. (3.84) becomes

$$u_1(x, t) = \frac{4\lambda_{2r}}{e^{E_3} + e^{E_4}}. \quad (3.88)$$

Taking $e^{-2i\lambda_{2i}x + 2i\lambda_{2i}^2t - 2i\lambda_{2r}^2t}$ as a common factor, the solution reads

$$u_1(x, t) = \frac{4\lambda_{2r} e^{2i\lambda_{2i}x - 2i\lambda_{2i}^2t + 2i\lambda_{2r}^2t}}{e^{2\lambda_{2r}x - 4\lambda_{2i}\lambda_{2r}t - \ln\gamma} + e^{-2\lambda_{2r}x + 4\lambda_{2i}\lambda_{2r}t + \ln\gamma}}, \quad (3.89)$$

or

$$u_1(x, t) = 2\lambda_{2r} e^{2i\lambda_{2i}x - 2i\lambda_{2i}^2t + 2i\lambda_{2r}^2t} \operatorname{sech} \left[2\lambda_{2r} \left(x - 2\lambda_{2i}t - \frac{\ln\gamma}{2\lambda_{2r}} \right) \right]. \quad (3.90)$$

From the last expression, we can clearly see that $2 \lambda_{2i}$ plays the role of the pulse speed. To get the more applicable form of the solitonic solution, we do the final renaming step, where we rename $2 \lambda_{2r} \rightarrow A$, $\ln \gamma / 2 \lambda_{2r} \rightarrow x_0$, and $2 \lambda_{2i} \rightarrow -v$

$$u_1(x, t) = A e^{-i v x - \frac{i v^2}{2} t + \frac{i A^2}{2} t} \operatorname{sech} \left[A (x - x_0 + v t) \right]. \quad (3.91)$$

Finally, the solution becomes

$$u_1(x, t) = A e^{i \Phi_1(x, t)} \operatorname{sech} \left[A (x - x_0 + v t) \right], \quad (3.92)$$

where A is the height of the soliton, $1/A$ represents its width, and the phase of the soliton is given by

$$\Phi_1(x, t) = \left(-v x + \left(\frac{A^2}{2} - \frac{v^2}{2} \right) t \right). \quad (3.93)$$

Figures 3.1 and 3.2 show the two cases of the soliton solution, the movable and non-movable solitonic solutions.

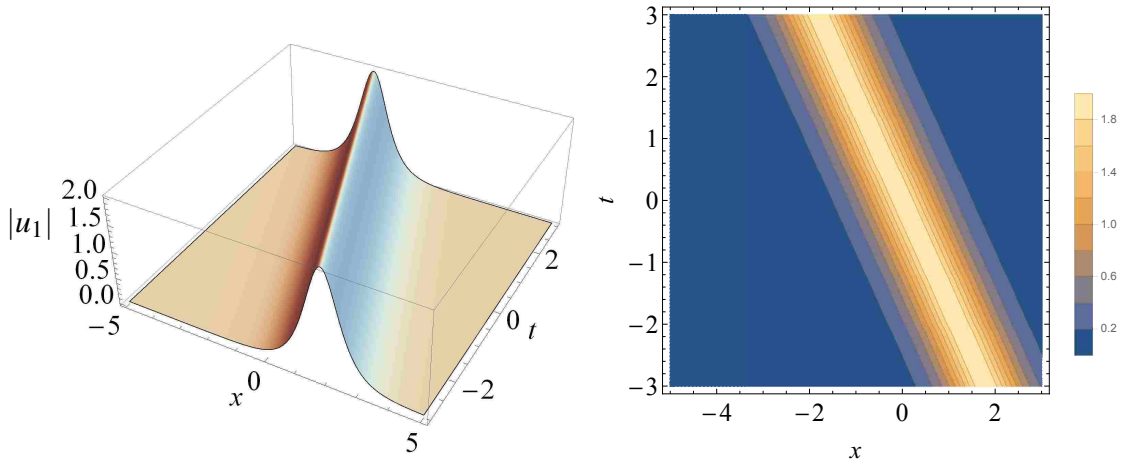


Figure 3.1: Movable solitonic solution of the fundamental NLSE, $A = 2$, $x_0 = 0$, and $v = 0.6$. Evolution of the movable soliton (left). Contour plot of the solution (right).

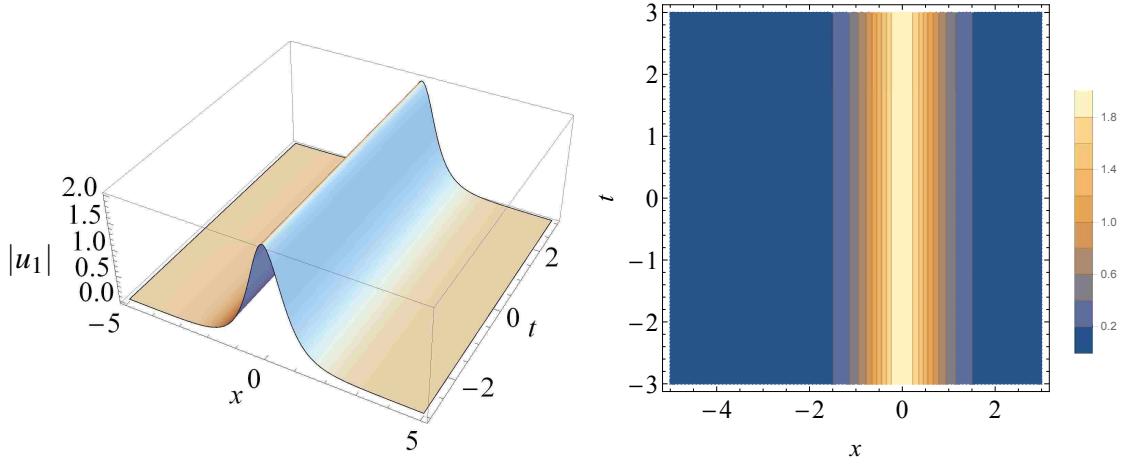


Figure 3.2: Non-movable solitonic solution of the fundamental NLSE, $A = 2$, $x_0 = 0$, and $\nu = 0$. Evolution of the non-movable soliton (left). Contour plot of the solution (right).

Peregrine Soliton of the Fundamental NLSE

The next interesting solution of this nonlinear model is the rogue wave. This type of solution is localized in both space and time. Many studies succeeded to derive the Peregrine soliton and higher order rogue waves from different versions of the NLSE using the LP and DT method [67–74]. It has been shown that, to derive such solution, a periodic seed solution is required to construct a successful DT of the LP [67, 68]. For Eq. (3.42), we use the same Lax Pair in the previous section with a real constant Λ matrix is given by

$$\Lambda = \begin{bmatrix} \lambda_1 & 0 \\ 0 & \lambda_2 \end{bmatrix}. \quad (3.94)$$

From the derivatives of the auxiliary field with respect to x and t , we get the following eight equations

$$-u_0 \phi_1 - \lambda_1 \psi_1 + \psi_{1x} = 0, \quad (3.95)$$

$$-u_0 \phi_2 - \lambda_2 \psi_2 + \psi_{2x} = 0, \quad (3.96)$$

$$\lambda_1 \phi_1 + u_0^* \psi_1 + \phi_{1x} = 0, \quad (3.97)$$

$$\lambda_2 \phi_2 + u_0^* \psi_2 + \phi_{2x} = 0, \quad (3.98)$$

$$-i \lambda_1^2 \psi_1 - u_0 (i \lambda_1 \phi_1 + \frac{i}{2} u_0^* \psi_1) + \psi_{1t} - \frac{i}{2} \phi_1 u_{0x} = 0, \quad (3.99)$$

$$-i \lambda_2^2 \psi_2 - u_0 (i \lambda_2 \phi_2 + \frac{i}{2} u_0^* \psi_2) + \psi_{2t} - \frac{i}{2} \phi_2 u_{0x} = 0, \quad (3.100)$$

$$i \lambda_1^2 \phi_1 + \frac{i}{2} u_0 u_0^* \phi_1 + i \lambda_1 u_0^* \psi_1 + \phi_{1t} - \frac{i}{2} \psi_1 u_{0x}^* = 0, \quad (3.101)$$

$$i \lambda_2^2 \phi_2 + \frac{i}{2} u_0 u_0^* \phi_2 + i \lambda_2 u_0^* \psi_2 + \phi_{2t} - \frac{i}{2} \psi_2 u_{0x}^* = 0. \quad (3.102)$$

Next, we find two functions of the auxiliary field, ψ_1 and ϕ_1 , then we use the two relations in Eq. (3.49) to find the other two functions, ψ_2 and ϕ_2 . From Eq. (3.95), we get the expression of ϕ_1 as

$$\phi_1 = \frac{-\lambda_1 \psi_1 + \psi_{1x}}{u_0}, \quad (3.103)$$

and plug it in Eq. (3.97) to get

$$\lambda_1 \left(\frac{-\lambda_1 \psi_1 + \psi_{1x}}{u_0} \right) + u_0^* \psi_1 + \frac{(-\lambda_1 \psi_{1x} + \psi_{1xx})u_0 - u_{0x}(-\lambda_1 \psi_1 + \psi_{1x})}{u_0^2} = 0. \quad (3.104)$$

Employing the periodic seed solution given by

$$u_0 = e^{it}, \quad (3.105)$$

with $\lambda_1 = 1$, and solving Eq. (3.104) for ψ_1 , we get

$$\psi_1 = C_1(t) + x C_2(t). \quad (3.106)$$

In order to find the two functions, $C_1(t)$ and $C_2(t)$, firstly, we use the expression of ϕ_1 , Eq. (3.103), and then we substitute the expression of ψ_1 , (3.106), in Eqs. (3.99) and (3.101). The following two equations are obtained

$$\frac{-i}{2} \left(C_1(t) + (2+x) C_2(t) + 2i \left(\frac{dC_1(t)}{dt} + x \frac{dC_2(t)}{dt} \right) \right) = 0, \quad (3.107)$$

and

$$\frac{i}{2} e^{-it} \left(C_1(t) + (1+x) C_2(t) + 2i \left(\frac{dC_1(t)}{dt} + (x-1) \frac{dC_2(t)}{dt} \right) \right) = 0. \quad (3.108)$$

Consequently, the two equations for $C_1(t)$ will read

$$C_1(t) = -(2+x) C_2(t) - 2i \left(\frac{dC_1(t)}{dt} + x \frac{dC_2(t)}{dt} \right), \quad (3.109)$$

and

$$C_1(t) = -(1+x) C_2(t) - 2i \left(\frac{dC_1(t)}{dt} + (x-1) \frac{dC_2(t)}{dt} \right). \quad (3.110)$$

Equating the above two expressions of $C_1(t)$, we end up with one equation for $C_2(t)$ as

$$-2i \frac{dC_2(t)}{dt} - C_2(t) = 0, \quad (3.111)$$

which leads to

$$C_2(t) = C_3 e^{\frac{it}{2}}, \quad (3.112)$$

where C_3 is the integration constant. Employing the expression of $C_2(t)$ in Eq. (3.109) or Eq. (3.110), and solving for $C_1(t)$

$$C_1(t) = it C_3 e^{\frac{it}{2}} + C_4 e^{\frac{it}{2}}, \quad (3.113)$$

where C_4 is the integration constant. Now, we can construct the four functions of the seed auxiliary field, ψ_1 and ϕ_1 by using $C_2(t)$ and $C_1(t)$ in Eqs. (3.112) and (3.113), respectively, and ψ_2 and ϕ_2 by applying the relations in Eq. (3.49), as follows

$$\psi_1 = e^{\frac{it}{2}} (C_4 + C_3 (it + x)), \quad (3.114)$$

$$\psi_2 = e^{\frac{it}{2}} (C_3 - C_4 + i C_3 t - C_3 x), \quad (3.115)$$

$$\phi_1 = e^{-\frac{it}{2}} (C_3 - C_4 - i C_3 t - C_3 x), \quad (3.116)$$

$$\phi_2 = -e^{-\frac{it}{2}} (C_4 + C_3 (x - it)), \quad (3.117)$$

where the seed of the auxiliary field is formed from the above expressions. Applying the DT in Eq. (3.72), $U_0[1]$ will read

$$U_0[1] = \begin{bmatrix} 0 & u_0 + \frac{2(\lambda_1 - \lambda_2) \psi_1 \psi_2}{-\phi_2 \psi_1 + \phi_1 \psi_2} \\ -u_0^* + \frac{2(\lambda_1 - \lambda_2) \phi_1 \phi_2}{-\phi_2 \psi_1 + \phi_1 \psi_2} & 0 \end{bmatrix}, \quad (3.118)$$

and hence

$$U_0[1]_{(11)} = 0, \quad (3.119)$$

$$U_0[1]_{(12)} = -\frac{e^{it} [2C_4^2 + 2C_3(C_4 + 2C_4x) + C_3^2(-1 - 4it + 2t^2 + 2x + 2x^2)]}{2C_4^2 + 2C_3(C_4 + 2C_4x) + C_3^2(1 + 2t^2 + 2x + 2x^2)}, \quad (3.120)$$

$$U_0[1]_{(21)} = \frac{e^{-it} [2C_4^2 + 2C_3(C_4 + 2C_4x) + C_3^2(-1 + 4it + 2t^2 + 2x + 2x^2)]}{2C_4^2 + 2C_3(C_4 + 2C_4x) + C_3^2(1 + 2t^2 + 2x + 2x^2)}, \quad (3.121)$$

$$U_0[1]_{(12)} = 0, \quad (3.122)$$

where we used $\lambda_1 = -\lambda_2$. Since $U_0[1]$ should have the same form as U_0 in Eq. (3.45), it represents the desired Peregrine solution of Eq. (3.42), $U_0[1]_{(12)} = u_1$ and $U_0[1]_{(21)} = -u_1^*$, given by

$$u_1(x,t) = -e^{it} \frac{[2C_4^2 + 2C_3(C_4 + 2C_4x) + C_3^2(-1 - 4it + 2t^2 + 2x + 2x^2)]}{2C_4^2 + 2C_3(C_4 + 2C_4x) + C_3^2(1 + 2t^2 + 2x + 2x^2)}, \quad (3.123)$$

see Figure (3.3).

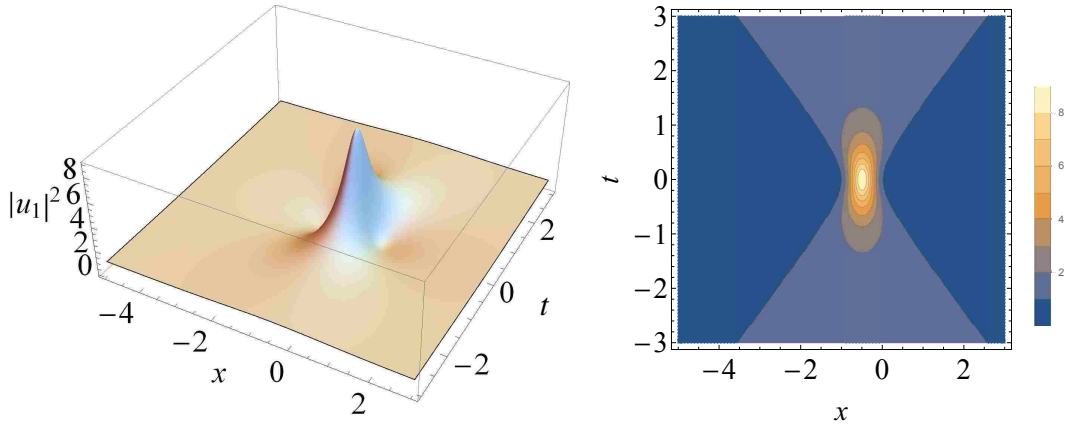


Figure 3.3: First order Rogue wave solution of the fundamental NLSE, $C_3 = C_4 = 1$. Evolution of the Peregrine soliton (left). Contour plot of the solution (right).

The spatial and temporal profiles of the Peregrine solution are shown in Figure 3.4. As one can observe, the peak of the envelope is located around $(x, t) = (-1.5, 0)$. This can be understood by the solution in (3.123).

3.3.2 LP and DT Method to NLSE with Linear Potential

The NLSE with linear potential or, the Gross-Pitaevskii equation is not less important than the fundamental one. This equation describes many nonlinear physical

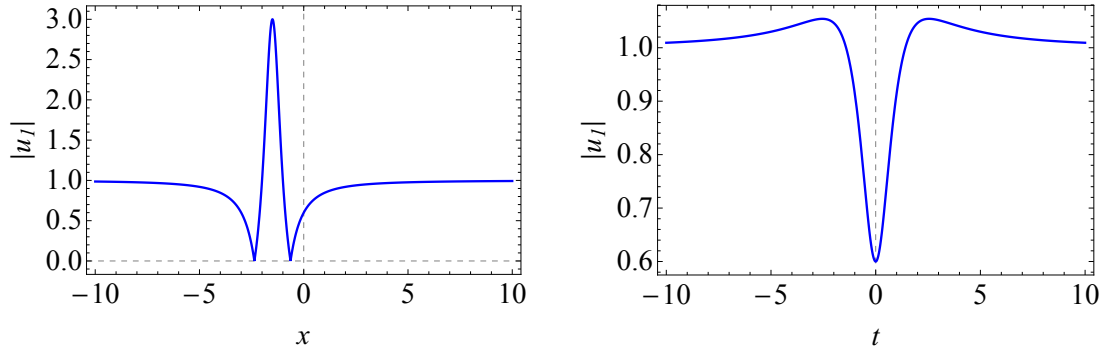


Figure 3.4: First order Rogue wave solution of the fundamental NLSE, $C_3 = C_4 = 1$. Spatial (left) and temporal (right) profiles of the Peregrine soliton.

systems. The interaction between atoms with a mean field potential and the BEC in the low temperature regime are two examples of its applications. This equation is given by

$$i u_t + u_{xx} - \beta^3 x u + \alpha^2 |u|^2 u = 0, \quad (3.124)$$

where β^3 and α^2 indicate the strength of potential force and the Kerr effect, respectively. Using the searching method in [65], the Lax Pair terms of Eq. (3.124) are defined as

$$U_0 = \begin{bmatrix} \frac{i\beta^2 t}{2} & \frac{\alpha u^*}{\sqrt{2}\beta} \\ -\frac{\alpha u}{\sqrt{2}\beta} & -\frac{i\beta^2 t}{2} \end{bmatrix}, \quad (3.125)$$

$$V_0 = -i \begin{bmatrix} \left(-\frac{\beta^4 t^2}{2} - \frac{\beta x}{2} + \frac{\alpha^2 u^* u}{2\beta^2}\right) & \left(\frac{i\alpha\beta^2 t u^*}{\sqrt{2}\beta} + \frac{\alpha u_x^*}{\sqrt{2}\beta^2}\right) \\ \left(\frac{-i\alpha\beta^2 t u}{\sqrt{2}\beta} + \frac{\alpha u_x}{\sqrt{2}\beta^2}\right) & \left(\frac{\beta^4 t^2}{2} + \frac{\beta x}{2} - \frac{\alpha^2 u^* u}{2\beta^2}\right) \end{bmatrix}, \quad (3.126)$$

$$U_1 = \begin{bmatrix} 1 & 0 \\ 0 & -1 \end{bmatrix}, \quad V_1 = \begin{bmatrix} 2\beta^2 t & -i\sqrt{2}\frac{\alpha}{\beta} u^* \\ i\sqrt{2}\frac{\alpha}{\beta} u^* & -2\beta^2 t \end{bmatrix}, \quad (3.127)$$

$$V_2 = i \begin{bmatrix} 2 & 0 \\ 0 & -2 \end{bmatrix}, \quad (3.128)$$

with a real constant Λ matrix is given by

$$\Lambda = \begin{bmatrix} \lambda_1 & 0 \\ 0 & \lambda_2 \end{bmatrix}. \quad (3.129)$$

Solitonic Solution with Linear Potential

For the sake of solitonic behaviour, we consider the seed solution to be zero.

Thus, the terms of the Lax Pair read

$$U_0 = \begin{bmatrix} \frac{i\beta^2 t}{2} & 0 \\ 0 & -\frac{i\beta^2 t}{2} \end{bmatrix}, \quad (3.130)$$

$$V_0 = -i \begin{bmatrix} (-\frac{\beta^4 t^2}{2} - \frac{\beta x}{2}) & 0 \\ 0 & (\frac{\beta^4 t^2}{2} + \frac{\beta x}{2}) \end{bmatrix}, \quad (3.131)$$

$$V_1 = \begin{bmatrix} 2\beta^2 t & 0 \\ 0 & -2\beta^2 t \end{bmatrix}, \quad (3.132)$$

where U_1 , V_2 , and Λ are independent of the seed solution. From the derivatives of the auxiliary field with respect to x and t , we get the following eight equations

$$\psi_{1x} = \frac{1}{2} \beta (i\beta^2 t + 2\lambda_1) \psi_1, \quad (3.133)$$

$$\psi_{2x} = \frac{1}{2} \beta (i\beta^2 t + 2\lambda_2) \psi_2, \quad (3.134)$$

$$\phi_{1x} = -\frac{1}{2} \beta (i\beta^2 t + 2\lambda_1) \phi_1, \quad (3.135)$$

$$\phi_{2x} = -\frac{1}{2} \beta (i\beta^2 t + 2\lambda_2) \phi_2, \quad (3.136)$$

$$\psi_{1t} = \frac{i}{2} \beta^2 (\beta x + (\beta^2 t - 2i\lambda_1)^2) \psi_1, \quad (3.137)$$

$$\psi_{2t} = \frac{i}{2} \beta^2 (\beta x + (\beta^2 t - 2i\lambda_2)^2) \psi_2, \quad (3.138)$$

$$\phi_{1t} = -\frac{i}{2} \beta^2 (\beta x + (\beta^2 t - 2i\lambda_1)^2) \phi_1, \quad (3.139)$$

$$\phi_{2t} = -\frac{i}{2} \beta^2 (\beta x + (\beta^2 t - 2i\lambda_2)^2) \phi_2. \quad (3.140)$$

Solving the above eight equations yields to

$$\psi_1(x, t) = C_1 [e^{\frac{i}{2} x (\beta^3 t - 2i\beta\lambda_1)} e^{(\frac{i}{6} \beta^6 t^3 + \beta^4 \lambda_1 t^2 - 2i\beta^2 \lambda_1^2 t)}], \quad (3.141)$$

$$\psi_2(x, t) = C_2 [e^{\frac{i}{2} x (\beta^3 t - 2i\beta\lambda_2)} e^{(\frac{i}{6} \beta^6 t^3 + \beta^4 \lambda_2 t^2 - 2i\beta^2 \lambda_2^2 t)}], \quad (3.142)$$

$$\phi_1(x, t) = C_3 [e^{-\frac{i}{2} x (\beta^3 t - 2i\beta\lambda_1)} e^{(-\frac{i}{6} \beta^6 t^3 - \beta^4 \lambda_1 t^2 + 2i\beta^2 \lambda_1^2 t)}], \quad (3.143)$$

$$\phi_2(x, t) = C_4 [e^{-\frac{i}{2} x (\beta^3 t - 2i\beta\lambda_2)} e^{(-\frac{i}{6} \beta^6 t^3 - \beta^4 \lambda_2 t^2 + 2i\beta^2 \lambda_2^2 t)}], \quad (3.144)$$

where $C_1, C_2, C_3,$ and C_4 are real parameters. From Eqs. (3.141)-(3.144), one can construct the seed of the auxiliary field. Using the definition of Darboux Transformation, we find the four elements of $U_0[1]$ matrix as follows

$$U_0[1]_{(11)} = \frac{i}{2} \beta^2 t, \quad (3.145)$$

$$U_0[1]_{(12)} = \frac{2(\lambda_1 - \lambda_2) C_1 C_2 e^{i\beta^3 x t + \frac{i}{3} \beta^6 t^3 + (2\beta x + 2\beta^4 t^2)(\lambda_1 + \lambda_2)}}{C_2 C_3 e^{2\beta(2i\beta\lambda_1^2 t + \lambda_2 x + \beta^3 \lambda_2 t^2)} - C_1 C_4 e^{2\beta(\lambda_1 x + \beta(\beta^2 \lambda_1 t + 2i\lambda_1^2 t))}}, \quad (3.146)$$

$$U_0[1]_{(21)} = \frac{2(\lambda_1 - \lambda_2) C_3 C_4 e^{-\frac{i}{3} \beta^6 t^3}}{-C_1 C_4 e^{\beta(\beta^2 t - 2i\lambda_1)(ix + 2\beta\lambda_1 t)} + C_2 C_3 e^{\beta(\beta^2 t - 2i\lambda_2)(ix + 2\beta\lambda_2 t)}}, \quad (3.147)$$

$$U_0[1]_{(22)} = -\frac{i}{2} \beta^2 t. \quad (3.148)$$

Based on the expression of U_0 matrix in Eq. (3.125), $U_0[1]_{(21)}$ represents $-u_1 \alpha / \sqrt{2} \beta$, while $U_0[1]_{(12)}$ represents $u_1^* \alpha / \sqrt{2} \beta$, where u_1 is the achieved new solution of Eq. (3.124). Thus, the relation between the parameters $C_1, C_2, C_3,$ and C_4 must give the same relation as what is in Eq. (3.79). It is worth mentioning that due to the potential

force, the resulted solitonic solution is movable, even if v does not appear explicitly. Using the relation between the parameters in (3.79) and Eq. (3.147) with $\lambda_1 = -\lambda_2$, the solution reads

$$u_1(x, t) = \frac{2\sqrt{2}\beta(2\lambda_2)e^{-\frac{i}{3}\beta^6 t^3}}{\alpha\left[\frac{C_4}{C_2}e^{\beta(\beta^2 t + 2i\lambda_2)(ix - 2\beta\lambda_2 t)} + \frac{C_2}{C_4}e^{\beta(\beta^2 t - 2i\lambda_2)(ix + 2\beta\lambda_2 t)}\right]}. \quad (3.149)$$

Expanding all brackets, taking $e^{-4i\beta^2 t \lambda_2^2 + i\beta^3 x t}$ as a common factor from the denominator, and renaming $C_4/C_2 \rightarrow \gamma$

$$u_1(x, t) = \frac{4\sqrt{2}\beta\lambda_2 e^{-\frac{i}{3}\beta^6 t^3 + 4i\beta^2 t \lambda_2^2 - i\beta^3 x t}}{(e^{-2\beta\lambda_2 x - 2\beta^4 \lambda_2 t^2 + \ln\gamma} + e^{2\beta\lambda_2 x + 2\beta^4 \lambda_2 t^2 - \ln\gamma})\alpha}. \quad (3.150)$$

Clearly, this expression gives the sech form as follows

$$u_1(x, t) = 4\sqrt{2}\beta\alpha^{-1}\lambda_2 e^{-\frac{i}{3}\beta^6 t^3 + 4i\beta^2 t \lambda_2^2 - i\beta^3 x t} \operatorname{sech}[-2\beta\lambda_2 x - 2\beta^4 \lambda_2 t^2 + \ln\gamma], \quad (3.151)$$

or

$$u_1(x, t) = 4\sqrt{2}\beta\alpha^{-1}\lambda_2 e^{-\frac{i}{3}\beta^6 t^3 + 4i\beta^2 t \lambda_2^2 - i\beta^3 x t} \operatorname{sech}\left[-2\beta\lambda_2\left(x + 2\beta^3 t^2 - \frac{\ln\gamma}{2\beta\lambda_2}\right)\right]. \quad (3.152)$$

Renaming $2\sqrt{2}\alpha^{-1}\lambda_2\beta \rightarrow A$, $\ln\gamma/2\lambda_2\beta \rightarrow x_0$, $\beta^3 \rightarrow -v$, and $-2\beta\lambda_2 \rightarrow -A\alpha/\sqrt{2}$

$$u_1(x, t) = A e^{-\frac{i}{3}v^2 t^3 + i\frac{A^2\alpha^2}{2}t + i v x t} \operatorname{sech}\left[\frac{-A\alpha}{\sqrt{2}}(x - x_0 - v t^2)\right]. \quad (3.153)$$

Finally, the solution reads

$$u_1(x, t) = A e^{i\Phi_2(x, t)} \operatorname{sech}\left[\frac{-A\alpha}{\sqrt{2}}(x - x_0 - v t^2)\right], \quad (3.154)$$

where A is the height of the soliton, $-\sqrt{2}/A \alpha$ represents its width, and the phase of the soliton is given by

$$\Phi_2(x, t) = \left(\frac{-v^2 t^3}{3} + \left(\frac{A^2 \alpha^2}{2} + v x \right) t \right), \quad (3.155)$$

see Figure (3.5).

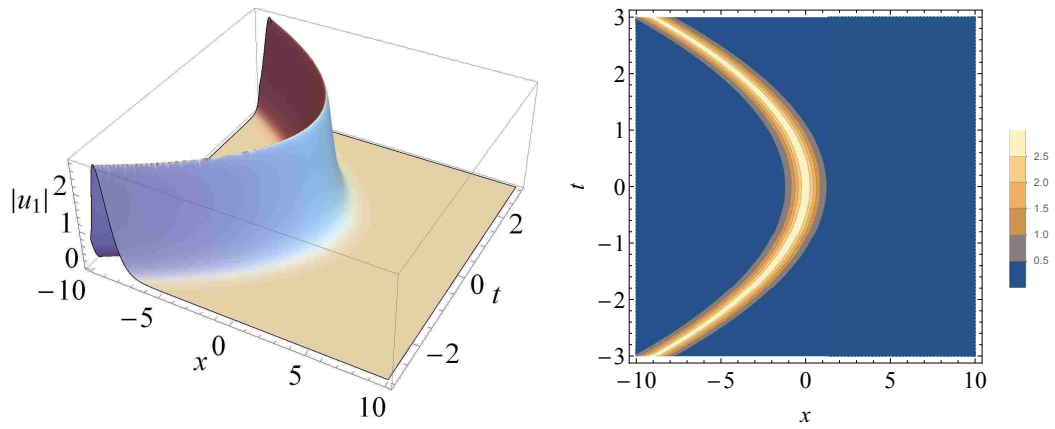


Figure 3.5: Solitonic solution of the fundamental NLSE with linear potential, $x_0 = 1$, $A = 1$, and $\alpha = 1$. Evolution of the soliton (left). Contour plot of the solution (right).

The main difference between the solution in the absence of the external potential, Eq. (3.92), and the solution in the presence of the potential, Eq. (3.154), is that in the absence of potential, the phase of the soliton solution is a linear function of t , while, in the presence of the potential, the phase is a cubic function of t . In addition, the center-of-mass in the case of linear potential is being accelerated, namely $x_{com} = x_0 + v t^2$. This is of course is expected since the linear potential corresponds to a constant force. This situation is similar to the free fall problem under the force of gravity which is constant near the surface of Earth.

Chapter 4: Iterative Power Series (IPS) Method

Often, using power series solutions turns to be useless because the resulting solution diverges at a finite radius of convergence. The divergence is intrinsic to the nature of the solution in the sense that it persists to exist even with an infinite power series expansion. In this chapter, we present a new iterative procedure, the *Iterative power series* (IPS) method, which is based on successive power series expansions providing a high accuracy numerical scheme. This method solves the typical problem of finite radius of convergence showing that the radius of convergence can be extended arbitrarily to any large value. This value could, in principle, approach infinity achieving exact solutions.

Briefly, the present technique is based on iterative power series expansions of the solution. The domain of the independent variable, say x , is divided into a number I of segments each of width Δ , where Δ is smaller than the radius of convergence. A power series solution is obtained by expanding the solution around the left end of the first segment using the initial conditions given with the problem. Similarly, a power series solution is obtained by expanding around the start of the second segment but now using the first series to calculate the initial conditions. This is repeated I times till a solution at $x = I \times \Delta$ is obtained. In the limit $I \rightarrow \infty$ and $\Delta \rightarrow 0$ the series solution becomes an exact solution. This scheme is effectively equivalent to an iterative procedure of repeated iterative calculation of the recursion relations of the power series in the first segment.

4.1 Mathematical Formalism of the IPS Method

In this section, we give a systematic description of the present method. Consider a general ordinary differential equation of the form

$$F \left[f(x), f'(x), f''(x), \dots, f^{(m)}(x), g(x) \right] = 0, \quad x \in (x_0, x_\infty], \quad (4.1)$$

with m initial conditions

$$f^{(i)}(x_0) = a_i \times i!, \quad i = 0, 1, 2, \dots, m-1, \quad (4.2)$$

where $f^{(i)}$ is the i th derivative of $f(x)$, a_i are real constants, and $g(x)$ is a known function. The factor $i!$ is introduced, without loss of generality, for the constants a_i to correspond to the coefficients of the power series expansion below. At first, we divide the interval $[x_0, x]$ into a number of I identical segments each of width $\Delta = (x - x_0)/I$. Then we expand $f(x)$ in a power series around the beginning of each interval, namely

$$f^i(x) = \sum_{n=0}^{n_{max}} a_n^i \left(x - (x_0 + i \Delta) \right)^n, \quad i \Delta \leq x \leq (i+1) \Delta, \quad 0 \leq i < I, \quad (4.3)$$

where $f^i(x)$ is the power series expansion around the start of the i th segment, n_{max} is the number of terms in the power series expansion, and a_n^i are the coefficients of the power series. For additional clarification, in Figure 4.1 we employ the exact solitonic solution of the fundamental NLSE to show the I segments of width Δ , where the dots represent the iterative initial point of each round.

Recursion relations between the coefficients are obtained upon substituting the power series solution, Eq. (4.3), in the differential equation, Eq. (4.1), which can be expressed in terms of the first m coefficients corresponding to the initial conditions

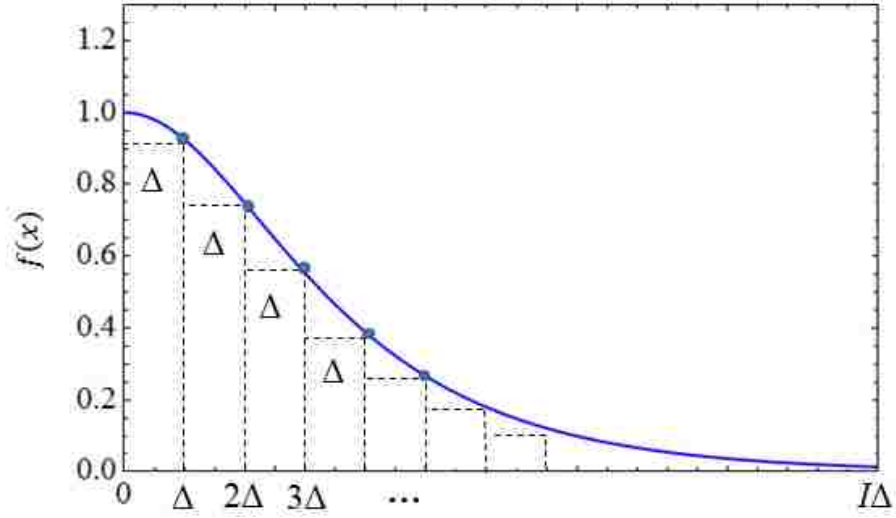


Figure 4.1: I segments of the IPS method. The blue curve corresponds to the solitonic solution of the fundamental NLSE.

$$a_n^i = a_n^i(\{a_k^i\}), \quad 0 \leq k < m, \quad n \geq m, \quad (4.4)$$

where $\{a_k^i\}$ denotes the set of coefficients $a_0^i, a_1^i, \dots, a_{m-1}^i$. The essential idea of the IPS method is to calculate the coefficients $\{a_k^{i+1}\}$ of the $(i+1)$ th power series from the i th series according to Eq. (4.2),

$$a_k^{i+1} = \frac{1}{k!} \left. \frac{d^k}{dx^k} f^i(x) \right|_{x=x_0+(i+1)\Delta}, \quad (4.5)$$

which upon using (4.3) reads

$$a_k^{i+1} = \frac{1}{k!} \sum_{n=0}^{n_{\max}} a_{n+k}^i \times \frac{d^k}{d\Delta^k} \Delta^{n+k}, \quad (4.6)$$

and simplifies to

$$a_k^{i+1} = \sum_{n=0}^{n_{\max}} a_{n+k}^i \times \binom{n+k}{k} \Delta^n, \quad (4.7)$$

and then imposes the condition $n_{max} > k$. Here, $\binom{n+k}{k}$ is the binomial function. The last equation is the basis for the IPS algorithm. Starting from the initial conditions $\{a_k^0\}$ for the power series of the zeroth interval, an iterative application of Eq. (4.7) leads to the coefficients of the I th interval, namely $\{a_k^I\}$ which give the solution at the desired point, $x = x_0 + I\Delta$,

$$f^I(x) = \sum_{n=0}^{n_{max}} a_n^I \times \left(x - (x_0 + I\Delta)\right)^n. \quad (4.8)$$

Both analytical and numerical schemes may be deduced from this algorithm. For the numerical scheme, the value of Δ used is inserted as a number $\Delta = (x_\infty - x_0)/I$. On the other hand, leaving x as a variable, results in an analytical solution in terms of a power series in x which is equivalent to a functional transformation on the zeroth order series, i.e., the coefficients of the i th series are functional transformation of the $(i-1)$ th series. In such a case the last power series for the I th interval corresponds to I such functional transformations and all power series expansions of the zeroth up to $(I-1)$ th intervals will be included in the I th expansion.

The coefficient a_0^i of each i th expansion represents the value of the solution at $x = x_0 + i\Delta$. which gives a discrete representation of $f(x)$. Therefore, in the limit $I \rightarrow \infty$, the discrete representation turns to a continuous one and thus we conjecture that the exact solution is obtained in the limits of $I \rightarrow \infty$ and $n_{max} \rightarrow \infty$

$$f(x) = \lim_{I \rightarrow \infty} \sum_{n=0}^{\infty} a_n^I \times \left(x - (x_0 + I\Delta)\right)^n. \quad (4.9)$$

In summary, the IPS procedure can be reduced to the following algorithm

$$f(\Delta) = a_0 + a_1 \Delta + a_2 \Delta^2 + \dots + a_{n_{max}} \Delta^{n_{max}} + O(\Delta^{n_{max}+1}), \quad (4.10)$$

$$a_0 = f(\Delta), \quad a_1 = f'(\Delta), \quad a_2 = \frac{f''(\Delta)}{2}, \quad \dots \quad a_{m-1} = \frac{f^{(m-1)}(\Delta)}{m-1}, \quad (4.11)$$

where $a_m = a_m(a_0, a_1, a_2, \dots, a_{m-1})$ are the recursion relations obtained from the differential equation. We have removed the superscripts that indicate the index of the iteration for convenience. The scheme is thus described simply as follows: One starts with Eq. (4.10) to calculate $f(\Delta)$, followed by updating the initial conditions according to Eq. (4.11), and then using the updated values back in Eq. (4.10), and so on. The procedure has to be repeated I times with $\Delta = (x - x_0)/I$.

This procedure is general and it is applicable for both, homogeneous and inhomogeneous nonlinear differential equations. However, in the homogeneous case, further reduction takes place, where the recursion relations will be independent of I .

Despite the radius of convergence of the generated power series at each iteration was not examined, we conclude that it will not differ very considerably from the radius of convergence of the initial power series. The following systematic reduction in error supports our intuition.

The upper bound of the error in the IPS method can be estimated as follows. At each iterative step an error of order $\Delta^{n_{max}+1}$ results from terminating the power series at n_{max} . This error will be magnified I times due to the iterative procedure. As a result, the upper bound of the error of the IPS method is

$$E_{IPS} = I (\Delta)^{n_{max}+1}. \quad (4.12)$$

We end this section by Figure 4.2 that illustrates the iterative loop of the IPS method starting with $i = 0$.

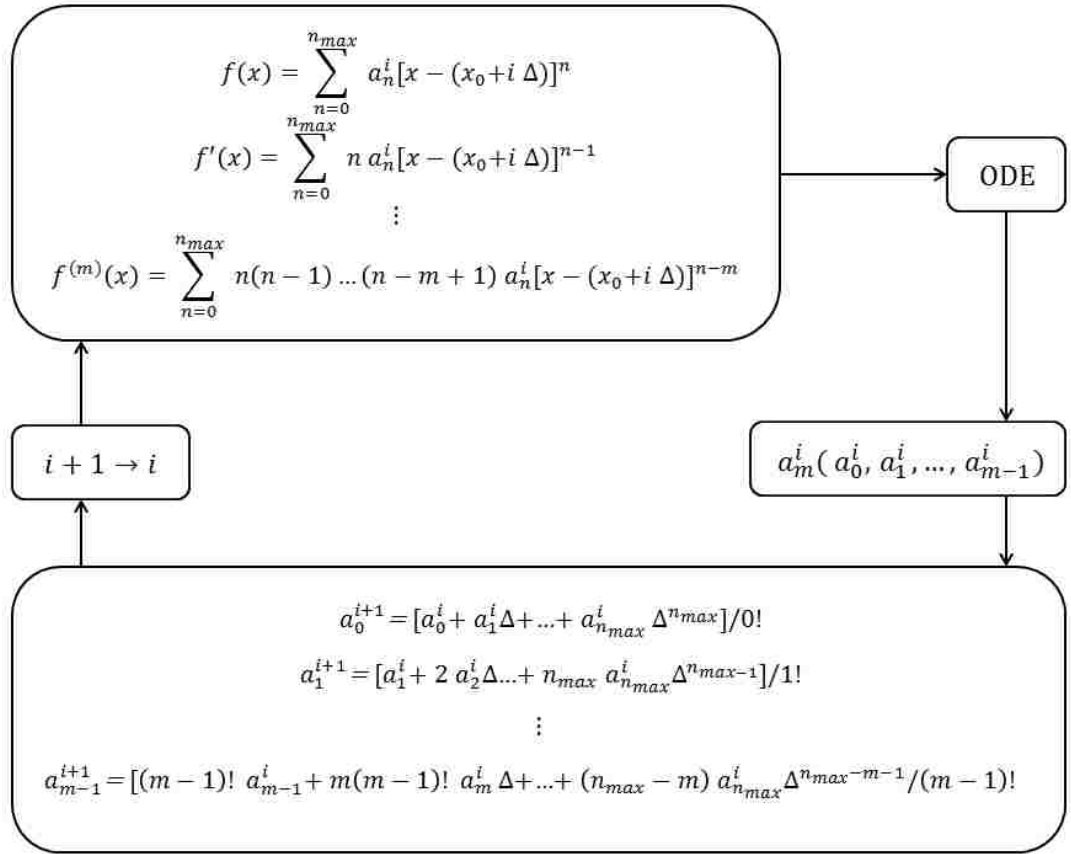


Figure 4.2: Schematic loop of the IPS method.

4.2 Application of IPS Method to NLSEs

Here we are interested in the application of the IPS method to three different versions of the NLSE, the fundamental NLSE, the NLSE with power law nonlinearity, and the higher order NLSE to demonstrate the physical implementations of the technique. Other applications will be dealt with through the next chapters.

4.2.1 IPS Method to the Fundamental NLSE

The fundamental NLSE could be written as

$$\frac{i}{2} u_t + \frac{1}{2} u_{xx} + |u|^2 u = 0, \quad (4.13)$$

where we take $\sigma_1 = +1$ and $\sigma_2 = +2$. Using Eq. (3.2) in Eq. (4.13) yields to the ordinary version

$$\frac{1}{2} Z - \frac{1}{2} Z'' - Z^3 = 0. \quad (4.14)$$

This is a homogeneous second order nonlinear differential equation, where the prime indicates differentiation with respect to x . The well-known fundamental soliton is one of the analytical exact solutions of Eq. (4.14) given by

$$Z(x) = A \operatorname{sech}(A x), \quad (4.15)$$

where A is the amplitude of the envelope. First, we start by expanding the solution, $Z(x)$, in power series around the initial point $x_0 = 0$

$$Z^0(x) = \sum_{n=0}^{n_{max}} a_n^0(x)^n, \quad (4.16)$$

and similarly for the derivatives, $Z^{0'}$ and $Z^{0''}$. Substituting in Eq. (4.14), the coefficients, a_n^0 , for $n \geq 2$, can be found recursively in terms of the initial conditions a_0^0 and a_1^0 through the recursion relations. The first two recursion relations are given by

$$a_2^0 = \frac{1}{2} \left[a_0^0 - 2 (a_0^0)^3 \right], \quad (4.17)$$

$$a_3^0 = \frac{1}{6} [a_1^0 - 6 (a_0^0)^2 a_1^0]. \quad (4.18)$$

Recalculating Z^0 and $Z^{0'}$ at $x = \Delta$ gives

$$a_0^1 = Z^0(\Delta), \quad a_1^1 = Z^{0'}(\Delta). \quad (4.19)$$

Now, a_0^1 and a_1^1 play the role of the initial conditions for the next series expansion, where we expand the solution and its derivatives in power series around $x_0 = \Delta$

$$Z^1(x) = \sum_{n=0}^{n_{max}} a_n^1 (x - \Delta)^n. \quad (4.20)$$

Resubstituting these power series expansions in the differential equation, we get the new recursion relations $a_n^1(a_0^1, a_1^1)$. The next iterative step is to calculate $Z^1(x)$ and its first two derivatives at $t = 2\Delta$ which will give the initial conditions of the new power series. It should be mentioned here that for this equation and the upcoming equations in this chapter, we study homogeneous cases, and hence, repeating this process I times will produce identical recursion relations as in (4.17) and (4.18).

Figure 4.3 shows the stationary soliton solution of Eq. (4.14) at different iterations $I = 10, 30, 50, 70, 90, 110, 130$ together with the exact solution obtained by (4.15) where the amplitude is taken to be $A = 1$. The divergence is delaying with the number of iterations in the IPS solution. Knowing that, using the power series method to solve such equation renders the divergence to appear at $x < \pi/2$.

In Figure 4.4, we show the series solution of Eq. (4.14) at iteration, $I = 1000$, and number of terms in power series expansion, $n_{max} = 8$, where the divergence problem is almost eliminated. The right of the figure shows the difference between the series and the exact solutions. As one can see, a high accuracy of the IPS solution is attained, where the error is in the range of 3×10^{-15} which is acceptable.

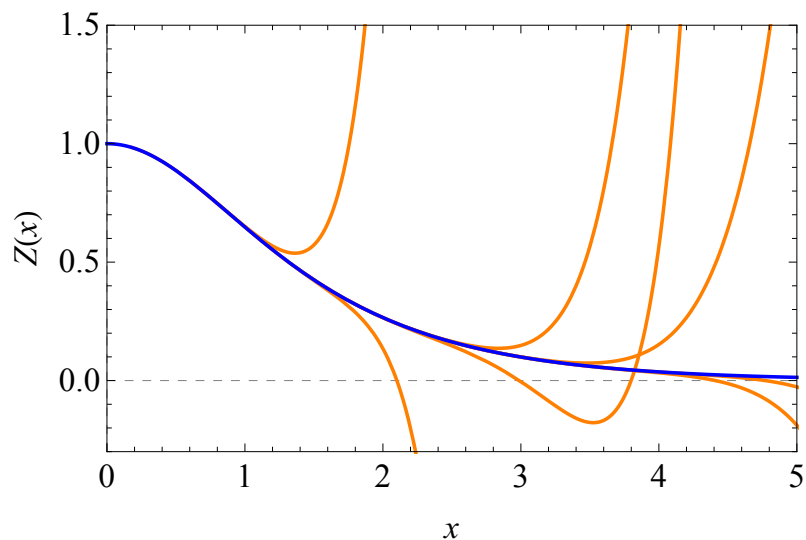


Figure 4.3: Solitonic solution of Eq. (4.14). The blue curve corresponds to the exact solution given by Eq. (4.15) and the diverging orange curves correspond to the IPS method at different iterations, with $\Delta = 0.02$, and $n_{max} = 8$.

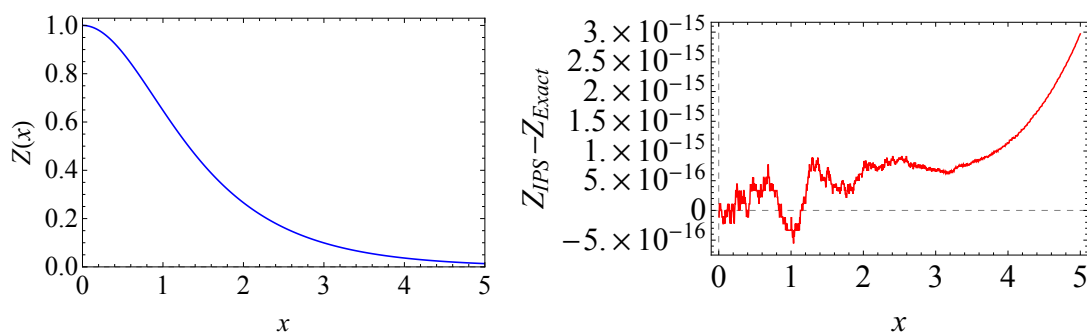


Figure 4.4: Solitonic solution of Eq. (4.14). Left: The IPS solution, with $a_0^0 = 1$, $a_1^0 = 0$, $n_{max} = 8$, $I = 1000$, and $\Delta = 0.005$. Right: The difference between the IPS solution and the exact solution given by (4.15).

4.2.2 Mathematica Code

Here we, respectively, present two codes that are used to generate and progress the recursion relations and the IPS method of Figures 4.3 and 4.4. These codes are compiled using Wolfram Mathematica 10.4.

Code A

```

ClearAll [ "Global '*"]
nmax = 8; nn = 300; Δ = 0.02; a[0] = 1; a[1] = 0;
Z[x_] := Sum [ a[n] (x - 0)^n, { n, 0, nmax } ];
ode = 1/2 Z[x] - Z[x]^3 - 1/2 Z''[x];
ZZ0 = Z[x]; ZZ1 = Z'[x];
Do [ { a[i] = Solve [ SeriesCoefficient [ ode, { x, 0, i - 2 } ] == 0,
a[i] ] [[ 1 ] ] [[ 1 ] ] [[ 2 ] ] }, { i, 2, nmax } ];
plots = Array [ m000, nn ];
Do [ {
a0 = ReplaceAll [ ZZ0, x → ii Δ ];
a1 = ReplaceAll [ ZZ1, x → ii Δ ];
Clear[ a ];
a[0] = a0;
a[1] = a1;
Z[x_] := Sum [ a[n] (x - ii Δ)^n, { n, 0, nmax } ];
ZZ0 = Z[x]; ZZ1 = Z'[x];
Do [ { a[i] = Solve [ SeriesCoefficient [ ode, { x, (ii) Δ, i - 2 } ] == 0,
a[i] ] [[ 1 ] ] [[ 1 ] ] [[ 2 ] ] }, { i, 2, nmax } ];
plots [ [ ii ] ] = Plot [ ZZ0, { x, (ii - 1) Δ, 5 } ];
plotexact = Plot [ Sech[ x ], { x, 0, 5 } ];
}, { ii, 1, nn } ]
Show [ plots[ [ nn ] ], plotexact ]

```

Code B

```

ClearAll [ "Global '*"]
nmax = 8; a[0] = a0; a[1] = a1;
Z[x_] := Sum [ a[n] (x - 0)^n, { n, 0, nmax } ];
ode =  $\frac{1}{2} Z[x] - Z[x]^3 - \frac{1}{2} Z''[x]$ ;
Do [ { a[i] = Simplify [ a[i] /. Solve [ SeriesCoefficient [ ode, { x, 0, i - 2 } ] ==
0, a[i] ] ] [ [ 1 ] ] ]; Print [ a[i] ] }, { i, 2, nmax } ];
a0 = 1; a1 = 0; x0 = 0; xf = 5; nn = 1000;  $\Delta = \frac{xf-x0}{nn}$ ;
matrix1 = Array [ m000, {nn, 2} ];
matrix2 = Array [ m000, {nn, 2} ];
Do [ {
a2 =  $\frac{1}{2} (a0 - 2 a0^3)$ ;
a3 =  $\frac{1}{6} (a1 - 6 a0^2 a1)$ ;
a4 =  $\frac{1}{24} a0 (1 - 8 a0^2 + 12 a0^4 - 12 a1^2)$ ;
a5 =  $\frac{-1}{120} a1 (-1 + 48 a0^2 - 108 a0^4 + 12 a1^2)$ ;
a6 =  $\frac{1}{720} (a0 - 50 a0^3 + 204 a0^5 - 216 a0^7 - 132 a0 a1^2 + 504 a0^3 a1^2)$ ;
a7 =  $\frac{1}{5040} (a1 - 414 a0^2 a1 + 2556 a0^4 a1 - 3528 a0^6 a1 - 132 a1^3 + 1512 a0^2 a1^3)$ ;
a8 =  $\frac{1}{40320} a0 (1 - 416 a0^2 + 3384 a0^4 - 8640 a0^6 + 7056 a0^8 - 1224 a1^2 + 15552 a0^2 a1^2 -$ 
30240 a0^4 a1^2 + 3024 a1^4);
a0 = a0 + a1  $\Delta$  + a2  $\Delta^2$  + a3  $\Delta^3$  + a4  $\Delta^4$  + a5  $\Delta^5$  + a6  $\Delta^6$  + a7  $\Delta^7$  + a8  $\Delta^8$ ;
a1 = a1 + 2 a2  $\Delta$  + 3 a3  $\Delta^2$  + 4 a4  $\Delta^3$  + 5 a5  $\Delta^4$  + 6 a6  $\Delta^5$  + 7 a7  $\Delta^6$  + 8 a8  $\Delta^7$ ;
matrix1[ [ ii, 1 ] ] = (ii) $\Delta$ ;
matrix1[ [ ii, 2 ] ] = a0;
matrix2[ [ ii, 1 ] ] = (ii) $\Delta$ ;
matrix2[ [ ii, 2 ] ] = a0 - Sech [ (ii) $\Delta$  ];
}, {ii, 1, nn} ]
solitonIPS = ListLinePlot [ matrix1 ]
solitonDiff = ListLinePlot [ matrix2 ]

```

4.2.3 IPS Method to NLSE with Power Law Nonlinearity

Now, let us employ the IPS method on the NLSE with power law nonlinearity

$$\frac{1}{2} Z - \frac{1}{2} Z'' - Z^5 = 0, \quad (4.21)$$

and compare our results with the exact analytical solution given by (3.12). Expanding the solution, $Z(x)$, in power series around $x_0 = 0$, the first two recursion relations are formed as

$$a_2^0 = \frac{1}{2} \left[a_0^0 - 2 (a_0^0)^5 \right], \quad (4.22)$$

$$a_3^0 = \frac{1}{6} \left[a_1^0 - 10 (a_0^0)^4 a_1^0 \right], \quad (4.23)$$

and then following the same steps mentioned in the previous subsection. The values of the initial conditions, a_0^0 , and a_1^0 , can be easily found from (3.12) and its first derivative at the initial point, $x_0 = 0$

$$Z(0) = \left(\frac{3}{2} \right)^{\frac{1}{4}} = a_0^0, \quad (4.24)$$

$$Z'(0) = 0 = a_1^0. \quad (4.25)$$

Figure 4.5 indicates the IPS solution of Eq. (4.21), where the high efficiency can be seen from the error curve.

4.2.4 IPS Method to Higher Order NLSE

In the case of much shorter optical lasers, say in the femtosecond domain, it is necessary to include higher order effects to the fundamental NLSE such as, third-order dispersion (TOD), self steepening (SS), and self-frequency shift due to stimulated Ra-

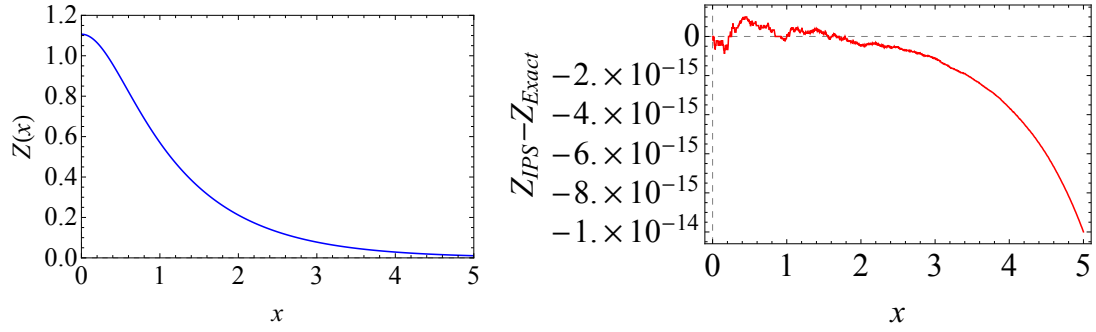


Figure 4.5: Solitonic solution of Eq. (4.21). Left: The IPS solution, with initial values $a_0^0 = \left(\frac{3}{2}\right)^{\frac{1}{4}}$ and $a_1^0 = 0$. The power series is expanded up to $n_{max} = 8$, with the iteration number $I = 1000$ and $\Delta = 0.005$. Right: The difference between the IPS solution and the exact solution given by Eq. (3.12).

man scattering (SRS). The equation representing such case is called a higher order NLSE (HONLSE) and is given by

$$i u_t + \sigma_1 u_{xx} + \sigma_2 |u|^2 u - i \sigma_3 u_{xxx} - i \sigma_4 (|u|^2 u)_x - i \sigma_5 u (|u|^2)_x = 0, \quad (4.26)$$

where the real coefficients, σ_1 , σ_2 , σ_3 , σ_4 , and σ_5 , correspond to the GVD, the SPM induced by the Kerr effect, TOD, SS, and SRS effects, respectively. This equation is studied in several works such as [75–77]. The SS effect means a change in the pulse shape due to the intensity dependence of the group velocity, which causes a steep intensity edge towards the back of the pulse. In the SRS, the input pulse is exposed to energy loss or gain. In the loss case, the Stokes scattering takes place where the lost energy is absorbed by the medium in the form of vibrations and rotations, hence the output pulse propagates at a lower frequency. However, in the gain case, the anti-Stokes scattering takes place, where the output pulse propagates at a higher frequency than the original one. The following special case of Eq. (4.26), for $\sigma_3 = \sigma_4 = 0$, is known to be nonintegrable

$$i u_t + \sigma_1 u_{xx} + \sigma_2 |u|^2 u - \sigma_5 u (|u|^2)_x = 0. \quad (4.27)$$

Using the solution in (3.2), the ordinary version for $\sigma_1 = \sigma_2 = 1$ reads

$$Z - Z'' - Z^3 + 2\sigma_5 Z^2 Z' = 0. \quad (4.28)$$

To employ the IPS method on this equation, we start by expanding the solution, $Z(x)$, and its derivatives, $Z^{0'}$ and $Z^{0''}$ in power series around the initial point $x_0 = 0$. The following first two recursion relations are obtained as

$$a_2^0 = \frac{1}{2} \left[a_0^0 - (a_0^0)^2 + 2\sigma_5 (a_0^0)^2 a_1^0 \right], \quad (4.29)$$

$$a_3^0 = \frac{1}{6} \left[a_1^0 - 3(a_0^0)^2 a_1^0 + 2\sigma_5 (a_0^0)^3 - 2\sigma_5 (a_0^0)^5 + 4\sigma_5 a_0^0 (a_1^0)^2 + 4\sigma_5^2 (a_0^0)^4 a_1^0 \right]. \quad (4.30)$$

For the sake of applicable initial conditions, we first search for the initial conditions that lead to the constant solutions. To know these initial conditions, we set a constant solution $Z(x) = C$, thus, the second and last terms in the ordinary equation (4.28) vanish and the equation ends up with

$$C - C^3 = 0. \quad (4.31)$$

Solving the algebraic equation (4.31) gives $C = -1, 0$, or 1 , therefore, for $a_0^0 = -1, 0, 1$ and $a_1^0 = 0$, Eq. (4.28) admits constant solutions.

Next, we search around these values for interesting solutions. Let us start by examining the influence of the sign of SRS factor for $a_0^0 = 0.1$ and $a_1^0 = 0$, with $I = 10000$. For $\sigma_5 = +0.02$, the solution is oscillating almost around 0. This is associated with an increase in both the amplitude and the frequency. However, for $\sigma_5 = -0.02$, the solution is oscillating almost around 1. This is associated with a decrease in the amplitude while the frequency is kept unchanged. These results are shown in Figure 4.6.

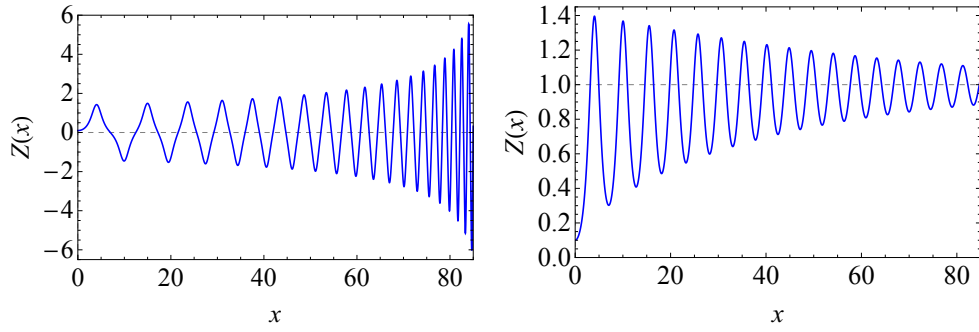


Figure 4.6: Oscillating solutions of Eq. (4.28) using IPS method with initial values $a_0^0 = 0.1$ and $a_1^0 = 0$. The power series is expanded up to $n_{max} = 8$, with the iteration number $I = 10000$ and $\Delta = 0.0085$. Left: The SRS factor is $\sigma_5 = +0.02$. Right: The SRS factor is $\sigma_5 = -0.02$.

Figure 4.7 presents a localized behaviour of the solution for $x \in (0, 20]$, when $a_0^0 = 1.429660329$ and $a_1^0 = 0$, where the SRS factor is taken to be $\sigma_5 = -0.02$. This value of a_0^0 is obtained by gradually increasing its value starting from $a_0^0 = 0.1$. We consider this initial condition, $a_0^0 = 1.429660329$, as a critical point that separates the oscillating solution from the localized solution.

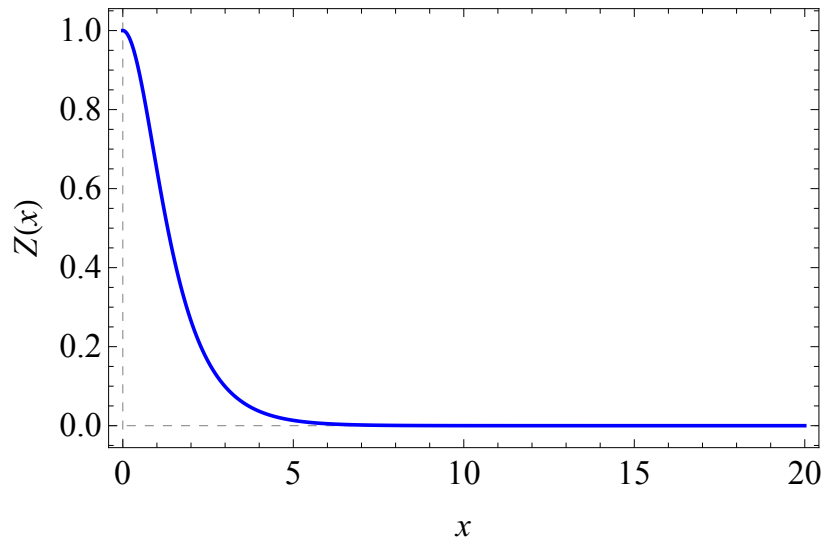


Figure 4.7: The IPS Localized solution of Eq. (4.28) with initial values $a_0^0 = 1.429660329$ and $a_1^0 = 0$, and the SRS factor is $\sigma_5 = -0.02$. The power series is expanded up to $n_{max} = 8$, with the iteration number $I = 10000$ and $\Delta = 0.002$.

In the following discussion, we will make a quick and simple comparison between the obtained IPS solutions, Figures 4.4 and 4.7, for Eqs. (4.14) and (4.28), respectively. To make such comparison, we will normalize the solution in Figure 4.7, $Z(x)_{HONLSE} = Z(x)/1.429660329$. Figure 4.8 illustrates this comparison. As one can see, the two solutions look similar while the difference takes the range of 10^{-3} .

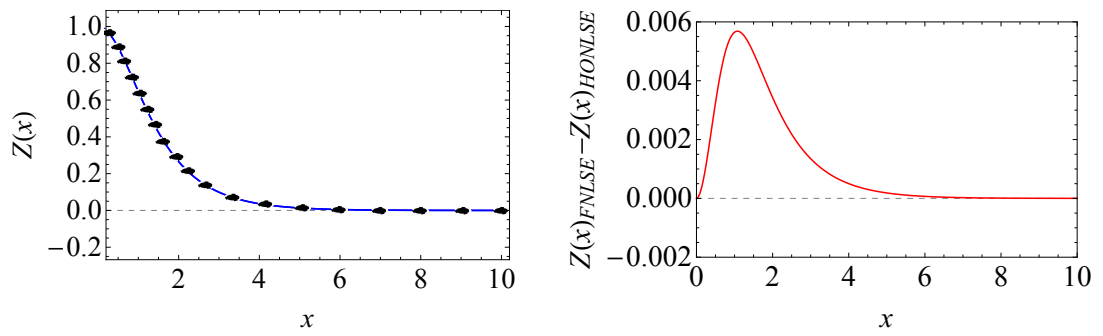


Figure 4.8: Left: Localized solutions of Eqs. (4.28) and (4.14), dotted curve corresponds to the normalized representation of Figure 4.7 and the blue curve corresponds to the solution in Figure 4.4. Right: The difference between the two solutions.

Chapter 5: Application of IPS Method to Fluid Flow Dynamics

The fluid dynamics and heat transfer of a viscous incompressible fluid flow past stretching surfaces - such as a sheet or tube - have attracted considerable interests of many researchers because of their importance in many industrial applications such as the quality of certain products. One of the most interesting conditions for stretching surfaces problems is the velocity at the surface, where it mainly figures the fluid characteristics based upon two essential factors, fluid viscosity and suction parameter. A remarkable interest of several researchers concentrated on tracking the existence of dual solutions for the flow within a certain range of unsteadiness and suction parameters [78–88]. Although, the literature reveals numerous research papers discussing the flow over a stretching sheet and moving plate [89–97], there are only few studies focusing on the problem of flow past a stretching cylinder or tube, see [79–81] and references therein.

In this chapter we will employ the IPS technique on heat and mass transfer over a shrinking permeable cylinder described in Zaimi *et al.* [79] and Elnajjar *et al.* [81]. A worth materialized work is presented in Appendix. For completeness, we redescribe precisely the physical model. The flow is considered of an unsteady, laminar, viscous and incompressible fluid with uniform velocity U and uniform temperature T_∞ over a permeable shrinking circular cylinder. The cylinder is assumed to be infinitely long and the flow has constant properties. The diameter of the cylinder is assumed to be time dependant with the radius $a(t) = r_0 \sqrt{1 - \beta t}$, where r_0 is a positive constant, β is the constant of expansion/contraction strength, and t is the time. Clearly, the cylinder's radius is shrinking with time if β is positive and stretching with time if β is negative. Notice that, since the flow is axisymmetric, the flow field should be a function of the radial coordinate, r , and the longitudinal, z .

5.1 Heat and Mass Transfer Model

The governing equations for the unsteady and incompressible fluid without body force are the continuity, momentum and energy equations. These equations in cylindrical coordinate system with azimuthal symmetry, (r, z) , are given by

$$\frac{1}{r} \frac{\partial}{\partial r} (r u_r) + \frac{\partial u_z}{\partial z} = 0, \quad (5.1)$$

$$\frac{\partial u_r}{\partial t} + u_r \frac{\partial u_r}{\partial r} + u_z \frac{\partial u_r}{\partial z} = -\frac{1}{\rho} \frac{\partial p}{\partial r} + \nu \left(\frac{\partial^2 u_r}{\partial r^2} + \frac{1}{r} \frac{\partial u_r}{\partial r} + \frac{\partial^2 u_r}{\partial z^2} - \frac{u_r}{r^2} \right), \quad (5.2)$$

$$\frac{\partial u_z}{\partial t} + u_r \frac{\partial u_z}{\partial r} + u_z \frac{\partial u_z}{\partial z} = -\frac{1}{\rho} \frac{\partial p}{\partial z} + \nu \left(\frac{\partial^2 u_z}{\partial r^2} + \frac{1}{r} \frac{\partial u_z}{\partial r} + \frac{\partial^2 u_z}{\partial z^2} \right), \quad (5.3)$$

and

$$\frac{\partial T}{\partial t} + u_r \frac{\partial T}{\partial r} = \alpha \left(\frac{1}{r} \frac{\partial}{\partial r} \left(r \frac{\partial T}{\partial r} \right) \right), \quad (5.4)$$

where r and z are the polar coordinates in the radial and axial directions, respectively, u_r and u_z are the fluid velocity components in the radial and axial directions, respectively, and T is the fluid temperature. The function p represents the fluid pressure, and the parameters ν , ρ , and α denote the fluid viscosity, the fluid density, and the fluid thermal diffusivity, respectively. Notice that, we assumed that there is no azimuthal velocity component. The assumed boundary conditions associated with Eqs. (5.1)-(5.4) for the velocity components and the temperature are given by

$$u_r = -\frac{2 \nu \gamma}{r_0 \sqrt{1 - \beta t}}, \quad u_z = -\frac{4 \nu z}{r_0^2 (1 - \beta t)}, \quad T_s = \frac{c_0}{\sqrt{1 - \beta t}} + T_\infty \quad \text{at } r = a(t), \quad (5.5)$$

and

$$u_z = 0, \quad T = T_\infty \quad \text{as } r \rightarrow \infty, \quad (5.6)$$

where T_s is the constant surface temperature and c_0 is a positive constant. The similarity transformations which convert Eqs. (5.1)-(5.4) into nonlinear ordinary differential equations are given by [79] and [81]

$$u_r = -\frac{2\nu}{r_0\sqrt{1-\beta t}} \frac{f(\eta)}{\sqrt{\eta}}, \quad u_z = \frac{4\nu z}{r_0^2(1-\beta t)} f'(\eta), \quad (5.7)$$

$$T = (T_s - T_\infty)(\theta(\eta) - T_\infty) + T_\infty, \quad (5.8)$$

where $f'(\eta) = df/d\eta$ and η is the similarity variable given by

$$\eta = \left(\frac{r}{r_0}\right)^2 \frac{1}{1-\beta t}. \quad (5.9)$$

In addition, it should be noted that f represents the dimensionless stream function and θ represents the normalized temperature. Applying the above similarity transformations, Eqs. (5.1)-(5.4) and the boundary conditions (5.5)-(5.6) reduce the system of three variables, t, r , and z , and three functions, u_r, u_z , and T , into a system of one variable, η , and two functions, f and θ , as

$$\eta f''' + f'' + ff'' - f'^2 - S(\eta f'' + f') = 0, \quad (5.10)$$

$$\eta \theta'' + \theta'(1 + \text{Pr} f - S\text{Pr} \eta) - S\text{Pr} \theta = 0, \quad (5.11)$$

subject to

$$f(1) = \gamma, \quad f'(1) = -1, \quad f'(\infty) = 0, \quad \theta(1) = 1, \quad \theta(\infty) = 0, \quad (5.12)$$

where $S = r_0^2 \beta / 4 \nu$ is the unsteadiness parameter representing the strength of contraction/expansion, $\gamma = -r_0 U / 2 \nu$ is the suction parameter, and $\text{Pr} = \nu / \alpha$ is the Prandtl number.

In the next section, we will solve Eqs. (5.10) and (5.11) subject to the boundary conditions (5.12) using the IPS technique in the ranges $0 \leq \gamma \leq 7$ and $-4 \leq S \leq 0$ at $\text{Pr} = 0.7$. We will also study the normalized skin friction coefficient, $f''(1)$, and the normalized heat transfer rate, $-\theta'(1)$.

5.2 IPS Method to Heat and Mass Transfer Model

The following is a detailed implementation of the IPS method used to solve Eqs. (5.10) and (5.11) subject to the boundary conditions (5.12). First, we need to render Eq. (5.10) to be an initial-value problem; i.e.

$$f''' = \frac{1}{\eta} (-f'' - f f'' + f'^2 + S (\eta f'' + f')), \quad (5.13)$$

with

$$f(1) = \gamma, \quad f'(1) = -1, \quad f''(1) = \lambda, \quad (5.14)$$

where λ must be chosen using the shooting method [81] so that the solution satisfies the boundary condition $f'(\infty) = 0$. Notice that, setting different initial values for λ in the shooting method, dual solutions are obtained.

We start by expanding $f(\eta)$ in power series around the initial point $\eta_0 = 1$

$$f^0(\eta) = \sum_{n=0}^{n_{max}} a_n^0 (\eta - 1)^n, \quad (5.15)$$

and the derivatives, $f^{0'}$, $f^{0''}$, and $f^{0'''}$ can be calculated simply by differentiating this series. Substituting in Eq. (5.10), the coefficients, a_n^0 , for $n \geq 3$, can be found recursively in terms of the initial conditions a_0^0 , a_1^0 , and a_2^0 through the recursion relations.

The first two recursion relations are given by

$$a_3^0 = \frac{1}{6} \left[(a_1^0)^2 - 2a_2^0(1 + a_0^0 - S) + a_1^0 S \right], \quad (5.16)$$

$$a_4^0 = \frac{1}{24} \left[(a_1^0)^2 (S - 2 - a_0^0) + 2a_2^0 \left(2 + (a_0^0)^2 + a_0^0(3 - 2S) - S + S^2 \right) + a_1^0 \left(2a_2^0 + S(S - 2 - a_0^0) \right) \right] \quad (5.17)$$

Recalculating $f^0(\eta)$, $f^{0'}(\eta)$, and $f^{0''}(\eta)$ at $\eta = 1 + \Delta$ gives

$$a_0^1 = f^0(\Delta), \quad a_1^1 = f^{0'}(\Delta), \quad a_2^1 = \frac{f^{0''}(\Delta)}{2}. \quad (5.18)$$

Now, a_0^1 , a_1^1 , and a_2^1 play the role of the initial conditions for the next series expansion, where we expand the solution and its derivatives in power series around $\eta_0 = 1 + \Delta$

$$f^1(\eta) = \sum_{n=0}^{n_{max}} a_n^1 (\eta - (1 + \Delta))^n. \quad (5.19)$$

Resubstituting these power series expansions in the differential equation, we get the new recursion relations $a_n^1(a_0^1, a_1^1, a_2^1)$. The next iterative step is to calculate $f^1(\eta)$ and its first two derivatives at $\eta = 1 + 2\Delta$ which will give the initial conditions for the new power series. Repeating this process I times, the general forms of the first two recursion relations of Eq. (5.10) are found to be

$$a_3^I = \frac{1}{6(1 + I\Delta)} \left[(a_1^I)^2 - 2a_2^I(1 + a_0^I - S - SI\Delta) + a_1^I S \right], \quad (5.20)$$

$$a_4^I = \frac{1}{24(1 + I\Delta)^2} \left[(a_1^I)^2 \left(-2 - a_0^I + S + SI\Delta \right) + a_1^I \left(2a_2^I(1 + I\Delta) + S(-2 - a_0^I + S + SI\Delta) \right) \right]$$

$$+ 2a_2^I \left(S(-1 - I\Delta) + (S + SI\Delta)^2 + 2 + (a_0^I)^2 + a_0^I(3 - 2S - 2SI\Delta) \right) \Big], \quad (5.21)$$

where

$$a_0^I = f^{I-1}(\Delta), \quad a_1^I = (f^{I-1})'(\Delta), \quad a_2^I = \frac{(f^{I-1})''(\Delta)}{2}. \quad (5.22)$$

In order to obtain accurate numerical results, we have to pay attention to the selection of the numerical algorithm parameters, I , n_{max} , and the infinity of the independent variable domain, η_∞ .

It is worth mentioning that we succeeded to find the explicit analytical form of the first solution for (5.10) subject to (5.12) under a condition $S = -1/\gamma$; that is

$$f(\eta) = \gamma e^{\frac{(1-\eta)}{\gamma}}. \quad (5.23)$$

This exact solution will play a crucial role in proving the advantages of our IPS method. The IPS solution of the problem (5.10)-(5.12) at three different iterations $I = 1, 2$, and 3 together with the exact solution obtained by (5.23) when $S = -1$ and $\gamma = 1$ are displayed in Figure 5.1. It is clearly seen that, increasing the number of iterations in the IPS method delays the divergence point.

To achieve an ‘‘optimal choice’’ of η_∞ , we solve the problem with $\eta_\infty = 7, 8, \dots, 17$. Table 5.1 shows the values of λ up to 50 digits corresponding to the values of η_∞ . It is clearly seen that, the value of λ stabilizes at around $\eta_\infty = 15$; hence we choose $\eta_\infty = 15$ as the optimal value for the rest of the calculations in the entire paper. It should be noted that most of the used numerical schemes for such type of problems, [79–81, 88], had chosen $\eta_\infty = 7$ to represent the infinity which, definitely, gave lower order of accuracy. This conclusion can be easily tested via the exact solution (5.23) which gives $f'(7) = -0.00247875$ and $f'(15) = -8.31529 \times 10^{-7}$. However, we will only show

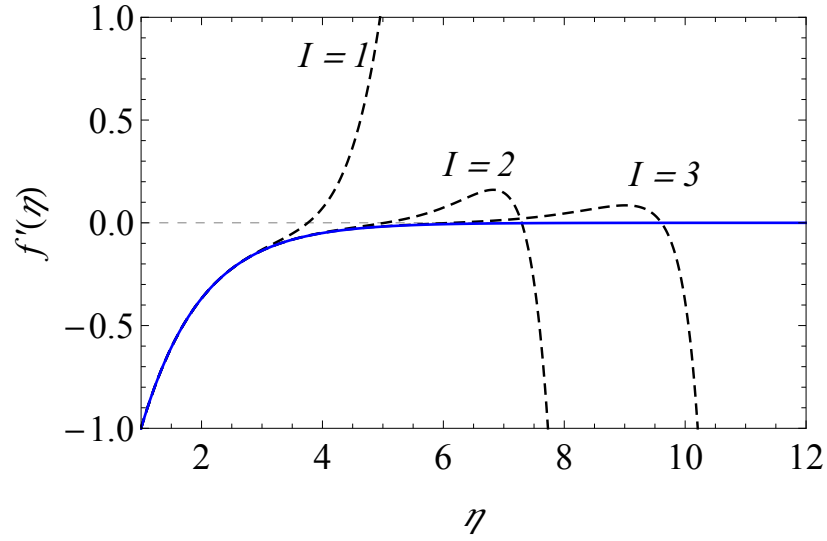


Figure 5.1: Velocity profiles, $f'(\eta)$, for the first solution; exact (blue) and approximate (dashed) solutions at different I with $S = -1$ and $\gamma = 1$. The power series is expanded up to $n_{max} = 8$, $\Delta = 0.014$.

the interval up to $\eta_\infty = 8$ for the rest of the coming figures.

Table 5.1: Stabilization of λ values with η_∞ at $\gamma = 1$ and $S = -1$.

η_∞	λ
7	1.06032130948772355259169445286450439527129433161564
8	<u>1.02826614125492573507123370718399515004546832373446</u>
9	<u>1.01244316459533191876326159442255228857229463473780</u>
10	<u>1.00535010609275538041830857835707790239466505001516</u>
11	<u>1.00221279175507729615034859048196423158532888754168</u>
12	<u>1.00084874204304334646862685662321915732040012124886</u>
13	<u>1.00030312215822976659593816307972112761442861473174</u>
14	<u>1.00016671718702637162776598969384662018793573810246</u>
15	<u>1.00003031221582297665959381630797211276144286147317</u>
16	<u>1.00003031221582297665959381630797211276144286147317</u>
17	<u>1.00003031221582297665959381630797211276144286147317</u>

Table 5.2 presents the Central Processing Unit (CPU) time in seconds, which is machine-dependent, versus the E_{IPS} given by Eq. (4.12) of the IPS method for the first solution at $\gamma = 2$ and $S = -1$, where n_{max} varies from 3 to 8.

Table 5.2: The upper bound of the error for the first solution at $\gamma = 2$ and $S = -1$ versus the CPU time at different values of n_{max} .

n_{max}	E_{IPS}	CPU time (seconds)
3	$\approx 10^{-5}$	0.0156001
4	$\approx 10^{-7}$	0.0312002
5	$\approx 10^{-9}$	0.0780005
6	$\approx 10^{-10}$	0.156001
7	$\approx 10^{-12}$	0.296402
8	$\approx 10^{-14}$	0.546004

The exact solution, (5.23), provides a unique possibility to calculate the error of the IPS method and compare it with that of other numerical methods. Figure 5.2 presents a comparison between the error of the IPS method and the explicit Runge-Kutta method of order four (ERK4) for the problem at $\gamma = 1$ and $S = -1$. The advantages of the IPS technique over the other one is notable.

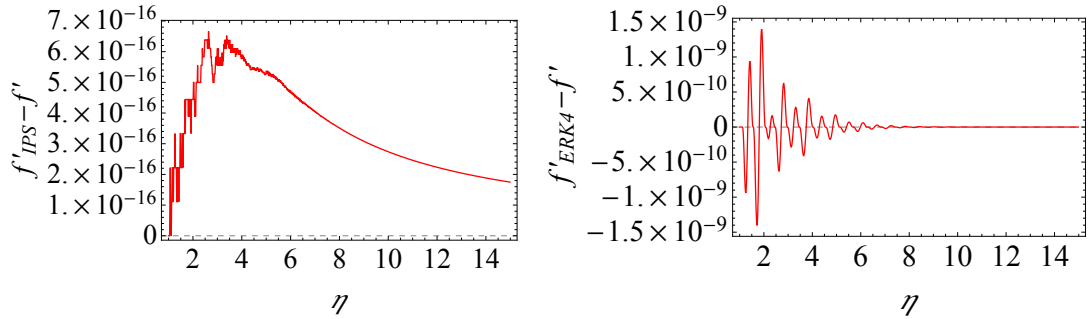


Figure 5.2: Error of the IPS method (left) and the ERK4 (right) for the case of $\gamma = 1$ and $S = -1$. The error is defined as the difference between the numerical solution and the exact solution (5.23). The power series is expanded up to $n_{max} = 8$, $I = 1000$ and $\Delta = 0.014$.

A further comparison is done in Figure 5.3 on the normalized skin friction coefficient, $f''(1)$, as a function of S with Zaimi *et al.* [79] and Elnajjar *et al.* [81] for the case when $\gamma = 0$. Excellent agreements are obtained. It should be mentioned herein that Elnajjar *et al.* [81] used a combination of the implicit Runge-Kutta method and the shooting method while Zaimi *et al.* [79] implemented the shooting method described

in the book by Jaluria and Torrance [82].

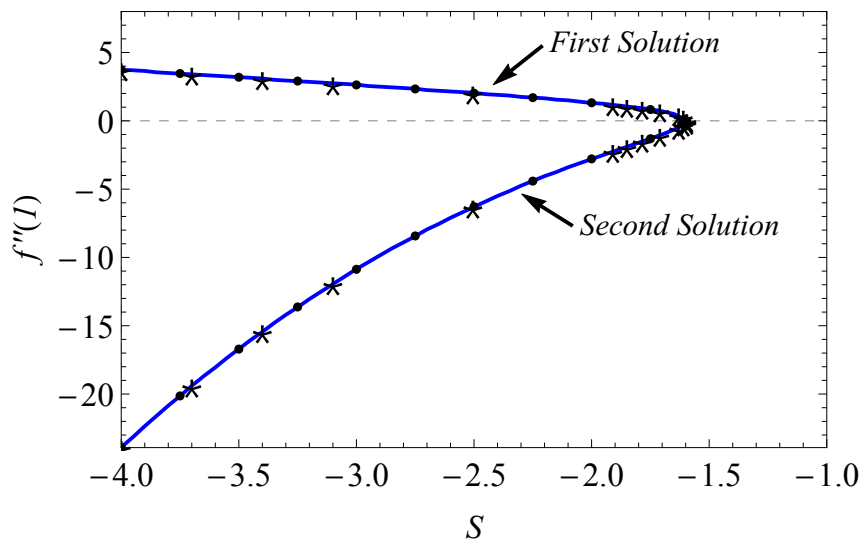


Figure 5.3: Normalized skin friction coefficient, $f''(1)$, as a function of S for $\gamma = 0$. The IPS (solid blue), the Zaimi *et al.* [79] (●), and the Elnajjar *et al.* [81] (*) solutions.

Notice that, several recent studies such as [81–87] reported the existence of a critical value of S (named S_c) at which the problem has no solution (for $S > S_c$), only one solution (at $S = S_c$), and dual solutions (for $S < S_c$).

Figure 5.4 shows the first and second solutions of the velocity profiles for $\gamma = 0, 1, 3, 5, 7$ with a fixed unsteadiness parameter, $S = 2$. It is clearly seen that, the first solution for the fluid velocity inside the boundary layer region increases as γ increases, while the second solution shows an opposite trend. In addition, the two solutions of the velocity profile become steeper with higher magnitudes as γ increases. These observations emphasize the effect of increasing the suction parameter of the cylinder's wall which is to decrease the boundary layer thickness.

Figure 5.5 displays the first and second solutions of the velocity profiles for $S = 1, 2, 3, 4$ with a fixed value of the suction parameter, $\gamma = 1$. Generally speaking, the behaviour of $f'(\eta)$ is very similar to the case of the variable suction parameter;

that is increasing the unsteadiness parameter produces steeper behaviour in the velocity profiles for the first solution while the second solution shows an opposite trend. In agreement result with the case of the variable suction parameter in Figure 5.4, increasing the unsteadiness parameter will then cause a reduction in the thickness of the boundary layer.

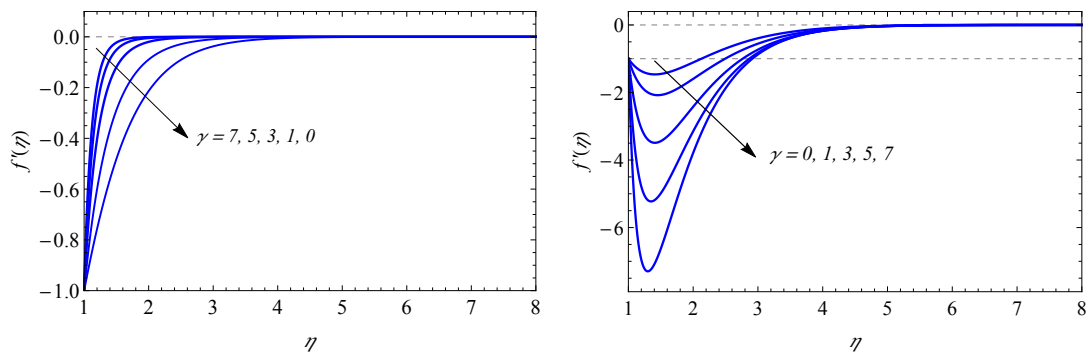


Figure 5.4: Velocity profiles, $f'(\eta)$, for different values of γ at $S = 2$: First solution (left) and second solution (right). The power series is expanded up to $n_{max} = 8$, $I = 1000$ and $\Delta = 0.014$.

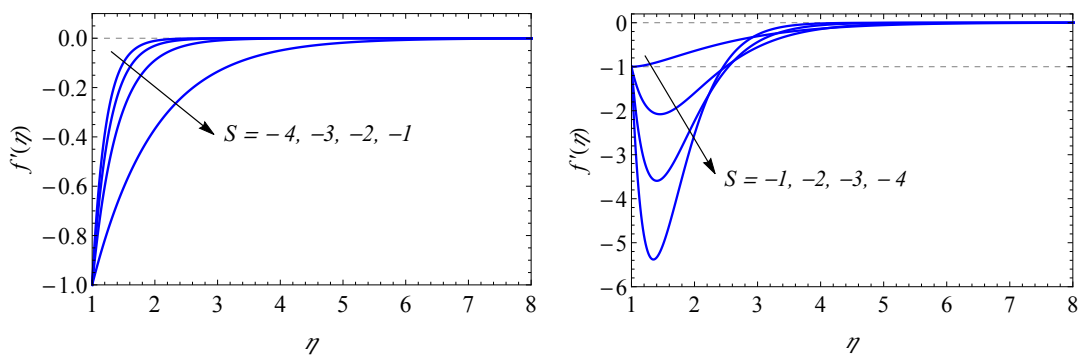


Figure 5.5: Velocity profiles, $f'(\eta)$, for different values of S at $\gamma = 1$: First solution (left) and second solution (right). The power series is expanded up to $n_{max} = 8$, $I = 1000$ and $\Delta = 0.014$.

As a consequence of the results in Figure 5.4, increasing the suction parameter causes an increment in the normalized skin friction coefficient for the first solution and decrement in the normalized skin friction coefficient for the second solution, as clearly

shown in Figure 5.6.

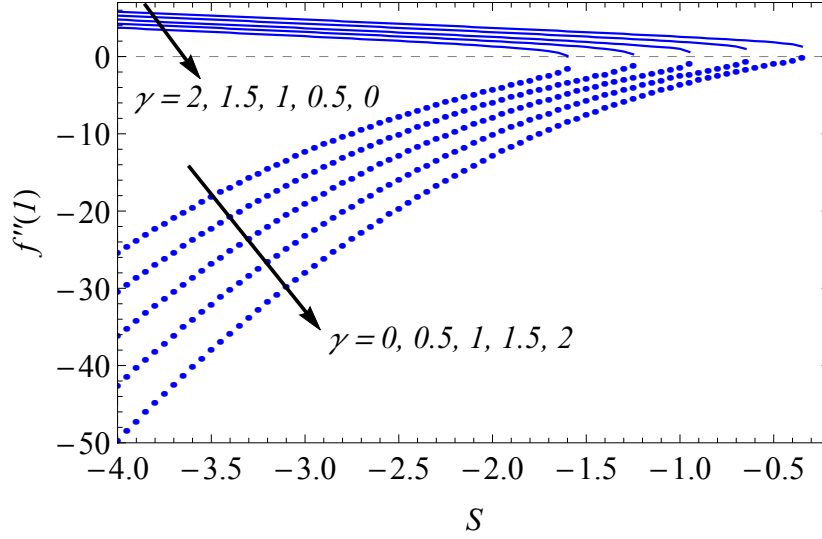


Figure 5.6: Normalized skin friction coefficient, $f''(1)$, as a function of S for different values of γ : The first solution (solid) and second solution (dotted). The power series is expanded up to $n_{max} = 8$, $I = 1000$ and $\Delta = 0.014$.

In a similar way, for the energy equation

$$\theta'' = \frac{1}{\eta} \left(-\theta'(1 + \text{Pr } f - S \text{ Pr } \eta) + S \text{ Pr } \theta \right), \quad (5.24)$$

subject to

$$\theta(1) = 1, \quad \theta'(1) = \sigma, \quad (5.25)$$

where σ must be chosen using the shooting method [81] so that the solution satisfies the boundary condition $\theta(\infty) = 0$. We expand $\theta(\eta)$ in power series around the same initial point

$$\theta^0(\eta) = \sum_{n=0}^{n_{max}} b_n^0 (\eta - 1)^n, \quad (5.26)$$

and similarly for the derivatives, $\theta^{0'}$ and $\theta^{0''}$. Substituting in Eq. (5.11), the coefficients, b_n^0 , for $n \geq 2$, are found recursively in terms of the initial conditions b_0^0 and b_1^0 through the recursion relations. The first two recursion relations are given by

$$b_2^0 = \frac{1}{2} \left[b_0^0 \text{Pr} S + b_1^0 (-1 - a_0^0 \text{Pr} + \text{Pr} S) \right], \quad (5.27)$$

$$b_3^0 = \frac{1}{6} \left[b_0^0 \text{Pr} S \left(-2 - a_0^0 \text{Pr} + S \text{Pr} \right) + b_1^0 \left(2 + (a_0^0)^2 \text{Pr}^2 - \text{Pr} S + \text{Pr}^2 S^2 - a_1^0 \text{Pr} + a_0^0 \text{Pr} (3 - 2 \text{Pr} S) \right) \right]. \quad (5.28)$$

Employing the IPS method, the first two recursion relations are found to be

$$b_2^I = \frac{1}{2(1+I\Delta)} \left[b_0^I \text{Pr} S + b_1^I (-1 - a_0^I \text{Pr} + \text{Pr} S + I\Delta \text{Pr} S) \right], \quad (5.29)$$

$$b_3^I = \frac{1}{6(1+I\Delta)^2} \left[b_0^I \text{Pr} S \left(-2 - a_0^I \text{Pr} + S(1+I\Delta) \text{Pr} \right) + b_1^I \left(2 + (a_0^I)^2 \text{Pr}^2 - \text{Pr} S + \text{Pr}^2 S^2 - \text{Pr} S I \Delta + 2 \text{Pr}^2 S^2 I \Delta + \text{Pr}^2 S^2 I^2 \Delta^2 - a_1^I \text{Pr} (1+I\Delta) + a_0^I \text{Pr} (3 - 2 \text{Pr} S (1+I\Delta)) \right) \right], \quad (5.30)$$

where

$$b_0^I = \theta^{I-1}(\Delta), \quad b_1^I = (\theta^{I-1})'(\Delta). \quad (5.31)$$

Figure 5.7 presents the temperature profiles of the fluid flow, $\theta(\eta)$, at $S = 2$ and $\gamma = 0, 1, 3, 5, 7$. It is obviously noticeable that both solutions for temperature profiles admit similar behaviour, where they become wider and more relaxed as the suction parameter decreases. These behaviours inspire us to conclude that the developed thermal boundary layer and the corresponding rate of heat transfer are decreasing as S increases. However, the second solution depicts more relaxed behaviour compared with the first solution.

Figure 5.8 presents the temperature profiles of the fluid flow, $\theta(\eta)$, at $\gamma = 1$ and

$S = 1, 2, 3, 4$. Clearly, the increase in the unsteadiness parameter or the suction parameter leads to the same trend.

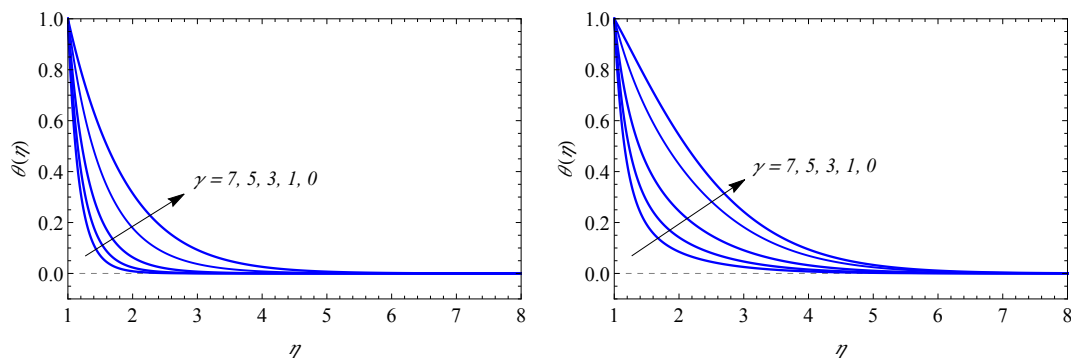


Figure 5.7: Temperature profiles, $\theta(\eta)$, for different values of γ at $S = 2$: First solution (left) and second solution (right). The power series is expanded up to $n_{max} = 8$, $I = 1000$ and $\Delta = 0.014$.

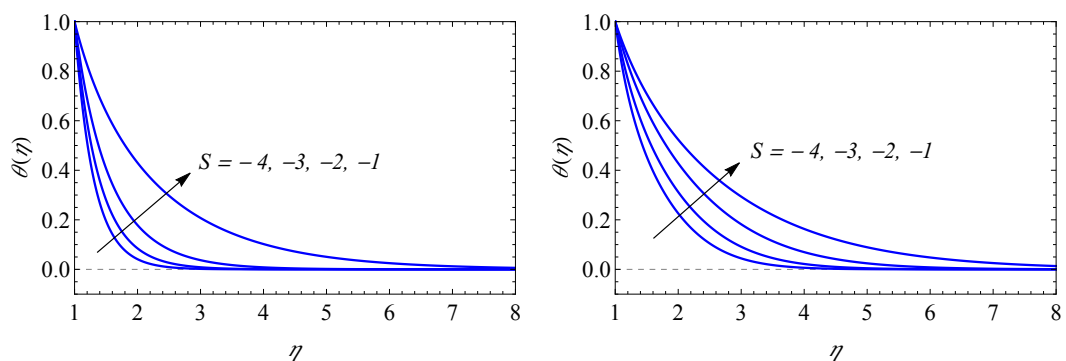


Figure 5.8: Temperature profiles, $\theta(\eta)$, for different values of S at $\gamma = 1$: First solution (left) and second solution (right). The power series is expanded up to $n_{max} = 8$, $I = 1000$ and $\Delta = 0.014$.

The slight difference between the first and second temperature profiles indicates that the second solution reflects higher thermal boundary layer than the first solution, and thus, a larger rate of the heat transfer as confirmed by Figure 5.9.

The variation of both the normalized skin friction coefficient, $f''(1)$, and the heat transfer rate, $\theta'(1)$, as functions of S , are shown, respectively, in Figures 5.6 and 5.9 for

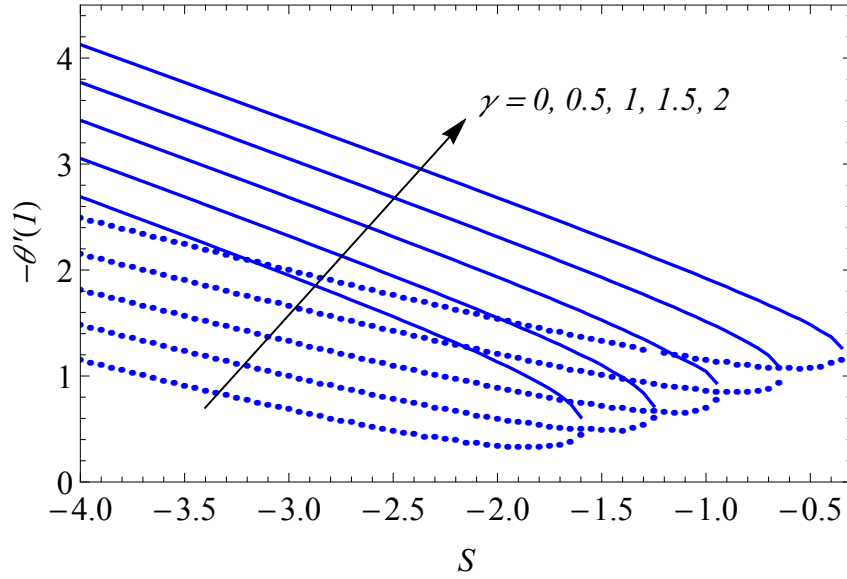


Figure 5.9: Heat transfer rate, $-\theta'(1)$, as a function of S for different values of γ : The first solution (solid) and second solution (dotted). The power series is expanded up to $n_{max} = 8$, $I = 1000$ and $\Delta = 0.014$.

$\gamma = 0, 0.5, 1, 1.5, 2$. The results demonstrate the existence of a critical value S_c in the S -domain at which the problem has no solution for $S > S_c$, only one solution at $S = S_c$, and dual solutions for $S < S_c$. Figure 5.6 shows that, $|f''(1)|$ increases as γ increases which is due to the increase in the surface shear stress coefficient. Moreover, we observe that, $|f''(1)|$ is decreasing with S . However, Figure 5.9 clearly shows that increasing γ will definitely increase the heat transfer rate while increasing S causes a decrease in the heat transfer rate.

Finally, we finish our discussion of this chapter with Figure 5.10 which presents an overview of the solution for problems (5.10) and (5.11) subject to the boundary conditions (5.12) in the $\gamma - S$ domain for $Pr = 0.7$ and $0 \leq \gamma \leq 2$. The straight line in this figure represents the occurrence of unique solution of the problem.

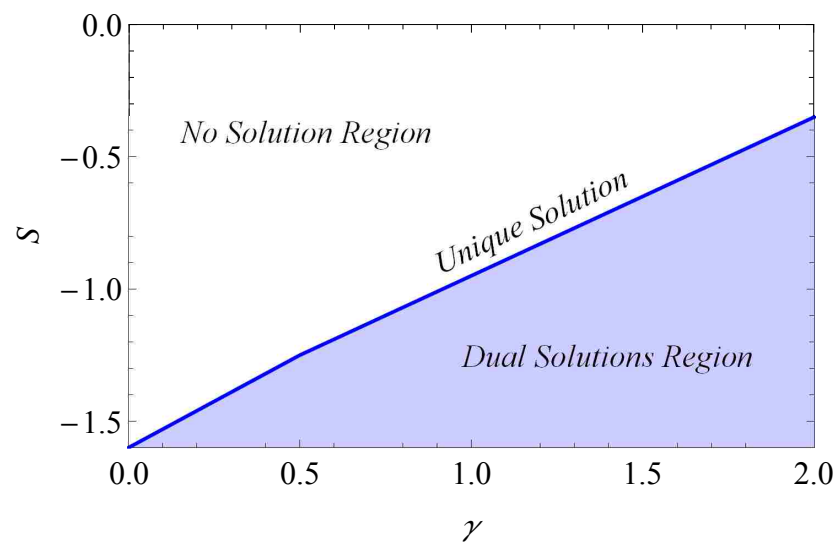


Figure 5.10: An overview of the solution for problems (5.10) and (5.11) subject to the boundary conditions (5.12) in the $\gamma - S$ domain.

Chapter 6: Application of IPS Method to Chaotic Systems

In a random event such as, the flipping of the a coin, the present observation has no connection to the previous one. This event is called a non-deterministic system. This contrasts with a chaotic dynamics where the current outcome does depend on the previous state in a deterministic way, but the way of the measurements made on the system does not allow the prediction of the system's state. Chaotic dynamics, as a very interesting phenomenon, has been studied in several publications such as [98] and [99].

Chaos has a very vigorous connection with nonlinearity. Whenever there is a chaotic behavior, there will be an accompanied nonlinearity, but not the opposite. One necessary condition for the nonlinear system to present chaos is involving at least three variables. There is no one definition of chaos term, however, here we use the definition mentioned in [100]: "*Chaos is aperiodic long-term behaviour in a deterministic system that exhibits sensitive dependence on initial conditions*". Aperiodic term means that the solutions of the system do not settle down to a steady state or a periodic behaviour as time goes to ∞ , while sensitive dependence on initial conditions implies that two solutions starting very close to each other will rapidly diverge to two completely different results.

The bulk of this chapter is devoted on studying the Lorenz system [101], one of the most important systems that admits chaos, using the IPS method.

6.1 Lorenz System

In 1963 E. Lorenz attempted to construct a simple system of differential equations that can be used to explain the unpredictable behaviours of the weather from the

thermal convection model [101].

Motion of a fluid can be described by a system of differential equations that consist of infinitely many variables. Roughly speaking, if the fluid is hotter than the surrounding, it will rise up because its density is less than the surrounding and donate heat to its surrounding as well. If it slowly loses energy, it will convect. The behaviour of this convection could form different patterns starting from no flow, passing through a simple roll, and ending up with a chaotic pattern.

Lorenz's simplification based on pretending that all variables that describe the fluid motion stay constant except three variables, the fluid velocity or the convection rate, $x(t)$, and the horizontal and vertical fluid temperature, $y(t)$ and $z(t)$. Lorenz came up with a dynamical system of these three time dependent variables. It is called the Lorenz system and is defined by the following three equations

$$x' = \text{Pr} (y - x), \quad (6.1)$$

$$y' = \text{Ra} x - y - x z, \quad (6.2)$$

$$z' = x y - \gamma z, \quad (6.3)$$

with the initial conditions

$$x(0) = 0, \quad y(0) = 1, \quad z(0) = 0, \quad (6.4)$$

where Pr is the Prandtl number mentioned in the previous chapter, $\text{Ra} = g \beta \Delta T d^3 / \nu \alpha$ is the Rayleigh number, where the parameters g , β , ΔT , d , ν , and α denote acceleration due to gravity, the constant of expansion/contraction strength, the temperature difference, the length of the system, the fluid viscosity, and the fluid thermal diffusivity, respectively, γ is a real positive parameter related to the physical size of the system,

and the prime denotes differentiation with respect to the time, t .

The nonlinearity of the system (6.1)-(6.3) appears on the two quadratic terms, xz and xy , in Eqs. (6.2) and (6.3). This system also shows an interesting symmetry $(x, y) \rightarrow (-x, -y)$, which implies that if $(x(t), y(t), z(t))$ is a solution of the system, $(-x(t), -y(t), z(t))$ is a solution as well.

The Rayleigh number measures how hard the fluid system is being heated, which implies how hard the system will be driven to dissipation. Despite the simplicity of this system, it could behave chaotically depending on the parameter values. It is well-known that chaotic behaviour appears when $Ra > 24.74$. Below this value, the system behaves non-chaotically [101]. In the chaotic regime, the solution of Lorenz model never settles down to an equilibrium or to a periodic state, instead, it oscillates irregularly and takes an aperiodic behaviour. The original chaotic case of Lorenz was $Pr = 10$, $Ra = 28$, and $\gamma = 8/3$. Lorenz found that when he started with two slightly different initial conditions, the resulting two solutions became totally different as $t \rightarrow \infty$. This is telling us why the prediction of the future weather is impossible, very small error in measuring the current weather parameters will lead to a completely wrong prediction of its future state, since this small error will keep amplifying and eventually, lead to a wrong conclusion. This is what we meant by the extremely sensitivity to initial conditions.

In the coming discussion, we will solve Eqs. (6.1)-(6.3) subject to the initial conditions (6.4) using our IPS method and set $Pr = 10$, $Ra = 28$, and $\gamma = 8/3$, where we consider the chaotic Lorenz behaviour in the time range $t \in (0, 50]$.

6.2 IPS Method to Lorenz System

The following is a detailed application of the IPS method used to solve Eqs. (6.1-6.3) subject to the initial conditions (6.4). As we mentioned in chapter 4, we start by expanding each of $x(t)$, $y(t)$, and $z(t)$ in power series around the initial point $t_0 = 0$

$$x^0(t) = \sum_{n=0}^{n_{max}} a_n^0 t^n, \quad (6.5)$$

$$y^0(t) = \sum_{n=0}^{n_{max}} b_n^0 t^n, \quad (6.6)$$

$$z^0(t) = \sum_{n=0}^{n_{max}} c_n^0 t^n, \quad (6.7)$$

and the derivatives, $x^{0'}$, $y^{0'}$, and $z^{0'}$ can be calculated simply by differentiating these series expansions. Substituting in the Lorenz equations, (6.1), (6.2), and (6.3), the coefficients, a_n^0 , b_n^0 , and c_n^0 , for $n \geq 1$, can be found recursively in terms of the initial condition a_0^0 , b_0^0 , and c_0^0 through the recursion relations. The first two recursion relations for each function are given by

$$a_1^0 = \text{Pr} [a_0^0 + b_0^0], \quad (6.8)$$

$$a_2^0 = \frac{1}{2} [-\text{Pr} b_0^0 - \text{Pr} a_0^0 c_0^0 + \text{Pr}^2 a_0^0 - \text{Pr}^2 b_0^0 + \text{Pr} \text{Ra} a_0^0], \quad (6.9)$$

$$b_1^0 = -b_0^0 - a_0^0 c_0^0 + \text{Ra} a_0^0, \quad (6.10)$$

$$b_2^0 = \frac{1}{2} [a_0^0(1 + \text{Pr})(c_0^0 - \text{Ra}) - b_0^0(-1 + (a_0^0)^2 + \text{Pr} c_0^0 - \text{Pr} \text{Ra}) + \gamma a_0^0 c_0^0], \quad (6.11)$$

$$c_1^0 = a_0^0 b_0^0 - \gamma c_0^0, \quad (6.12)$$

$$c_2^0 = \frac{1}{2} [\text{Pr} (b_0^0)^2 + (a_0^0)^2(\text{Ra} - c_0^0) + \gamma^2 c_0^0 - a_0^0 b_0^0(1 + \text{Pr} + \text{Ra})]. \quad (6.13)$$

Recalculating $x^0(t)$, $y^0(t)$, and $z^0(t)$ at $t = \Delta$ gives

$$a_0^1 = x^0(\Delta), \quad b_0^1 = y^0(\Delta), \quad c_0^1 = z^0(\Delta). \quad (6.14)$$

As we know, a_0^1 , b_0^1 , and c_0^1 will play the role of the initial conditions for the next series expansion, where we expand the three solutions and their derivatives in power series around $t_0 = \Delta$

$$x^1(t) = \sum_{n=0}^{n_{max}} a_n^1 (t - \Delta)^n, \quad (6.15)$$

$$y^1(t) = \sum_{n=0}^{n_{max}} b_n^1 (t - \Delta)^n, \quad (6.16)$$

$$z^1(t) = \sum_{n=0}^{n_{max}} c_n^1 (t - \Delta)^n. \quad (6.17)$$

Resubstituting these power series expansions in the three differential equations, we get the new recursion relations $a_n^1(a_0^1, b_0^1, c_0^1)$, $b_n^1(a_0^1, b_0^1, c_0^1)$, and $c_n^1(a_0^1, b_0^1, c_0^1)$. The next iterative step is to calculate $x^1(t)$, $y^1(t)$, and $z^1(t)$ and their first derivatives at $t = 2\Delta$ which will give the initial conditions for the new power series. Repeating this process I times, the general forms of the iterative recursion relations will not differ from the above recursion relations (6.8-6.13) due to the homogeneity of the system.

In Figure 6.1, we plot $y(t)$, as a functions of t and show the interval up to $t = 5$, where the power series is expanded up to $n_{max} = 8$, the iteration number $I = 10000$, and $\Delta = 0.002$. The figure shows also the quick divergence of the zeroth iterative power series expansion, while the power series is expanded up to $n_{max} = 20$. In Figure 6.2 we combine the three Lorenz variables, where we used same parameters as Figure 6.1.

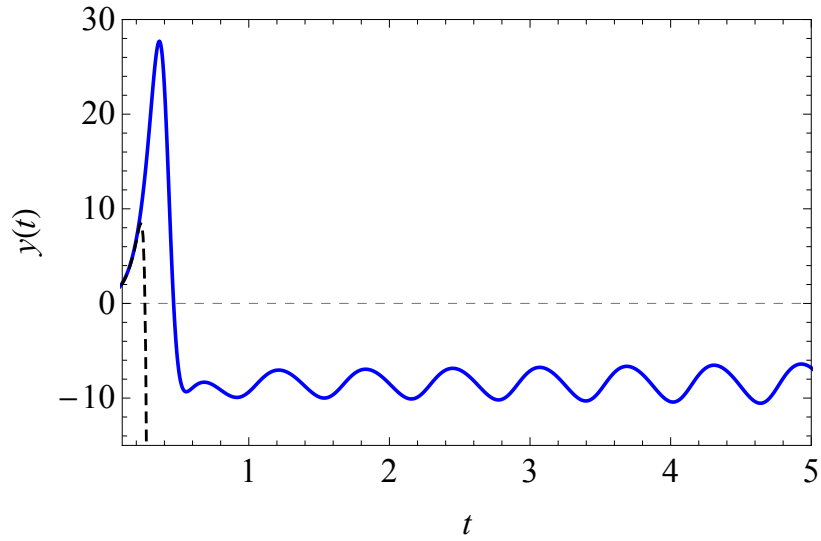


Figure 6.1: Trajectory, $y(t)$ (blue), of the chaotic Lorenz model with $\text{Pr} = 10$, $\text{Ra} = 28$, and $\gamma = 8/3$ and initial condition $(a_0^0, b_0^0, c_0^0) = (0, 1, 0)$. The power series is expanded up to $n_{\max} = 8$, with $I = 10000$ and $\Delta = 0.002$. The dashed curve represents the zeroth order series solution with $n_{\max} = 20$.

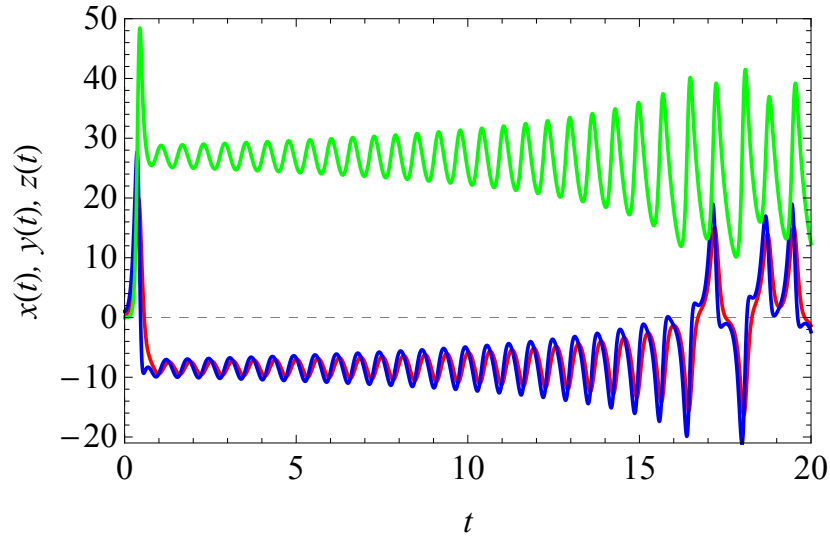


Figure 6.2: Trajectories, $x(t)$ (red), $y(t)$ (blue), and $z(t)$ (green) of the chaotic Lorenz model with $\text{Pr} = 10$, $\text{Ra} = 28$, and $\gamma = 8/3$ and initial condition $(a_0^0, b_0^0, c_0^0) = (0, 1, 0)$. The power series is expanded up to $n_{\max} = 8$, with $I = 10000$ and $\Delta = 0.002$.

It is well-known that the Lorenz system does not admit a closed form solution. Comparing our result with another numerical method such as ERK4 will not be decisive. Instead, we will manipulate the iteration number, I , in a systematic way to show the

systematic control on accuracy of the IPS method. This systematic analysis is illustrated in Figures 6.3-6.5. In Figure 6.3, we show two solutions with two different values of Δ associated with $I = 7500$ and 8000 . We believe that the obtained solution using $I = 8000$ is more accurate than the one obtained by $I = 7500$. A clear sign on this is mentioned in Eq. (4.12) where a systematic reduction upon increasing the number of iterations or the number of terms in the power series is achieved. The two solutions are overlapping up to just less than $t = 40$ and then they split. As a consequence, in Figure 6.4 we again plot two solutions with two different Δ associated with $I = 8000$ and 8500 . Here, the two solutions are overlapping just above $t = 40$ and then they split. Notice that, the overlapping length is increasing as Δ decreases. We have enough confidence to assert that the overlapping part represents a true behaviour of the solution since the three curves concurred to it. If we now employ the ERK4, Figure 6.5, one can observe that its solution overlaps with the IPS solution, $I = 8000$, just up to about $t = 38$, which boosts our beliefs.

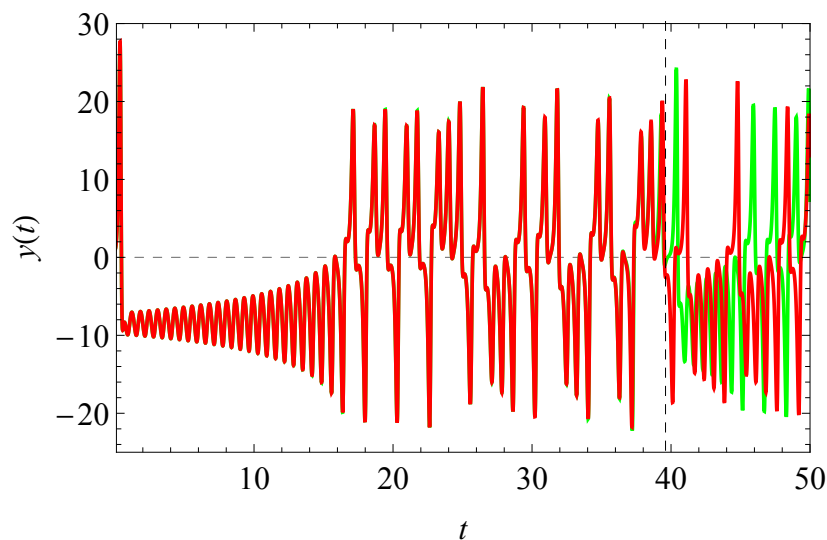


Figure 6.3: Two $y(t)$ solutions of the Lorenz system with $Pr = 10$, $Ra = 28$, $\gamma = 8/3$ and the initial conditions $(a_0^0, b_0^0, c_0^0) = (0, 1, 0)$. The IPS solutions are expanded up to $n_{max} = 8$, with $I = 7500$ (green curve) and with $I = 8000$ (red curve).

Next, we study the sensitivity to initial conditions of the Lorenz system by plotting two

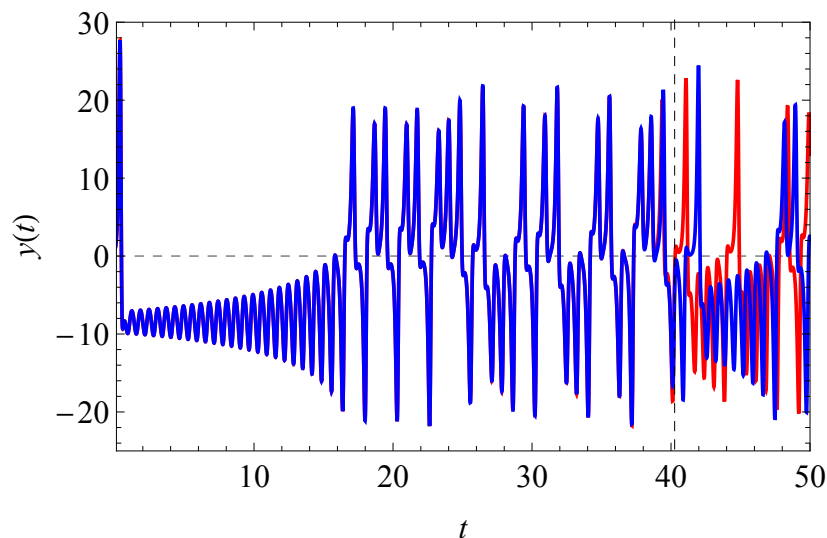


Figure 6.4: Two $y(t)$ solutions of the Lorenz system with $\text{Pr} = 10$, $\text{Ra} = 28$, $\gamma = 8/3$ and the initial conditions $(a_0^0, b_0^0, c_0^0) = (0, 1, 0)$. The IPS solutions are expanded up to $n_{\max} = 8$, with $I = 8000$ (red curve) and with $I = 8500$ (blue curve).

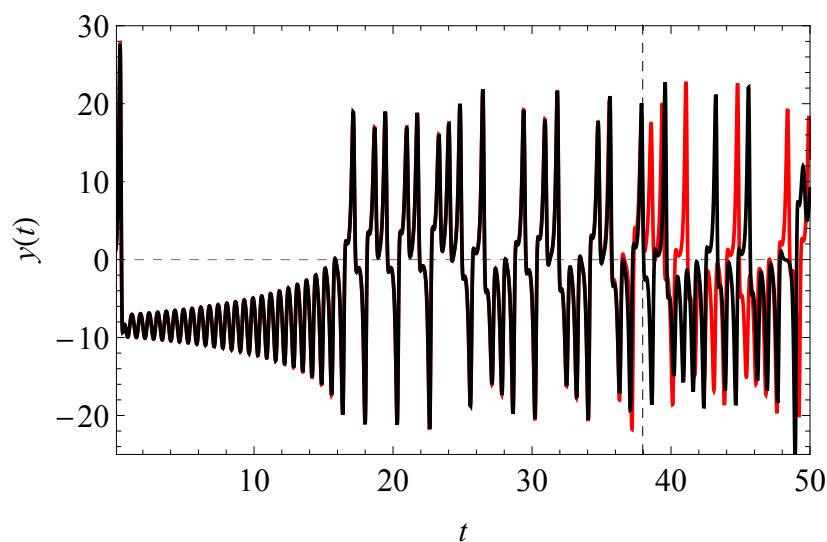


Figure 6.5: Two $y(t)$ solutions of the Lorenz system with $\text{Pr} = 10$, $\text{Ra} = 28$, $\gamma = 8/3$ and the initial conditions $(a_0^0, b_0^0, c_0^0) = (0, 1, 0)$. The IPS solution is expanded up to $n_{\max} = 8$, with $I = 8000$ (red curve) and The ERK4 solution (black curve).

evaluations of $y(t)$ in Figure 6.6 that are differing by only 0.0001. The time range is $t \in (0, 50]$, with $I = 1000$, $\Delta = 0.005$, and $n_{\max} = 8$. The two solutions behave identically in the range of $t \in (0, 30)$, but, the difference is notable after that.

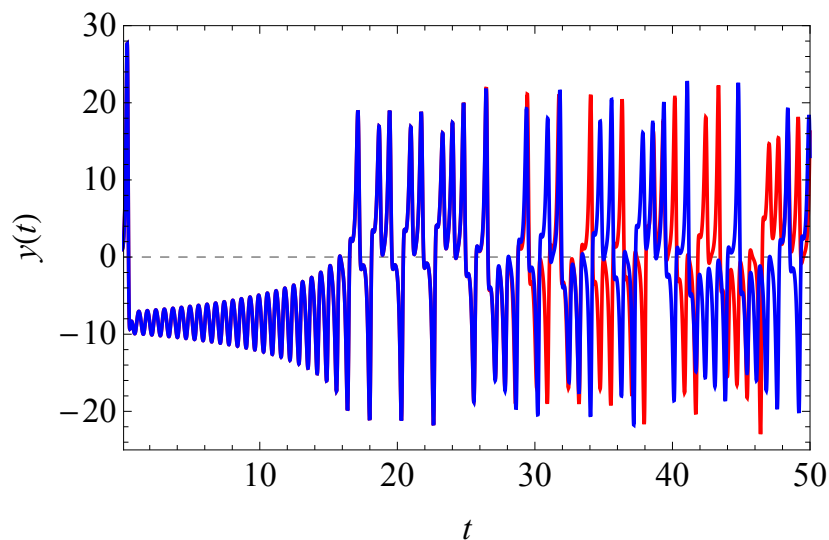


Figure 6.6: Two $y(t)$ solutions of the Lorenz system with $\text{Pr} = 10$, $\text{Ra} = 28$, and $\gamma = 8/3$ and the initial conditions $(a_0^0, b_0^0, c_0^0) = (0, 1, 0)$ (blue), and $(0, 1.0001, 0)$ (red). The power series is expanded up to $n_{max} = 8$, with $I = 10000$ and $\Delta = 0.005$.

Furthermore, Lorenz discovered that the phase space of any two variables will lead to the same strange structure later named as Lorenz's butterfly or Lorenz attractor. In the Lorenz's butterfly, the two solutions wind around two points alternatively. He concluded that all solutions tend to this same complicated attractor. He had a trajectory look at this phase space in a two-dimensional plane, and found a repeatedly cross between the two solutions, however, he noted that the intersection between the two solutions never occurs in the three-dimensional trajectory picture.

Finally, we end up our discussion with Figure 6.7 which presents three Lorenz attractors with $I = 10000$, $\Delta = 0.003$, and $n_{max} = 8$.

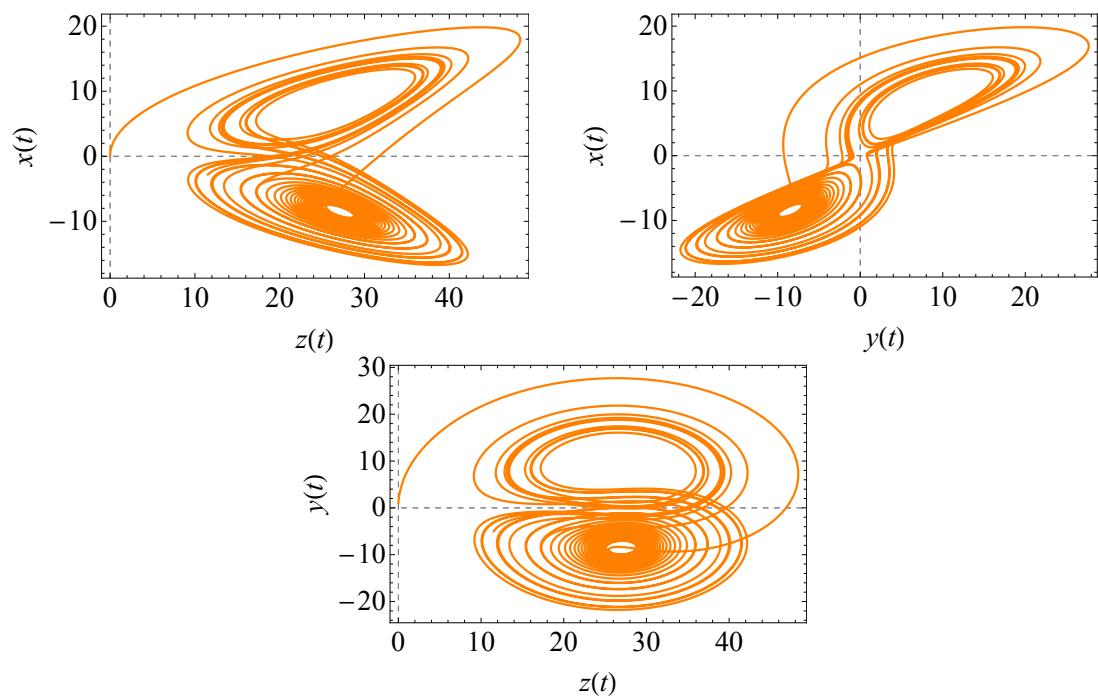


Figure 6.7: Three chaotic projections of the phase space of the Lorenz system with $Pr = 10$, $Ra = 28$, and $\gamma = 8/3$ and initial condition $(a_0^0, b_0^0, c_0^0) = (0, 1, 0)$. The power series is expanded up to $n_{max} = 8$, $I = 10000$ and $\Delta = 0.003$ for $t \in (0, 30]$.

Chapter 7: Conclusions and Future Remarks

In this thesis, we presented a new numerical technique for solving nonlinear BVPs based on iterative power series solutions. This technique is a modified version of the PS method. We called it the iterative power series (IPS) method. We have demonstrated its efficiency and accuracy throughout several nonlinear physical systems. We have shown that our method excels over the ERK4 by orders of magnitude in accuracy. Moreover, the accuracy in our method is systematically controlled such that the error can be reduced to any arbitrary small value.

In chapter 4, we demonstrated the present technique by applying it to three interesting versions of the NLSE. First, we found the solitonic solution of the fundamental NLSE and compared it with its well-known exact form. The result of the comparison emphasized the power of the IPS method where the difference between the two techniques was in the range of 3×10^{-15} for $I = 1000$, $\Delta = 0.005$, and $n_{max} = 8$. Next, we found the solitonic solution of the NLSE with power law nonlinearity. Here, we compared the IPS result with the exact solution found from the separation of variables method in chapter 3. The difference was in the range of 1×10^{-14} for $I = 1000$, $\Delta = 0.005$, and $n_{max} = 8$. The last considered system in this chapter was the nonintegrable form of the higher order NLSE. We reached to well approximated oscillating and localized solutions. The localized solution was compared with the solitonic solution of the fundamental NLSE.

In chapter 5, we successfully studied the unsteady viscous flow over a contracting cylinder using the IPS technique. The velocity and temperature profiles of the ordinary version of Navier-Stokes equations in the ranges $0 \leq \gamma \leq 7$ and $-4 \leq S \leq 0$ at $Pr = 0.7$ were obtained. Moreover, we analyzed the normalized skin friction coeffi-

cient, $f''(1)$, and the normalized heat transfer rate, $-\theta'(1)$. The IPS results showed its efficiency compared to the ERK4.

The Last considered model was mentioned in chapter 6. Here, we succeeded in employing the IPS method to the Lorenz system and figured out the evaluations of its three variables in the chaotic regime. We also constructed the Lorenz attractors using the IPS method.

The IPS method could be extended to PDEs. This will be worth working on in order to find out some interesting traveling solutions of such equations.

The convergence of the IPS method is considered for a future work. Although we do not have a solid proof yet, we strongly believe that the method is convergent. This is conjectured by the systematic reduction in error upon increasing the number of iterations or the number of terms in the power series.

We believe this technique will serve researchers in different fields working on nonlinear systems. In particular, the technique will be very useful for systems described by nonintegrable nonlinear differential equations.

References

- [1] Adomian, G., 1994. The decomposition method. Solving Frontier Problems of Physics Kluwer, Boston, MA.
- [2] Shabat, A. and Zakharov, V., 1972. Exact theory of two-dimensional self-focusing and one-dimensional self-modulation of waves in nonlinear media. Soviet physics JETP, 34(1), p.62.
- [3] Gardner, C.S., Greene, J.M., Kruskal, M.D. and Miura, R.M., 1967. Method for solving the Korteweg-deVries equation. Physical Review Letters, 19(19), p.1095.
- [4] Levitan, B.M., 1987. Inverse Sturm-Liouville Problems. VSP.
- [5] Liao, S.J., 1999. An explicit, totally analytic approximate solution for Blasius viscous flow problems. International Journal of Non-Linear Mechanics, 34(4), pp.759-778.
- [6] Liao, S., 2004. On the homotopy analysis method for nonlinear problems. Applied Mathematics and Computation, 147(2), pp.499-513.
- [7] Fairen, V., Lopez, V. and Conde, L., 1988. Power series approximation to solutions of nonlinear systems of differential equations. American Journal of Physics, 56(1), pp.57-61.
- [8] Lopez-Sandoval, E., Mello, A., Godina-Nava, J.J. and Samana, A.R., 2015, October. Power series solution for solving nonlinear burgers-type equations. In Abstract and Applied Analysis (Vol. 2015). Hindawi Publishing Corporation.
- [9] Lopez-Sandoval, E., Mello, A. and Nava, J.J., 2012. Power series solution to non-linear partial differential equations of mathematical physics. arXiv preprint arXiv:1206.2346.

- [10] Nuseir, A.S. and Al-Hasson, A., 2012. Power series solution for nonlinear system of partial differential equations. *Applied Mathematical Sciences*, 6(104), pp.5147-5159.
- [11] Pickett, R.C., Lindgren, G.E. and Anderson, R.K., 1993. Power series solution of linear and nonlinear partial differential equations via symbolic programming. *Computers in Physics*, 7(1), pp.108-111.
- [12] Scraton, R.E., 1969, July. A note on the summation of divergent power series. In *Mathematical Proceedings of the Cambridge Philosophical Society* (Vol. 66, No. 1, pp. 109-114). Cambridge University Press.
- [13] Corliss, G. and Chang, Y.F., 1982. Solving ordinary differential equations using Taylor series. *ACM Transactions on Mathematical Software (TOMS)*, 8(2), pp.114-144.
- [14] Chang, Y.F. and Corliss, G., 1994. ATOMFT: solving ODEs and DAEs using Taylor series. *Computers and Mathematics with Applications*, 28(10-12), pp.209-233.
- [15] Barrio, R. and Blesa, F., 2009. Systematic search of symmetric periodic orbits in 2DOF Hamiltonian systems. *Chaos, Solitons and Fractals*, 41(2), pp.560-582.
- [16] Barrio, R., Blesa, F. and Serrano, S., 2009. Periodic, escape and chaotic orbits in the Copenhagen and the $(n+1)$ -body ring problems. *Communications in Nonlinear Science and Numerical Simulation*, 14(5), pp.2229-2238.
- [17] Barrio, R., 2006. Painting chaos: a gallery of sensitivity plots of classical problems. *International Journal of Bifurcation and Chaos*, 16(10), pp.2777-2798.
- [18] Barrio, R. and Serrano, S., 2007. A three-parametric study of the Lorenz model. *Physica D: Nonlinear Phenomena*, 229(1), pp.43-51.
- [19] Jorba, Á. and Zou, M., 2005. A software package for the numerical integration of ODEs by means of high-order Taylor methods. *Experimental Mathematics*,

- 14(1), pp.99-117.
- [20] Fibich, G., 2015. The nonlinear Schrödinger equation: singular solutions and optical collapse (Vol. 192). Springer.
- [21] Litvak, A.G. and Sergeev, A.M., 1978. One dimensional collapse of plasma waves. JETP lett, 27(10), pp.549-553.
- [22] Agrawal, G.P., 2011. Nonlinear fiber optics: its history and recent progress. JOSA B, 28(12), pp.A1-A10.
- [23] Garanovich, I.L., Longhi, S., Sukhorukov, A.A. and Kivshar, Y.S., 2012. Light propagation and localization in modulated photonic lattices and waveguides. Physics Reports, 518(1), pp.1-79.
- [24] Kivshar, Y.S. and Agrawal, G., 2003. Optical solitons: from fibers to photonic crystals. Academic press.
- [25] Hasegawa, A., 2000. An historical review of application of optical solitons for high speed communications. Chaos: An Interdisciplinary Journal of Nonlinear Science, 10(3), pp.475-485.
- [26] Russell, J.S., 1844. Report of the 14th Meeting of the British Association for the Advancement of Science, York, 1844.
- [27] Drazin, P.G. and Johnson, R.S., 1989. Solitons: an introduction (Vol. 2). Cambridge university press.
- [28] Taylor, J.R. ed., 1992. Optical solitons: theory and experiment (Vol. 10). Cambridge University Press.
- [29] Solli, D.R., Ropers, C., Koonath, P. and Jalali, B., 2007. Optical rogue waves. Nature, 450(7172), pp.1054-1057.
- [30] Dysthe, K., Krogstad, H.E. and Müller, P., 2008. Oceanic rogue waves. Annu. Rev. Fluid Mech., 40, pp.287-310.

- [31] Ankiewicz, A., Devine, N. and Akhmediev, N., 2009. Are rogue waves robust against perturbations?. *Physics Letters A*, 373(43), pp.3997-4000.
- [32] Marklund, M. and Stenflo, L., 2009. Exciting rogue waves. *Physics*, 2, p.86.
- [33] Kharif, C., Pelinovsky, E. and Slunyaev, A., 2010. *Rogue waves in the ocean*. Springer.
- [34] Wen, L., Li, L., Li, Z.D., Song, S.W., Zhang, X.F. and Liu, W.M., 2011. Matter rogue wave in Bose-Einstein condensates with attractive atomic interaction. *The European Physical Journal D-Atomic, Molecular, Optical and Plasma Physics*, 64(2), pp.473-478.
- [35] Shrira, V.I. and Geogjaev, V.V., 2010. What makes the Peregrine soliton so special as a prototype of freak waves?. *Journal of Engineering Mathematics*, 67(1), pp.11-22.
- [36] Peregrine, D.H., 1983. Water waves, nonlinear Schrödinger equations and their solutions. *The ANZIAM Journal*, 25(1), pp.16-43.
- [37] Ma, Y.C., 1979. The Perturbed Plane-Wave Solutions of the Cubic Schrödinger Equation. *Studies in Applied Mathematics*, 60(1), pp.43-58.
- [38] Akhmediev, N., Eleonskii, V.M. and Kulagin, N.E., 1985. Generation of periodic trains of picosecond pulses in an optical fiber: exact solutions. *Sov. Phys. JETP*, 62(5), pp.894-899.
- [39] Akhmediev, N.N. and Korneev, V.I., 1986. Modulation instability and periodic solutions of the nonlinear Schrödinger equation. *Theoretical and Mathematical Physics*, 69(2), pp.1089-1093.
- [40] Akhmediev, N.N., Eleonskii, V.M. and Kulagin, N.E., 1987. Exact first-order solutions of the nonlinear Schrödinger equation. *Theoretical and mathematical physics*, 72(2), pp.809-818.

- [41] Guo, B., Tian, L., Yan, Z., Ling, L. and Wang, Y., 2017. Rogue waves: Mathematical theory and applications in Physics. Walter de Gruyter GmbH and Co KG.
- [42] Carretero-Gonzalez, R., Frantzeskakis, D.J. and Kevrekidis, P.G., 2008. Nonlinear waves in Bose-Einstein condensates: physical relevance and mathematical techniques. *Nonlinearity*, 21(7), p.R139.
- [43] Bludov, Y.V., Konotop, V.V. and Akhmediev, N., 2009. Matter rogue waves. *Physical Review A*, 80(3), p.033610.
- [44] Heimbarg, T. and Jackson, A.D., 2005. On soliton propagation in biomembranes and nerves. *Proceedings of the National Academy of Sciences of the United States of America*, 102(28), pp.9790-9795.
- [45] Mollenauer, L.F. and Gordon, J.P., 2006. Solitons in optical fibers: fundamentals and applications. Academic Press.
- [46] Al Khawaja, U., 2010. Stability and dynamics of two-soliton molecules. *Physical Review E*, 81(5), p.056603.
- [47] Kibler, B., Fatome, J., Finot, C., Millot, G., Genty, G., Wetzel, B., Akhmediev, N., Dias, F. and Dudley, J.M., 2012. Observation of Kuznetsov-Ma soliton dynamics in optical fibre. *Scientific reports*, 2, p.463.
- [48] Hasegawa, A. and Kodama, Y., 1995. Solitons in optical communications (No. 7). Oxford University Press, USA.
- [49] Wazwaz, A.M., 2006. Reliable analysis for nonlinear Schrödinger equations with a cubic nonlinearity and a power law nonlinearity. *Mathematical and Computer Modelling*, 43(1), pp.178-184.
- [50] Triki, H., Hayat, T., Aldossary, O.M. and Biswas, A., 2012. Bright and dark solitons for the resonant nonlinear Schrödinger's equation with time-dependent coefficients. *Optics and Laser Technology*, 44(7), pp.2223-2231.

- [51] Taghizadeh, N., Mirzazadeh, M. and Paghaleh, A.S., 2012. Exact solutions for the nonlinear Schrödinger equation with power law nonlinearity. *Math. Sci. Lett.*, 1(1), pp.7-16.
- [52] Ye, J. and Zheng, C., 2012. Exact Projective Excitations of Nonautonomous Nonlinear Schrödinger System in $(1+ 1)$ -Dimensions. *Journal of Modern Physics*, 3(08), p.702.
- [53] Zhao, D., He, X.G. and Luo, H.G., 2009. Transformation from the nonautonomous to standard NLS equations. *The European Physical Journal D*, 53(2), pp.213-216.
- [54] Pérez-García, V.M., Torres, P.J. and Konotop, V.V., 2006. Similarity transformations for nonlinear Schrödinger equations with time-dependent coefficients. *Physica D: Nonlinear Phenomena*, 221(1), pp.31-36.
- [55] Kundu, A., 2009. Integrable nonautonomous nonlinear Schrödinger equations are equivalent to the standard autonomous equation. *Physical Review E*, 79(1), p.015601.
- [56] Kruglov, V.I., Peacock, A.C. and Harvey, J.D., 2003. Exact self-similar solutions of the generalized nonlinear Schrödinger equation with distributed coefficients. *Physical Review Letters*, 90(11), p.113902.
- [57] Al Khawaja, U. and Boudjemâa, A., 2012. Binding energy of soliton molecules in time-dependent harmonic potential and nonlinear interaction. *Physical Review E*, 86(3), p.036606.
- [58] He, X.G., Zhao, D., Li, L. and Luo, H.G., 2009. Engineering integrable nonautonomous nonlinear Schrödinger equations. *Physical Review E*, 79(5), p.056610.
- [59] Lax, P.D., 1968. Integrals of nonlinear equations of evolution and solitary waves. *Communications on pure and applied mathematics*, 21(5), pp.467-490.

- [60] Matveev, V.B., 1979. Darboux transformation and explicit solutions of the Kadomtcev-Petviashvili equation, depending on functional parameters. *Letters in Mathematical Physics*, 3(3), pp.213-216.
- [61] Al Khawaja, U., 2009. Soliton localization in Bose-Einstein condensates with time-dependent harmonic potential and scattering length. *Journal of Physics A: Mathematical and Theoretical*, 42(26), p.265206.
- [62] Guo, B., Ling, L. and Liu, Q.P., 2012. Nonlinear Schrödinger equation: generalized Darboux transformation and rogue wave solutions. *Physical Review E*, 85(2), p.026607.
- [63] Al Khawaja, U. and Taki, M., 2013. Rogue waves management by external potentials. *Physics Letters A*, 377(41), pp.2944-2949.
- [64] Al Khawaja, U., 2007. Exact solitonic solutions of the Gross-Pitaevskii equation with a linear potential. *Physical Review E*, 75(6), p.066607.
- [65] Al Khawaja, U., 2006. Lax pairs of time-dependent Gross-Pitaevskii equation. *Journal of Physics A: Mathematical and General*, 39(31), p.9679.
- [66] Salle, M.A. and Matveev, V.B., 1991. Darboux transformations and solitons.
- [67] Ling, L. and Zhao, L.C., 2013. Simple determinant representation for rogue waves of the nonlinear Schrödinger equation. *Physical Review E*, 88(4), p.043201.
- [68] He, J., Guo, L., Zhang, Y. and Chabchoub, A., 2014, November. Theoretical and experimental evidence of non-symmetric doubly localized rogue waves. In *Proc. R. Soc. A* (Vol. 470, No. 2171, p. 20140318). The Royal Society.
- [69] He, J., Xu, S. and Cheng, Y., 2015. The rational solutions of the mixed nonlinear Schrödinger equation. *AIP Advances*, 5(1), p.017105.
- [70] Degasperis, A. and Lombardo, S., 2013. Rational solitons of wave resonant-interaction models. *Physical Review E*, 88(5), p.052914.

- [71] Wang, L.H., Porsezian, K. and He, J.S., 2013. Breather and rogue wave solutions of a generalized nonlinear Schrödinger equation. *Physical Review E*, 87(5), p.053202.
- [72] Yong, X., Wang, G., Li, W., Huang, Y. and Gao, J., 2017. On the Darboux transformation of a generalized inhomogeneous higher-order nonlinear Schrödinger equation. *Nonlinear Dynamics*, 87(1), pp.75-82.
- [73] Wang, L., Zhang, J.H., Liu, C., Li, M. and Qi, F.H., 2016. Breather transition dynamics, Peregrine combs and walls, and modulation instability in a variable-coefficient nonlinear Schrödinger equation with higher-order effects. *Physical Review E*, 93(6), p.062217.
- [74] Chowdury, A., Kedziora, D.J., Ankiewicz, A. and Akhmediev, N., 2015. Breather solutions of the integrable quintic nonlinear Schrödinger equation and their interactions. *Physical Review E*, 91(2), p.022919.
- [75] Gedalin, M., Scott, T.C. and Band, Y.B., 1997. Optical solitary waves in the higher order nonlinear Schrödinger equation. *Physical review letters*, 78(3), p.448.
- [76] Yan, Z. and Dai, C., 2013. Optical rogue waves in the generalized inhomogeneous higher-order nonlinear Schrödinger equation with modulating coefficients. *Journal of Optics*, 15(6), p.064012.
- [77] Hong, W.P., 2003. New solitary-wave solutions for the higher order nonlinear Schrödinger equation with both real and imaginary Raman terms. *Zeitschrift für Naturforschung A*, 58(12), pp.667-671.
- [78] Weidman, P.D., Kubitschek, D.G. and Davis, A.M.J., 2006. The effect of transpiration on self-similar boundary layer flow over moving surfaces. *International journal of engineering science*, 44(11), pp.730-737.
- [79] Zaimi, K., Ishak, A. and Pop, I., 2014. Unsteady flow due to a contracting cylinder.

- der in a nanofluid using Buongiorno's model. *International Journal of Heat and Mass Transfer*, 68, pp.509-513.
- [80] Fang, T., Zhang, J. and Zhong, Y., 2012. Note on unsteady viscous flow on the outside of an expanding or contracting cylinder. *Communications in Nonlinear Science and Numerical Simulation*, 17(8), pp.3124-3128.
- [81] Elnajjar, E.J., Al-Mdallal, Q.M. and Allan, F.M., 2016. Unsteady Flow and Heat Transfer Characteristics of Fluid Flow Over a Shrinking Permeable Infinite Long Cylinder. *Journal of Heat Transfer*, 138(9), p.091008.
- [82] Jaluria, Y. and Torrance, K.E., 2003. *Computational heat transfer*. 2nd ed. New York NY, Taylor and Francis.
- [83] Merkin, J.H., 1986. On dual solutions occurring in mixed convection in a porous medium. *Journal of engineering Mathematics*, 20(2), pp.171-179.
- [84] Paullet, J. and Weidman, P., 2007. Analysis of stagnation point flow toward a stretching sheet. *International Journal of Non-Linear Mechanics*, 42(9), pp.1084-1091.
- [85] Harris, S.D., Ingham, D.B. and Pop, I., 2009. Mixed convection boundary-layer flow near the stagnation point on a vertical surface in a porous medium: Brinkman model with slip. *Transport in Porous Media*, 77(2), pp.267-285.
- [86] Postelnicu, A. and Pop, I., 2011. Falkner-Skan boundary layer flow of a power-law fluid past a stretching wedge. *Applied Mathematics and Computation*, 217(9), pp.4359-4368.
- [87] Rosca, A.V. and Pop, I., 2013. Flow and heat transfer over a vertical permeable stretching/shrinking sheet with a second order slip. *International Journal of Heat and Mass Transfer*, 60, pp.355-364.
- [88] Ishak, A., Nazar, R. and Pop, I., 2008. Uniform suction/blowing effect on flow and heat transfer due to a stretching cylinder. *Applied Mathematical Modelling*,

32(10), pp.2059-2066.

- [89] Bachok, N., Ishak, A. and Pop, I., 2012. Boundary layer stagnation-point flow and heat transfer over an exponentially stretching/shrinking sheet in a nanofluid. *International Journal of Heat and Mass Transfer*, 55(25), pp.8122-8128.
- [90] Ishak, A., Lok, Y.Y. and Pop, I., 2010. Stagnation-point flow over a shrinking sheet in a micropolar fluid. *Chemical Engineering Communications*, 197(11), pp.1417-1427.
- [91] Yacob, N.A., Ishak, A. and Pop, I., 2011. Melting heat transfer in boundary layer stagnation-point flow towards a stretching/shrinking sheet in a micropolar fluid. *Computers and Fluids*, 47(1), pp.16-21.
- [92] Wang, C.Y., 2008. Stagnation flow towards a shrinking sheet. *International Journal of Non-Linear Mechanics*, 43(5), pp.377-382.
- [93] Bachok, N., Ishak, A. and Pop, I., 2012. Unsteady boundary-layer flow and heat transfer of a nanofluid over a permeable stretching/shrinking sheet. *International Journal of Heat and Mass Transfer*, 55(7), pp.2102-2109.
- [94] Zhong, Y. and Fang, T., 2011. Unsteady stagnation-point flow over a plate moving along the direction of flow impingement. *International Journal of Heat and Mass Transfer*, 54(15), pp.3103-3108.
- [95] Bhattacharyya, K., Mukhopadhyay, S. and Layek, G.C., 2011. Slip effects on boundary layer stagnation-point flow and heat transfer towards a shrinking sheet. *International Journal of Heat and Mass Transfer*, 54(1), pp.308-313.
- [96] Aman, F. and Ishak, A., 2012. Mixed convection boundary layer flow towards a vertical plate with a convective surface boundary condition. *Mathematical Problems in Engineering*, 2012.
- [97] Bachok, N., Ishak, A. and Pop, I., 2013. Stagnation point flow toward a stretching/shrinking sheet with a convective surface boundary condition. *Journal of the*

Franklin Institute, 350(9), pp.2736-2744.

- [98] Rong, C.G. and Ning, D.X., 1998. From chaos to order: methodologies, perspectives and applications. World Scientific.
- [99] Lü, J., Lu, J.A. and Chen, S.H., 2002. Chaotic time series analysis and its applications. Wuhan: Wuhan University Publication.
- [100] Strogatz, S.H., 2014. Nonlinear dynamics and chaos: with applications to physics, biology, chemistry, and engineering. Hachette UK.
- [101] Lorenz, E.N., 1963. Deterministic nonperiodic flow. Journal of the atmospheric sciences, 20(2), pp.130-141.

Appendix

Hindawi
Complexity
Volume 2018, Article ID 8269541, 11 pages
<https://doi.org/10.1155/2018/8269541>



Research Article

A Numerical Algorithm for Solving Higher-Order Nonlinear BVPs with an Application on Fluid Flow over a Shrinking Permeable Infinite Long Cylinder

Laila Y. Al Sakkaf,¹ Qasem M. Al-Mdallal²,² and U. Al Khawaja¹

¹Department of Physics, United Arab Emirates University, P.O. Box 15551, AlAin, UAE

²Department of Mathematical Sciences, United Arab Emirates University, P.O. Box 15551, AlAin, UAE

Correspondence should be addressed to Qasem M. Al-Mdallal; q.almdallal@uaeu.ac.ae

Received 5 November 2017; Accepted 12 February 2018; Published 12 March 2018

Academic Editor: Mohamed Belhaq

Copyright © 2018 Laila Y. Al Sakkaf et al. This is an open access article distributed under the Creative Commons Attribution License, which permits unrestricted use, distribution, and reproduction in any medium, provided the original work is properly cited.

We present an efficient iterative power series method for nonlinear boundary-value problems that treats the typical divergence problem and increases arbitrarily the radius of convergence. This method is based on expanding the solution around an iterative initial point. We employ this method to study the unsteady, viscous, and incompressible laminar flow and heat transfer over a shrinking permeable cylinder. More precisely, we solve the unsteady nonlinear Navier–Stokes and energy equations after reducing them to a system of nonlinear boundary-value problems of ordinary differential equations. The present method successfully captures dual solutions for both the flow and heat transfer fields and a unique solution at a specific critical unsteadiness parameter. Comparisons with previous numerical methods and an exact solution verify the validity, accuracy, and efficiency of the present method.

1. Introduction

Numerous phenomena in engineering and applied science fields are governed by nonlinear boundary-value problems (BVPs). Therefore, BVPs have received a huge attention from mathematicians, physicists, and engineers for the sake of finding and analyzing their solutions. Generally speaking, finding the analytical solutions for nonlinear BVPs is far from trivial and often is impossible. Therefore, many numerical techniques have been developed to solve such type of problems. These methods include Adomian's decomposition method, homotopy perturbation method, variational iteration method, optimal homotopy asymptotic method, operational matrices techniques based on various orthogonal polynomials and wavelets, finite difference method, and spectral methods; the reader is referred to [1–6] and references therein.

The fluid dynamics and heat transfer of a viscous incompressible fluid flowing past stretching surfaces, such as a sheet or tube, have attracted considerable interests of many researchers because of their importance in many industrial applications such as the quality of certain products. One

of the most interesting conditions for stretching surfaces problems is the velocity at the surface, where it mainly figures the characteristics of the fluid based upon two essential factors, fluid viscosity and suction parameter. A remarkable interest of several researchers concentrated on tracking the existence of dual solutions for the flow within a certain range of unsteadiness and suction parameters [7–17]. Although, the literature reveals numerous research papers discussing the flow over a stretching sheet and moving plate [18–26], there are only few studies focusing on the problem of flowing past a stretching cylinder or tube; see [8–10] and references therein.

It is established that the differential equations describing the fluid flow BVPs are highly nonlinear and demand extremely accurate numerical schemes. In this work, we show that an iterative procedure, based on successive power series expansions, provides one such high accuracy numerical scheme. Often, using power series solutions turns to be useless because the resulting solution diverges at a finite radius of convergence. The divergence is intrinsic to the nature of the solution in the sense that it persists to exist even with an infinite power series expansion. The method presented here

solves this problem showing that the radius of convergence can be delayed arbitrarily to any large value. This value could, in principle, approach infinity achieving exact solutions.

Among the many different methods of solving nonlinear differential equations [27–33], the power series method is the most straight forward and efficient [34]. It has been used as a powerful numerical scheme for many problems [35–43] including chaotic systems [44–47]. Many numerical algorithms and codes have been developed based on this method [34–36, 44–48]. However, the abovementioned finiteness of radius of convergence is a serious problem that hinders the use of this method to wide class of differential equations, in particular the nonlinear ones. For instance, the nonlinear Schrödinger equation (NLSE) with cubic nonlinearity has $\text{sech}(x)$ as a solution. Using the power series method to solve this equation produces the power series of $\text{sech}(x)$, which is valid only for $x < \pi/2$.

Recognizing that a powerful numerical scheme based on this method is already established [34–36, 44–48], we nonetheless present a thorough investigation of the error associated with this method with the aim of showing how we can systemically reduce errors to infinitesimal values while having the Central Processing Unit (CPU) time within a reasonable range. We will show robustness and efficiency of the method via a highly demanding fluid flow boundary-value problem. Therefore, solving the problem of finite radius of convergence will open the door wide for applying the power series method to much larger class of differential equations, particularly the nonlinear ones.

Briefly, the present technique is based on iterative power series expansions of the solution. The domain of the independent variable, say η , is divided into a number I of segments each of width Δ , where Δ is smaller than the radius of convergence. A power series solution is obtained by expanding the solution around the left end of the first segment using the initial conditions given with the problem. Similarly, a power series solution is obtained by expanding around the start of the second segment but now using the first series to calculate the initial conditions. This is repeated I times till a solution at $\eta = I \times \Delta$ is obtained. In the limit $I \rightarrow \infty$ and $\Delta \rightarrow 0$ the series solution becomes an exact solution. This scheme is effectively equivalent to an iterative procedure of repeated iterative calculation of the recursion relations of the power series in the first segment. Another aim of this paper is to apply this method to study the unsteady flow and heat transfer characteristics of fluid flow over a shrinking permeable infinite long cylinder. We will show that the iterative numerical scheme resulting from this method is exceeding the efficiency of typical numerical methods used. In addition, we managed to find an exact solution which enabled us to calculate accurately the error for a finite value of number of iterations I . It should be noted that the present work is a part of the Master thesis [49].

The rest of the paper is organized as follows. In Section 2, a mathematical representation of our method is illustrated using a general form of nonlinear ordinary differential equation, while henceforth we call it *iterative power series method*. Sections 3 and 4 display the implementation of the iterative power series method on the heat and mass

transfer model. Section 5 focuses on analyzing the validity of this present technique and demonstrating its efficiency by drawing comparisons with the achieved exact analytical solution and other numerical methods. In Section 6, we analyze and discuss the properties of the solutions obtained. We end with a summary of our main conclusions in Section 7.

2. General Scheme of the Iterative Power Series (IPS) Method

In this section, we give a brief description of the present method. Consider a general ordinary differential equation of the form

$$F[f(\eta), f'(\eta), f''(\eta), \dots, f^{(m)}(\eta), g(\eta)] = 0, \quad (1)$$

$$\eta \in (\eta_0, \eta_{\infty}],$$

with m initial conditions

$$f^{(i)}(\eta_0) = a_i \times i!, \quad i = 0, 1, 2, \dots, m-1, \quad (2)$$

where $f^{(i)}$ is the i th derivative of $f(\eta)$, a_i are real constants, and $g(\eta)$ is a known function. The factor $i!$ is introduced, without loss of generality, for the constants a_i to correspond to the coefficients of the power series expansion below. At first, we divide the interval $[\eta_0, \eta]$ into a number of I identical segments each of width $\Delta = (\eta - \eta_0)/I$. Then we expand $f(\eta)$ in a power series around the beginning of each interval, namely,

$$f^i(\eta) = \sum_{n=0}^{n_{\max}} a_n^i (\eta - (\eta_0 + i\Delta))^n, \quad (3)$$

$$i\Delta \leq \eta \leq (i+1)\Delta, \quad 0 \leq i < I,$$

where $f^i(\eta)$ is the power series expansion around the start of the i th segment and a_n^i are the coefficients of the power series. Recursion relations between the coefficients are obtained upon substituting the power series solution, (3), into the differential equation, (1), which can be expressed in terms of the first m coefficients corresponding to the initial conditions

$$a_n^i = a_n^i(\{a_k^i\}), \quad 0 \leq k < m, \quad n \geq m, \quad (4)$$

where $\{a_k^i\}$ denotes the set of coefficients $a_0^i, a_1^i, \dots, a_{m-1}^i$. The essential idea of the IPS method is to calculate the coefficients $\{a_k^{i+1}\}$ of the $(i+1)$ th power series from the i th series according to (2),

$$a_k^{i+1} = \frac{1}{k!} \frac{d^k}{d\eta^k} f^i(\eta) \Big|_{\eta=\eta_0+(i+1)\Delta}, \quad (5)$$

which upon using (3) reads

$$a_k^{i+1} = \frac{1}{k!} \sum_{n=0}^{n_{\max}} a_{n+k}^i \times \frac{d^k}{d\Delta^k} \Delta^{n+k} \quad (6)$$

Complexity

3

and is simplified to

$$a_k^{i+1} = \sum_{n=0}^{n_{\max}} a_{n+k}^i \times \binom{n+k}{k} \Delta^n \quad (7)$$

and then imposes the condition $n_{\max} > k$. Here, $\binom{n+k}{k}$ is the binomial function. The last equation is the basis for the IPS algorithm. Starting from the initial conditions $\{a_k^0\}$ for the power series of the zeroth interval, an iterative application of (7) leads to the coefficients of the I th interval, namely, $\{a_k^I\}$ which give the solution at the desired point, $\eta = \eta_0 + I\Delta$,

$$f^I(\eta) = \sum_{n=0}^{n_{\max}} a_n^I \times (\eta - (\eta_0 + I\Delta))^n. \quad (8)$$

Both analytical and numerical schemes may be deduced from this algorithm. For the numerical scheme, the value of Δ used is inserted as a number $\Delta = (\eta_{\infty} - \eta_0)/I$. On the other hand, leaving η as a variable results in an analytical solution in terms of a power series in η which is equivalent to a functional transformation on the zeroth order series; that is, the coefficients of the i th series are functional transformation of the $(i-1)$ th series. In such a case the last power series for the I th interval corresponds to I such that functional transformations and all power series expansions of the zeroth up to $(I-1)$ th intervals will be included in the I th expansion.

The coefficient a_n^I of each i th expansion represents the value of the solution at $\eta = \eta_0 + i\Delta$, which gives a discrete representation of $f(\eta)$. Therefore, in the limit $I \rightarrow \infty$, the discrete representation turns to a continuous one and thus we conjecture that the exact solution is obtained in the limits of $I \rightarrow \infty$ and $n_{\max} \rightarrow \infty$

$$f(\eta) = \lim_{I \rightarrow \infty} \sum_{n=0}^{\infty} a_n^I \times (\eta - (\eta_0 + I\Delta))^n. \quad (9)$$

3. Heat and Mass Transfer Model

In this section we will employ the present numerical technique on heat and mass transfer over a shrinking permeable cylinder described in Zaimi et al. [8] and Elnajjar et al. [10]. For completeness, we redescribe precisely the physical model. The flow is considered an unsteady, laminar, viscous, and incompressible fluid with uniform velocity U and uniform temperature T_{∞} over a permeable shrinking circular cylinder. The cylinder is assumed to be infinitely long and the flow has constant properties. The diameter of the cylinder is assumed to be time dependent with the radius $a(t) = r_0 \sqrt{1 - \beta t}$, where r_0 is a positive constant, β is the constant of expansion/contraction strength, and t is the time. Clearly, the cylinder's radius is shrinking with time if β is positive and stretching with time if β is negative. Notice that since the flow is axisymmetric, the flow field should be a function of the radial coordinate, r , and the longitudinal. The governing equations for the unsteady and incompressible fluid without body force are the continuity, momentum, and

energy equations. These equations in cylindrical coordinate system, (r, z) , are given by

$$\begin{aligned} \frac{1}{r} \frac{\partial}{\partial r} (ru_r) + \frac{\partial u_z}{\partial z} &= 0, \\ \frac{\partial u_r}{\partial t} + u_r \frac{\partial u_r}{\partial r} + u_z \frac{\partial u_r}{\partial z} \\ &= -\frac{1}{\rho} \frac{\partial p}{\partial r} + \nu \left(\frac{\partial^2 u_r}{\partial r^2} + \frac{1}{r} \frac{\partial u_r}{\partial r} + \frac{\partial^2 u_r}{\partial z^2} - \frac{u_r}{r^2} \right), \\ \frac{\partial u_z}{\partial t} + u_r \frac{\partial u_z}{\partial r} + u_z \frac{\partial u_z}{\partial z} \\ &= -\frac{1}{\rho} \frac{\partial p}{\partial z} + \nu \left(\frac{\partial^2 u_z}{\partial r^2} + \frac{1}{r} \frac{\partial u_z}{\partial r} + \frac{\partial^2 u_z}{\partial z^2} \right), \\ \frac{\partial T}{\partial t} + u_r \frac{\partial T}{\partial r} &= \alpha \left(\frac{1}{r} \frac{\partial}{\partial r} \left(r \frac{\partial T}{\partial r} \right) \right), \end{aligned} \quad (10)$$

where r and z are the polar coordinates in the radial and axial directions, respectively, u_r and u_z are the fluid velocity components in the radial and axial directions, respectively, and T is the fluid temperature. The function p represents the fluid pressure and the parameters ν , ρ , and α denote the fluid viscosity, the fluid density, and the fluid thermal diffusivity, respectively. Notice that we assumed that there is no azimuthal velocity component. The assumed boundary conditions associated with (10) for the velocity components and the temperature are given by

$$\begin{aligned} u_r &= -\frac{2\nu\gamma}{r_0 \sqrt{1 - \beta t}}, \\ u_z &= -\frac{4\nu z}{r_0^2 (1 - \beta t)}, \\ T_s &= \frac{c_0}{\sqrt{1 - \beta t}} + T_{\infty} \end{aligned} \quad (11)$$

at $r = a(t)$,

$$u_z = 0,$$

$$T = T_{\infty}$$

as $r \rightarrow \infty$,

where T_s is the constant surface temperature and c_0 is a positive constant.

The similarity transformations which convert (10) into nonlinear ordinary differential equations are given by [8, 10]

$$\begin{aligned} u_r &= -\frac{2\nu}{r_0 \sqrt{1 - \beta t}} \frac{f(\eta)}{\sqrt{\eta}}, \\ u_z &= \frac{4\nu z}{r_0^2 (1 - \beta t)} f'(\eta), \\ T &= (T_s - T_{\infty}) (\theta(\eta) - T_{\infty}) + T_{\infty}, \end{aligned} \quad (12)$$

where $f'(\eta) = df/d\eta$ and η is the similarity variable given by

$$\eta = \left(\frac{r}{r_0}\right)^2 \frac{1}{1 - \beta t}. \quad (13)$$

In addition, it should be noted that f represents the dimensionless stream function and θ represents the normalized temperature. Applying the above similarity transformations, (10) and the boundary conditions (11) reduce to

$$\eta f''' + f'' + ff'' - f'^2 - S(\eta f'' + f') = 0, \quad (14)$$

$$\eta \theta'' + \theta' (1 + \text{Pr}f - \text{SPr}\eta) - \text{SPr}\theta = 0, \quad (15)$$

subject to

$$\begin{aligned} f(1) &= \gamma, \\ f'(1) &= -1, \\ f'(\infty) &= 0, \\ \theta(1) &= 1, \\ \theta(\infty) &= 0, \end{aligned} \quad (16)$$

where $S = r_0^2 \beta / 4\nu$ is the unsteadiness parameter representing the strength of contraction/expansion, $\gamma = -r_0 U / 2\nu$ is the suction parameter, and $\text{Pr} = \nu/\alpha$ is the Prandtl number.

Our main target is to solve (14) and (15), subject to the boundary conditions (16), using the present technique in the ranges $0 \leq \gamma \leq 7$ and $-4 \leq S \leq 0$ at $\text{Pr} = 0.7$. In this study, we will analyze the normalized skin friction coefficient, $f''(1)$, and the normalized heat transfer rate, $-\theta'(1)$.

4. IPS Method for Heat and Mass Transfer Model

The following is a detailed implementation of the IPS method used to solve (14) and (15) subject to the boundary conditions (16). It is worth mentioning that (14) includes only the variable f , while (15) includes both θ and f . Therefore, it is more convenient to find the variable f from (14) and then solve (15). Furthermore, for the sake of simplicity, we render (14) to an initial-value problem; that is,

$$f''' = \frac{1}{\eta} (-f'' - ff'' + f'^2 + S(\eta f'' + f')), \quad (17)$$

with

$$\begin{aligned} f(1) &= \gamma, \\ f'(1) &= -1, \\ f''(1) &= \lambda, \end{aligned} \quad (18)$$

where λ must be chosen using the shooting method [10] so that the solution satisfies the boundary condition $f'(\infty) = 0$. Notice that by setting different initial values for λ in the shooting method, dual solutions are obtained.

As mentioned in Section 2, we start by expanding $f(\eta)$ in power series around the initial point $\eta_0 = 1$

$$f^0(\eta) = \sum_{n=0}^{n_{\max}} a_n^0 (\eta - 1)^n, \quad (19)$$

and the derivatives, $f^{0'}$, $f^{0''}$, and $f^{0'''}$ can be calculated simply by differentiating this series. Substituted in (14), the coefficients, a_n^0 , for $n \geq 3$, can be found recursively in terms of the initial conditions a_0^0 , a_1^0 , and a_2^0 through the recursion relations. The first two recursion relations are given by

$$\begin{aligned} a_3^0 &= \frac{1}{6} [(a_1^0)^2 - 2a_2^0(1 + a_0^0 - S) + a_1^0 S], \\ a_4^0 &= \frac{1}{24} [(a_1^0)^2 (S - 2 - a_0^0) \\ &\quad + 2a_2^0 (2 + (a_0^0)^2 + a_0^0(3 - 2S) - S + S^2) \\ &\quad + a_1^0 (2a_2^0 + S(S - 2 - a_0^0))]. \end{aligned} \quad (20)$$

Recalculating $f^0(\eta)$, $f^{0'}(\eta)$, and $f^{0''}(\eta)$ at $\eta = 1 + \Delta$ gives

$$\begin{aligned} a_0^1 &= f^0(\Delta), \\ a_1^1 &= f^{0'}(\Delta), \\ a_2^1 &= \frac{f^{0''}(\Delta)}{2}. \end{aligned} \quad (21)$$

Now, a_0^1 , a_1^1 , and a_2^1 play the role of the initial conditions for the next series expansion, where we expand the solution and its derivatives in power series around $\eta_0 = 1 + \Delta$

$$f^1(\eta) = \sum_{n=0}^{n_{\max}} a_n^1 (\eta - (1 + \Delta))^n. \quad (22)$$

Resubstituting these power series expansions in the differential equation, we get the new recursion relations $a_n^1(a_0^1, a_1^1, a_2^1)$. The next iterative step is to calculate $f^1(\eta)$ and its first two derivatives at $\eta = 1 + 2\Delta$ which will give the initial conditions for the new power series. Repeating this process I times, the general forms of the first two recursion relations of (14) are found to be

$$\begin{aligned} a_3^I &= \frac{1}{6(1 + I\Delta)} [(a_1^I)^2 - 2a_2^I(1 + a_0^I - S - SI\Delta) \\ &\quad + a_1^I S], \end{aligned} \quad (23)$$

$$\begin{aligned} a_4^I &= \frac{1}{24(1 + I\Delta)^2} [(a_1^I)^2 (-2 - a_0^I + S + SI\Delta) \\ &\quad + a_1^I (2a_2^I(1 + I\Delta) + S(-2 - a_0^I + S + SI\Delta)) \\ &\quad + 2a_2^I (S(-1 - I\Delta) + (S + SI\Delta)^2 + 2 + (a_0^I)^2) \\ &\quad + a_0^I (3 - 2S - 2SI\Delta)], \end{aligned} \quad (24)$$

Complexity

5

where

$$\begin{aligned} a_0^I &= f^{I-1}(\Delta), \\ a_1^I &= (f^{I-1})'(\Delta), \\ a_2^I &= \frac{(f^{I-1})''(\Delta)}{2}. \end{aligned} \quad (25)$$

In summary, the IPS procedure can be reduced to the following algorithm:

$$f(\Delta) = a_0 + a_1\Delta + a_2\Delta^2 + a_3\Delta^3 + a_4\Delta^4 + O(\Delta^5), \quad (26)$$

$$a_0 = f(\Delta),$$

$$a_1 = f'(\Delta), \quad (27)$$

$$a_2 = \frac{f''(\Delta)}{2},$$

where $a_3 = a_3(a_0, a_1, a_2)$ and $a_4 = a_4(a_0, a_1, a_2)$ are the recursion relations obtained from the differential equation. We have removed the superscripts that indicate the index of the iteration for convenience. The scheme is thus described simply as follows: one starts with (26) to calculate $f(\Delta)$, followed by updating the initial conditions according to (27) and then using the updated values back in (26) and so on. The procedure has to be repeated I times with $\Delta = (\eta - 1)/I$.

Similarly, for the energy equation

$$\theta'' = \frac{1}{\eta} (-\theta' (1 + \text{Pr}f - \text{SPr}\eta) + \text{SPr}\theta), \quad (28)$$

subject to

$$\begin{aligned} \theta(1) &= 1, \\ \theta'(1) &= \sigma, \end{aligned} \quad (29)$$

where σ must be chosen using the shooting method [10] so that the solution satisfies the boundary condition $\theta(\infty) = 0$. We expand $\theta(\eta)$ in power series around the same initial point

$$\theta^0(\eta) = \sum_{n=0}^{n_{\max}} b_n^0 (\eta - 1)^n \quad (30)$$

and similarly for the derivatives, $\theta^{0'}$ and $\theta^{0''}$. Substituted in (15), the coefficients, b_n^0 , for $n \geq 2$, are found recursively in terms of the initial conditions b_0^0 and b_1^0 through the recursion relations. Employing the IPS method, the first two recursion relations are found to be

$$\begin{aligned} b_2^I &= \frac{1}{2(1 + I\Delta)} \left[b_0^I \text{Pr}S + b_1^I (-1 - a_0^I \text{Pr} + \text{Pr}S \right. \\ &\quad \left. + I\Delta \text{Pr}S) \right], \end{aligned}$$

$$\begin{aligned} b_3^I &= \frac{1}{6(1 + I\Delta)^2} \left[b_0^I \text{Pr}S (-2 - a_0^I \text{Pr} + S(1 + I\Delta) \text{Pr}) \right. \\ &\quad \left. + b_1^I (2 + (a_0^I)^2 \text{Pr}^2 - \text{Pr}S + \text{Pr}^2 S^2 - \text{Pr}SI\Delta \right. \\ &\quad \left. + 2\text{Pr}^2 S^2 I\Delta + \text{Pr}^2 S^2 I^2 \Delta^2 - a_1^I \text{Pr}(1 + I\Delta) \right. \\ &\quad \left. + a_0^I \text{Pr}(3 - 2\text{Pr}S(1 + I\Delta)) \right], \end{aligned} \quad (31)$$

where

$$\begin{aligned} b_0^I &= \theta^{I-1}(\Delta), \\ b_1^I &= (\theta^{I-1})'(\Delta). \end{aligned} \quad (32)$$

5. Validation

In this section we aim at demonstrating the performance and efficiency of the present numerical scheme. Firstly, in order to obtain accurate numerical results, we have to pay attention to the selection of the numerical algorithm parameters, I , n_{\max} , and η_{∞} . To achieve this target we focus on studying the following:

$$\begin{aligned} f''' &= \frac{1}{\eta} (-f'' - ff'' + f'^2 + S(\eta f'' + f')), \\ \eta &\in (1, \eta_{\infty}), \end{aligned} \quad (33)$$

with

$$\begin{aligned} f(1) &= \gamma, \\ f'(1) &= -1, \\ f''(1) &= \lambda, \end{aligned} \quad (34)$$

where λ is updated using the shooting method to satisfy the condition $f'(\infty) = 0$. Notice that several recent studies such as [10–16] reported the existence of a critical value of S (named S_c) at which the problem has no solution (for $S > S_c$), only one solution (at $S = S_c$), and dual solutions (for $S < S_c$). It is worth mentioning that we succeeded in finding the explicit analytical form of the first solution for (33) subject to (34) under a condition $S = -1/\gamma$; that is

$$f(\eta) = \gamma e^{(1-\eta)/\gamma}. \quad (35)$$

This exact solution will play a crucial role in proving the advantages of our numerical scheme.

The approximate solutions of the problems (33) and (34) at three different iterations $I = 1, 2$, and 3 , together with the exact solution obtained by (35) when $S = -1$ and $\gamma = 1$, are displayed in Figure 1. It is clearly seen that increasing the number of iterations in the IPS method delays the divergence point.

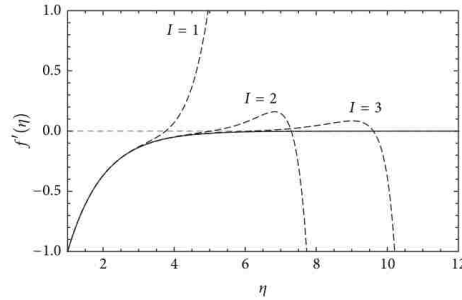
To achieve an ‘‘optimal choice’’ of η_{∞} , we solve the problem with $\eta_{\infty} = 7, 8, \dots, 17$. Table 1 shows the values of λ up to 50 digits corresponding to the values of η_{∞} . It is clearly

TABLE 1: Progressing of λ values with η_{∞} at $\gamma = 1$ and $S = -1$.

η_{∞}	λ
7	1.06032130948772355259169445286450439527129433161564
8	1.02826614125492573507123370718399515004546832373446
9	1.01244316459533191876326159442255228857229463473780
10	1.00535010609275538041830857835707790239466505001516
11	1.00221279175507729615034859048196423158532888754168
12	1.00084874204304334646862685662321915732040012124886
13	1.00030312215822976659593816307972112761442861473174
14	1.00016671718702637162776598969384662018793573810246
15	1.00003031221582297665959381630797211276144286147317
16	1.00003031221582297665959381630797211276144286147317
17	1.00003031221582297665959381630797211276144286147317

TABLE 2: The upper bound of the error for the first solution at $\gamma = 2$ and $S = -1$ versus the CPU time at different values of n_{\max} .

n_{\max}	E_{IPS}^*	CPU time (seconds)
3	$\approx 10^{-5}$	0.0156001
4	$\approx 10^{-7}$	0.0312002
5	$\approx 10^{-9}$	0.0780005
6	$\approx 10^{-10}$	0.156001
7	$\approx 10^{-12}$	0.296402
8	$\approx 10^{-14}$	0.546004

FIGURE 1: Velocity profiles, $f'(\eta)$, for the first solution; exact (solid) and approximate (dashed) solutions at different I with $S = -1$ and $\gamma = 1$.

seen that the value of λ stabilizes at around $\eta_{\infty} = 15$; hence we choose $\eta_{\infty} = 15$ as the optimal value for the rest of the calculations in the entire paper. It should be noted that most of the used numerical schemes for such type of problems, [8–10, 17], had chosen $\eta_{\infty} = 7$ to represent the infinity which, definitely, gave lower order of accuracy. This conclusion can be easily tested via the exact solution (35) which gives $f'(7) = -0.00247875$ and $f'(15) = -8.31529 \times 10^{-7}$. However, we will only show the interval up to $\eta_{\infty} = 8$ for the rest of the coming figures.

The upper bound of the error in the IPS method can be estimated as follows. At each iterative step an error of order $\Delta^{n_{\max}+1}$ results from terminating the power series at n_{\max} . This

error will be magnified I times due to the iterative procedure. As a result, the upper bound of the error of the IPS method is

$$E_{\text{IPS}} = I (\Delta)^{n_{\max}+1}. \quad (36)$$

Table 2 presents the CPU time in seconds, which is machine-dependent, versus the upper bound of the error, E_{IPS}^* , of the IPS method for the first solution at $\gamma = 2$ and $S = -1$, where n_{\max} varies from 3 to 8.

The exact solution, (35), provides a unique possibility of calculating the error of the IPS method and comparing it with that of other numerical methods. Figure 2 presents a comparison between the error of the IPS method and the explicit Runge–Kutta method of order four (ERK4) for the problem at $\gamma = 1$ and $S = -1$. The advantages of the present technique over the other one are notable.

A further comparison is done in Figure 3 on the normalized skin friction coefficient, $f''(1)$, as a function of S with Zaimi et al. [8] and Elnajjar et al. [10] for the case when $\gamma = 0$. Excellent agreements are obtained. It should be mentioned herein that Elnajjar et al. [10] used a combination of the implicit Runge–Kutta method and the shooting method while Zaimi et al. [8] implemented the shooting method described in the book by Jaluria and Torrance [11].

It is worth mentioning here that our technique successfully showed its definite capability to exceed the machine precision which is 10^{-14} . A clear sign on this is the systematic reduction in the error in Table 2 when compared with the exact solution. Moreover, all computations are performed with at least 14 decimal digits of precision, knowing that all computations are operated using Mathematica software 10.4 and carried out on a Lenovo PC with the following

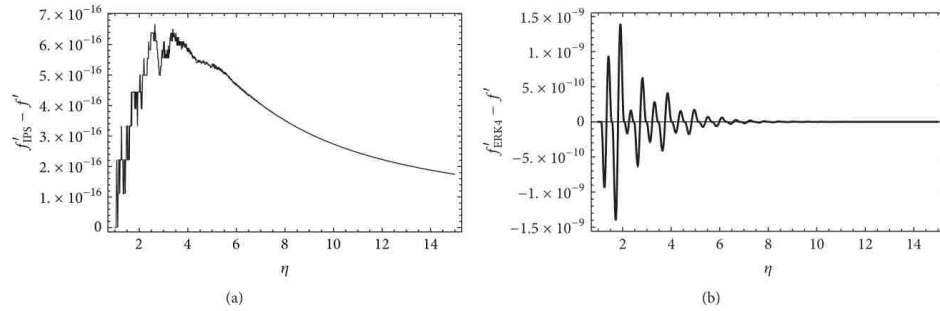


FIGURE 2: Error of the IPS method (a) and ERK4 (b) for the case of $\gamma = 1$ and $S = -1$. The error is defined as the difference between the numerical solution and the exact solution (35).

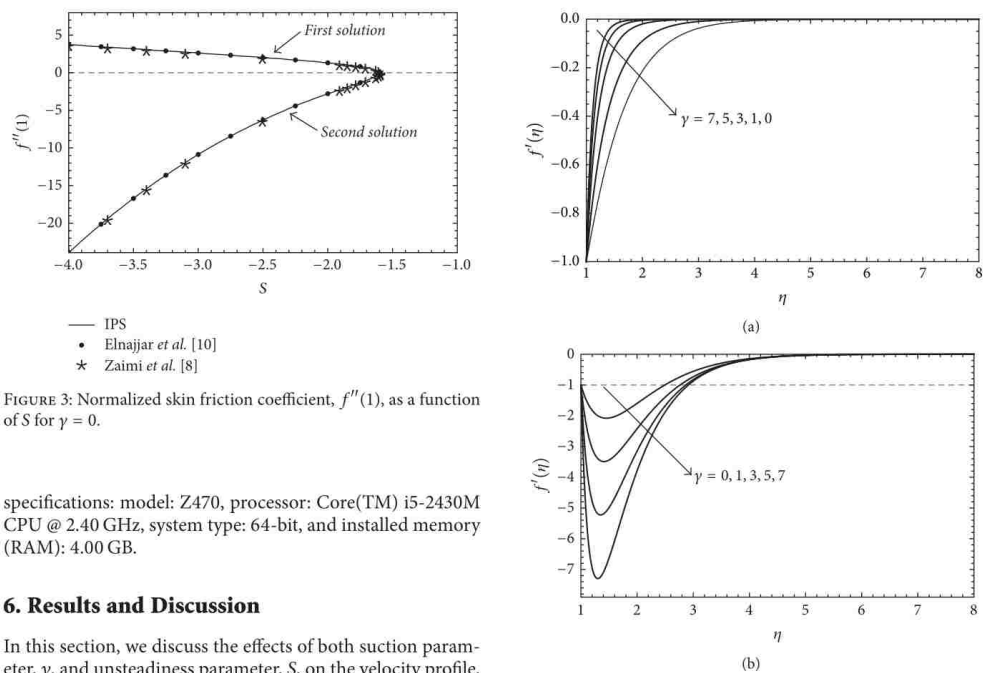


FIGURE 3: Normalized skin friction coefficient, $f''(1)$, as a function of S for $\gamma = 0$.

specifications: model: Z470, processor: Core(TM) i5-2430M CPU @ 2.40 GHz, system type: 64-bit, and installed memory (RAM): 4.00 GB.

6. Results and Discussion

In this section, we discuss the effects of both suction parameter, γ , and unsteadiness parameter, S , on the velocity profile, $f'(\eta)$, the normalized skin friction coefficient, $f''(1)$, the temperature profile, $\theta(\eta)$, and the heat transfer rate, $-\theta'(\eta)$. The numerical simulations are conducted at a fixed Prandtl number, $Pr = 0.7$, while the ranges considered for the other parameters are $0 \leq \gamma \leq 7$ and $-4 \leq S \leq -1$.

Figure 4 shows the first and second solutions of the velocity profiles for $\gamma = 0, 1, 3, 5, 7$ with a fixed unsteadiness parameter, $S = -2$. It is clearly seen that the first solution for the fluid velocity inside the boundary layer region increases as γ increases, while the second solution shows an opposite trend. In addition, the two solutions of the velocity profile

FIGURE 4: Velocity profiles, $f'(\eta)$, for different values of γ at $S = -2$: first solution (a) and second solution (b).

become steeper with higher magnitudes as γ increases. These observations emphasize the effect of increasing the suction parameter of the cylinder's wall which is to decrease the boundary layer thickness. Consequently, increasing the suction parameter causes an increment in the normalized skin friction coefficient for the first solution and decrement

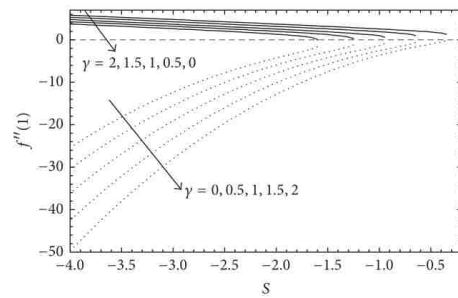


FIGURE 5: Normalized skin friction coefficient, $f''(1)$, as a function of S for different values of γ : the first solution (solid) and second solution (dotted).

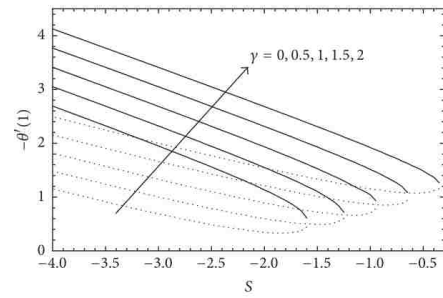


FIGURE 7: Heat transfer rate, $-\theta'(1)$, as a function of S for different values of γ : the first solution (solid) and second solution (dotted).

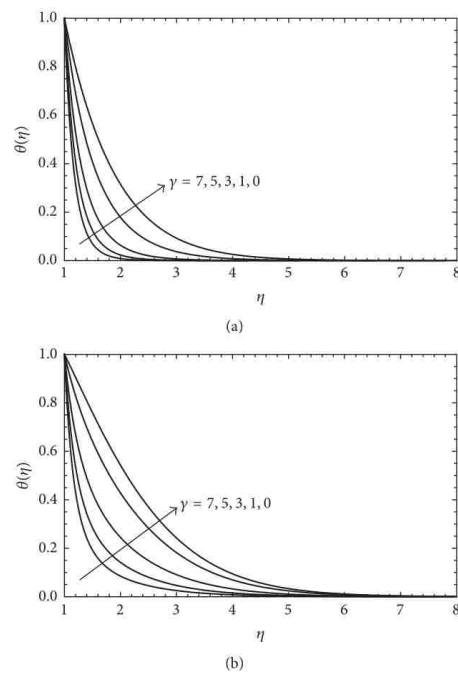


FIGURE 6: Temperature profiles, $\theta(\eta)$, for different values of γ at $S = -2$: first solution (a) and second solution (b).

in the normalized skin friction coefficient for the second solution, as clearly shown in Figure 5. These findings are consistent with the results reported by Elnajjar et al. [10] and Zaimi et al. [8].

Figure 6 presents the temperature profiles of the fluid flow, $\theta(\eta)$, at $S = -2$ and $\gamma = 0, 1, 3, 5, 7$. It is obviously noticeable that both solutions for temperature profiles admit

similar behaviour, where they become wider and more relaxed as the suction parameter decreases. These kinds of behaviour inspire us to conclude that the developed thermal boundary layer and the corresponding rate of heat transfer are decreasing as S increases. However, the second solution depicts more relaxed behaviour compared with the first solution. This slight difference between the first and second temperature profiles indicates that the second solution reflects higher thermal boundary layer than the first solution and, thus, a larger rate of the heat transfer as confirmed by Figure 7.

The variation of both the normalized skin friction coefficient, $f''(1)$, and the heat transfer rate, $-\theta'(1)$, as functions of S , are shown, respectively, in Figures 5 and 7 for $\gamma = 0, 0.5, 1, 1.5, 2$. The results demonstrate the existence of a critical value S_c in the S -domain at which the problem has no solution for $S > S_c$, only one solution at $S = S_c$, and dual solutions for $S < S_c$. Figure 5 shows that $|f''(1)|$ increases as γ increases which is due to the increase in the surface shear stress coefficient. Moreover, we observe that $|f''(1)|$ is decreasing with S . However, Figure 7 clearly shows that increasing γ will definitely increase the heat transfer rate while increasing S causes a decrease in the heat transfer rate.

Figure 8 displays the first and second solutions of the velocity profiles for $S = -1, -2, -3, -4$ with a fixed value of the suction parameter, $\gamma = 1$. Generally speaking, the behaviour of $f'(\eta)$ is very similar to the case of the variable suction parameter; that is, increasing the unsteadiness parameter produces steeper behaviour in the velocity profiles for the first solution while the second solution shows an opposite trend. In agreement with the case of the variable suction parameter in Figure 4, increasing the unsteadiness parameter will then cause a reduction in the thickness of the boundary layer.

Figure 9 presents the temperature profiles of the fluid flow, $\theta(\eta)$, at $\gamma = 1$ and $S = -1, -2, -3, -4$. Clearly, the increase in the unsteadiness parameter or the suction parameter leads to the same trend.

Finally, we end up our discussion with Figure 10 which presents an overview of the solution for problems (14) and (15) subject to the boundary conditions (16) in the γ - S domain

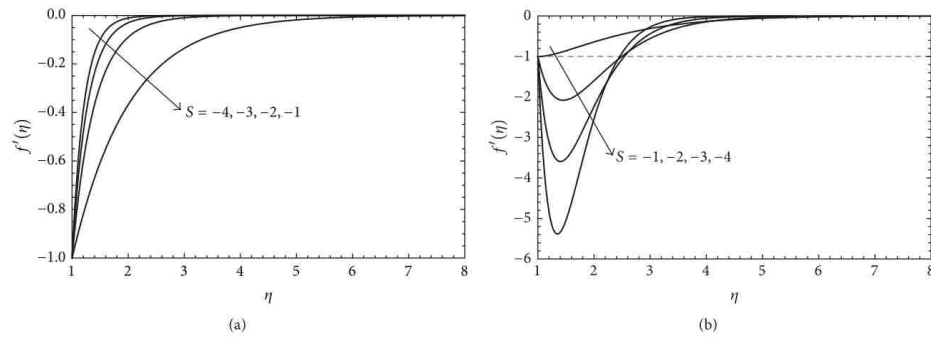


FIGURE 8: Velocity profiles, $f'(\eta)$, for different values of S at $\gamma = 1$: first solution (a) and second solution (b).

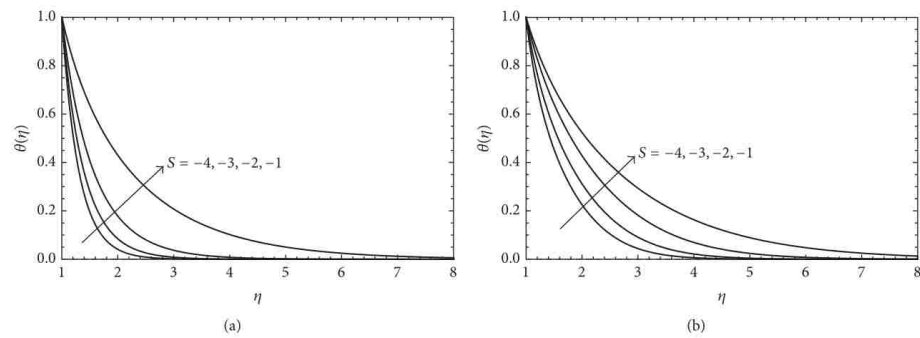


FIGURE 9: Temperature profiles, $\theta(\eta)$, for different values of S at $\gamma = 1$: first solution (a) and second solution (b).

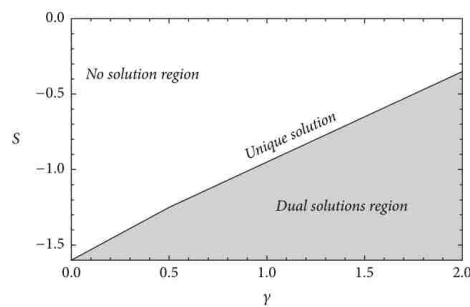


FIGURE 10: An overview of the solution for problems (14) and (15) subject to the boundary conditions (16) in the γ - S domain.

for $Pr = 0.7$ and $0 \leq \gamma \leq 2$. The straight line in this figure represents the occurrence of unique solution of the problem.

7. Conclusions

In this work, we presented a numerical technique for solving nonlinear BVPs based on iterative power series solutions. We have demonstrated its efficiency and accuracy through validation against the numerical ERK4. We have shown that our method excels over the ERK4 by orders of magnitude in accuracy. Moreover, the accuracy in our method is systematically controlled such that the error can be reduced to any arbitrary small value. We successfully studied the unsteady viscous flow over a contracting cylinder using the present technique. The velocity and temperature profiles of the ordinary version of Navier–Stokes equations for different suction and unsteadiness parameters are calculated. We have obtained the exact solution of the first solution of the fluid flow under a specific condition, $S = -1/\gamma$, and have employed it to emphasize the efficiency of the present numerical technique.

The convergence analysis of the IPS method is considered for a future work. However, we strongly believe that the method is convergent. This is conjectured by the systematic

reduction in error upon increasing the number of iterations or the number of terms in the power series. We believe that this technique will serve researchers in different fields working on nonlinear systems. In particular, the technique will be very useful for systems described by nonintegrable nonlinear differential equations.

Conflicts of Interest

The authors declare that they have no conflicts of interest.

Acknowledgments

The authors would like to express their sincere appreciation to the United Arab Emirates University, Al Ain, UAE, for providing the financial support with the UPAR (7) 2015 and the UPAR (4) 2016 grants.

References

- [1] A.-M. Wazwaz, "A reliable modification of Adomian decomposition method," *Applied Mathematics and Computation*, vol. 102, no. 1, pp. 77–86, 1999.
- [2] A.-M. Wazwaz, "Dual solutions for nonlinear boundary value problems by the variational iteration method," *International Journal of Numerical Methods for Heat & Fluid Flow*, vol. 27, no. 1, pp. 210–220, 2017.
- [3] V. Marinca and N. Herisanu, "The optimal homotopy asymptotic method: Engineering applications," *The Optimal Homotopy Asymptotic Method: Engineering Applications*, pp. 1–465, 2015.
- [4] Q. M. Al-Mdallal and F. M. Mahfouz, "Heat transfer from a heated non-rotating cylinder performing circular motion in a uniform stream," *International Journal of Heat and Mass Transfer*, vol. 112, pp. 147–157, 2017.
- [5] Q. M. Al-Mdallal, "Numerical simulation of viscous flow past a circular cylinder subject to a circular motion," *European Journal of Mechanics - B/Fluids*, vol. 49, no. part A, pp. 121–136, 2015.
- [6] Q. M. Al-Mdallal, "A numerical study of initial flow past a circular cylinder with combined streamwise and transverse oscillations," *Computers & Fluids*, vol. 63, pp. 174–183, 2012.
- [7] P. D. Weidman, D. G. Kubitschek, and A. M. J. Davis, "The effect of transpiration on self-similar boundary layer flow over moving surfaces," *International Journal of Engineering Science*, vol. 44, no. 11–12, pp. 730–737, 2006.
- [8] K. Zaimi, A. Ishak, and I. Pop, "Unsteady flow due to a contracting cylinder in a nanofluid using Buongiorno's model," *International Journal of Heat and Mass Transfer*, vol. 68, pp. 509–513, 2014.
- [9] T. Fang, J. Zhang, and Y. Zhong, "Note on unsteady viscous flow on the outside of an expanding or contracting cylinder," *Communications in Nonlinear Science and Numerical Simulation*, vol. 17, no. 8, pp. 3124–3128, 2012.
- [10] E. J. Elnajjar, Q. M. Al-Mdallal, and F. M. Allan, "Unsteady Flow and Heat Transfer Characteristics of Fluid Flow over a Shrinking Permeable Infinite Long Cylinder," *Journal of Heat Transfer*, vol. 138, no. 9, Article ID 092003, 2016.
- [11] Y. Jaluria and K. E. Torrance, *Comput Heat Transfer*, 2003.
- [12] J. H. Merkin, "On dual solutions occurring in mixed convection in a porous medium," *Journal of Engineering Mathematics*, vol. 20, no. 2, pp. 171–179, 1986.
- [13] J. Paullet and P. Weidman, "Analysis of stagnation point flow toward a stretching sheet," *International Journal of Non-Linear Mechanics*, vol. 42, no. 9, pp. 1084–1091, 2007.
- [14] S. D. Harris, D. B. Ingham, and I. Pop, "Mixed convection boundary-layer flow near the stagnation point on a vertical surface in a porous medium: brinkman model with slip," *Transport in Porous Media*, vol. 77, no. 2, pp. 267–285, 2009.
- [15] A. Postelnicu and I. Pop, "Falkner-Skan boundary layer flow of a power-law fluid past a stretching wedge," *Applied Mathematics and Computation*, vol. 217, no. 9, pp. 4359–4368, 2011.
- [16] A. V. Roşca and I. Pop, "Flow and heat transfer over a vertical permeable stretching/shrinking sheet with a second order slip," *International Journal of Heat and Mass Transfer*, vol. 60, no. 1, pp. 355–364, 2013.
- [17] A. Ishak, R. Nazar, and I. Pop, "Uniform suction/blowing effect on flow and heat transfer due to a stretching cylinder," *Applied Mathematical Modelling*, vol. 32, no. 10, pp. 2059–2066, 2008.
- [18] N. Bachok, A. Ishak, and I. Pop, "Boundary layer stagnation-point flow and heat transfer over an exponentially stretching/shrinking sheet in a nanofluid," *International Journal of Heat and Mass Transfer*, vol. 55, no. 25–26, pp. 8122–8128, 2012.
- [19] A. Ishak, Y. Y. Lok, and I. Pop, "Stagnation point flow over a shrinking sheet in micropolar fluid," *Chemical Engineering Communications*, vol. 197, no. 11, pp. 1417–1427, 2010.
- [20] N. A. Yacob, A. Ishak, and I. Pop, "Melting heat transfer in boundary layer stagnation-point flow towards a stretching/shrinking sheet in a micropolar fluid," *Computers & Fluids*, vol. 47, no. 1, pp. 16–21, 2011.
- [21] C. Y. Wang, "Stagnation flow towards a shrinking sheet," *International Journal of Non-Linear Mechanics*, vol. 43, no. 5, pp. 377–382, 2008.
- [22] N. Bachok, A. Ishak, and I. Pop, "Unsteady boundary-layer flow and heat transfer of a nanofluid over a permeable stretching/shrinking sheet," *International Journal of Heat and Mass Transfer*, vol. 55, no. 7–8, pp. 2102–2109, 2012.
- [23] Y. Zhong and T. Fang, "Unsteady stagnation-point flow over a plate moving along the direction of flow impingement," *International Journal of Heat and Mass Transfer*, vol. 54, no. 15–16, pp. 3103–3108, 2011.
- [24] K. Bhattacharyya, S. Mukhopadhyay, and G. C. Layek, "Slip effects on boundary layer stagnation-point flow and heat transfer towards a shrinking sheet," *International Journal of Heat and Mass Transfer*, vol. 54, no. 1–3, pp. 308–313, 2011.
- [25] F. Aman and A. Ishak, "Mixed convection boundary layer flow towards a vertical plate with a convective surface boundary condition," *Mathematical Problems in Engineering*, vol. 2012, Article ID 453457, 11 pages, 2012.
- [26] N. Bachok, A. Ishak, and I. Pop, "Stagnation point flow toward a stretching/shrinking sheet with a convective surface boundary condition," *Journal of The Franklin Institute*, vol. 350, no. 9, pp. 2736–2744, 2013.
- [27] A. D. Polyanin and V. F. Zaitsev, *Handbook of Nonlinear Partial Differential Equations*, CRC press, 2004.
- [28] C. S. Gardner, J. M. Greene, M. D. Kruskal, and R. M. Miura, "Method for solving the Korteweg-deVries equation," *Physical Review Letters*, vol. 19, no. 19, pp. 1095–1097, 1967.
- [29] P. D. Lax, "Integrals of nonlinear equations of evolution and solitary waves," *Communications on Pure and Applied Mathematics*, vol. 21, no. 5, pp. 467–490, 1968.
- [30] M. A. Salle and V. B. Matveev, *Darboux transformations and solitons*, 1991.

- [31] R. Hirota, "The Direct Method in Soliton Theory," in *Solitons*, pp. 157–176, Springer, Berlin, Heidelberg, 1980.
- [32] G. Adomian, *Solving Frontier Problems of Physics: The Decomposition Method*, Springer, The Netherlands, 1994.
- [33] S. Liao and Y. Tan, "A general approach to obtain series solutions of nonlinear differential equations," *Studies in Applied Mathematics*, vol. 119, no. 4, pp. 297–354, 2007.
- [34] R. Barrio, M. Rodriguez, A. Abad, and F. Blesa, "Breaking the limits: the Taylor series method," *Applied Mathematics and Computation*, vol. 217, no. 20, pp. 7940–7954, 2011.
- [35] G. Corliss and Y. F. Chang, "Solving ordinary differential equations using Taylor series," *ACM Transactions on Mathematical Software*, vol. 8, no. 2, pp. 114–144, 1982.
- [36] Y. F. Chang and G. Corliss, "ATOMFT: solving ODEs and DAEs using Taylor series," *Computers & Mathematics with Applications*, vol. 28, no. 10-12, pp. 209–233, 1994.
- [37] J. D. Pryce, "Solving high-index DAEs by Taylor series," *Numerical Algorithms*, vol. 19, no. 1-4, pp. 195–211, 1998.
- [38] R. Barrio, "Performance of the Taylor series method for ODEs/DAEs," *Applied Mathematics and Computation*, vol. 163, no. 2, pp. 525–545, 2005.
- [39] N. S. Nedialkov and J. D. Pryce, "Solving differential-algebraic equations by TAYLOR series. I. Computing TAYLOR coefficients," *BIT Numerical Mathematics*, vol. 45, no. 3, pp. 561–591, 2005.
- [40] N. S. Nedialkov and J. D. Pryce, "Solving differential-algebraic equations by Taylor series. (II): Computing the system Jacobian," *BIT Numerical Mathematics*, vol. 47, no. 1, pp. 121–135, 2007.
- [41] N. S. Nedialkov and J. D. Pryce, "Solving differential algebraic equations by Taylor series. (III): THE DAETS code," *JNAIAM. Journal of Numerical Analysis, Industrial and Applied Mathematics*, vol. 3, no. 1-2, pp. 61–80, 2008.
- [42] N. S. Nedialkov, K. R. Jackson, and G. F. Corliss, "Validated solutions of initial value problems for ordinary differential equations," *Applied Mathematics and Computation*, vol. 105, no. 1, pp. 21–68, 1999.
- [43] W. Tucker, "A Rigorous ODE Solver and Smale's 14th Problem," *Foundations of Computational Mathematics*, vol. 2, no. 1, pp. 53–117, 2002.
- [44] R. Barrio and F. Blesa, "Systematic search of symmetric periodic orbits in 2DOF Hamiltonian systems," *Chaos, Solitons & Fractals*, vol. 41, no. 2, pp. 560–582, 2009.
- [45] R. Barrio, F. Blesa, and S. Serrano, "Periodic, escape and chaotic orbits in the Copenhagen and the (n+ 1) body ring problems," *Communications in Nonlinear Science and Numerical Simulation*, vol. 14, no. 5, pp. 2229–2238, 2009.
- [46] R. Barrio, "Painting chaos: a gallery of sensitivity plots of classical problems," *International Journal of Bifurcation and Chaos*, vol. 16, no. 10, pp. 2777–2798, 2006.
- [47] R. Barrio and S. Serrano, "A three-parametric study of the Lorenz model," *Physica D: Nonlinear Phenomena*, vol. 229, no. 1, pp. 43–51, 2007.
- [48] À. Jorba and M. Zou, "A software package for the numerical integration of ODEs by means of high-order Taylor methods," *Experimental Mathematics*, vol. 14, no. 1, pp. 99–117, 2005.
- [49] L. Y. Al Sakkaf, *Iterative power series solutions of nonlinear partial differential equations with applications in nonlinear Science [M.S. thesis]*, United Arab Emirates University, Al Ain, United Arab Emirates, 2018.